Daniel Sousa Lapa Cupido Zagalo

Bachelor of Science

Development and testing safe fall strategies for lower limbs exoskeletons

Dissertation submitted in partial fulfillment
of the requirements for the degree of

Master of Science in
Biomedical Engineering

Co-advisers: Cristina Bayón Calderón, PhD.,
University of Twente

Cláudia Regina Pereira Quaresma, Associate Professor, Faculdade de Ciências e Tecnologia da Universidade Nova de Lisboa

FACULDADE DE
CIÊNCIAS E TECNOLOGIA
UNIVERSIDADE NOVA DE LISBOA

March, 2021

Development and testing safe fall strategies for lower limbs exoskeletons

This document was created using the (pdf)LaTeX processor, based in the "novathesis" template[1], developed at the Dep. Informática of FCT-NOVA [2].
[1] https://github.com/joaomlourenco/novathesis [2] http://www.di.fct.unl.pt

To my family, for making me who I am.
To Pedro, Rita and Bernardo, for inspiring me to be more.

Acknowledgements

First of all, I would like to thank the help and guidance of my advisor, Cristina Bayón. The process of completing this work left me flustered more than once, and Cristina helped me time and time again to regain focus. That is one lesson I won't forget any time soon. I would also like to thank Professor Cláudia Quaresma, for always showing availability for any questions or issues I might or could have. Feeling supported as I felt was a privilege.

On a personal note, this process was arguably the most challenging task I ever pursued. If a shared joy is a greater one, then a shared pain is without question a lesser one, and throughout this journey I was blessed to be able to share everything with Pedro, Rita, Bernardo and Francisca. I can only hope they know how much they mean to me, because words won't properly describe it. Lastly, I would like to thank my family. If in me there is any virtue to be found, it is there because of my family.

"Enquanto houver estrada para andar
A gente vai continuar..."
- Jorge Palma

Abstract

Loss of mobility is among the most impactful consequences of sustaining a spinal cord injury. Wheelchairs provide a considerable degree of mobility to their users, but are not without their drawbacks, most of which are caused by requiring prolonged periods of time in the sitting position. Recently, the field of lower limb exoskeletons has seen considerable developments, and the use of external power technologies has made it possible for users to walk for longer periods of time. However, current exoskeletons do not ensure balance during standing and walking conditions, which leaves their users vulnerable to situations of instability and falls. The goal of this thesis was to investigate safe fall strategies to reduce the severity of the impact in case of a loss of balance with a lower limb exoskeleton. The backwards fall scenario is examined, and a fall strategy is implemented in a simulation environment, using a combination of center of mass and hip joint angle reference signals. The results verified the model's ability to execute the proposed strategy by following the reference signals, and the strategy was shown to result in safer falls. Further work should be conducted to test this strategy in real-life human-exoskeleton fall scenarios, and to develop strategies for other fall scenarios.

Keywords: lower limb exoskeletons, safe falls, mobility technologies, fall control

Resumo

Perda de mobilidade é das consequências com maior impacto na vida de quem sofre uma lesão da medula espinhal. Cadeiras de rodas providenciam um nível considerável de mobilidade aos seus utilizadores, mas trazem os seus próprios problemas, sendo que a maioria dos quais são resultantes da necessidade dos seus utilizadores permanecerem sentados durante longos períodos de tempo. Mais recentemente, a área dos exosqueletos para membros inferiores tem visto desenvolvimento notável, e o uso de fontes de energia externas tem permitido que os seus utilizadores se desloquem a pé durante intervalos de tempo maiores. Contudo, estas tecnologias ainda não garantem equilíbrio constante dos seus utilizadores durante a marcha ou em pé, o que faz com que estes estejam vulneráveis a situações de instabilidade e quedas. Esta tese teve como objetivo investigar estratégias de queda segura para reduzir a severidade do impacto em caso de uma perda de equilíbrio utilizando um exosqueleto para membros inferiores. É examinado o cenário de uma queda para trás, e é implementada uma estratégia de queda num ambiente de simulação, recorrendo a uma combinação de sinais de referência de centro de massa e ângulo da articulação da anca. Os resultados verificaram a capacidade do modelo utilizado executar a estratégia proposta ao seguir os sinais de referência, e a estratégia mostrou resultar em quedas mais seguras. No futuro, a estratégia deve ser testada em cenários reais de quedas de um exosqueleto e o seu utilizador, e devem ser desenvolvidas estratégias para os restantes cenários de queda.

Palavras-chave: exosqueletos para membros inferiores, quedas seguras, tecnologias de mobilidade, controlo de queda

Contents

List of Figures xvii

List of Tables xix

Acronyms, Initialisms and Abbreviations xxi

1 Introduction 1

2 Concepts 5
- 2.1 Spinal Cord Injury . . . 5
- 2.2 Exoskeletons . . . 6
- 2.3 Falls . . . 6
  - 2.3.1 Falls and Exoskeletons . . . 7
- 2.4 Inverted Pendulum Model . . . 7

3 Literature Review 9
- 3.1 Balance Controllers in Exoskeletons . . . 9
- 3.2 Safe-fall Controllers in Exoskeletons . . . 13
- 3.3 Safe Falls in Healthy Individuals . . . 15
- 3.4 Conclusion on literature review . . . 19

4 Methods 21
- 4.1 Purpose of the controller . . . 21
- 4.2 Reference trajectory for the Center of Mass . . . 25
  - 4.2.1 Adapting the Center of Mass Reference . . . 27
- 4.3 Hip Actuation . . . 28
- 4.4 Center of Mass and Hip Angle Reference Tracking . . . 28
- 4.5 Integral Joint Torques . . . 30
- 4.6 Studying Fall Safety . . . 30
- 4.7 Performance Tracking . . . 31
- 4.8 Testing Protocol . . . 31

5 Results 37
- 5.1 Reference Tracking and Strategy Execution . . . 37

5.1.1 Center of Mass and Hip Angle Score Tracking 39
5.1.2 Joint Torque Involved in the Safe Fall Strategy 40
5.2 Fall Safety and Vertical Hip Impact Velocity 41
5.3 Performance Score 41

6 Discussion **49**
6.1 Conclusion 52

Bibliography **53**

A Initial Positions and Joint Angles **63**

B Center of Mass Reference Tracking Results **65**

C Hip Joint Angle Reference Tracking Results **71**

D Average Joint Torque Integral Results **77**

E Normalized Hip Vertical Velocity Results **83**

F Performance Score Results **89**

List of Figures

2.1 Inverted pendulum model used for skeletal dynamics. 8

3.1 Sketch of how CoM position is estimated in the MINDWALKER. 10
3.2 A diagram of the ATALANTE human-exoskeleton system. 12
3.3 The CAPTUR and TWICE exoskeletons. 13
3.4 Optimization procedure for the MBC and FSF to fit human balance responses. 14
3.5 Three-link model created to represent the dynamics of a human and human-exoskeleton fall. Representations of the human-exoskeleton model's position at specific instants in throughout a fall. 15
3.6 Schematics of the SIT and FALL trials for self-initiated backward descents. . 16
3.7 Descent kinematics associated with one-link, two-link and three-link models 17
3.8 Representation of the tether-release falling experiment. 18

4.1 Body segment lengths expressed as a fraction of body height H, as described by Winter. 22
4.2 Design features of the WE2 exoskeleton. 23
4.3 Overview of the process of execution for the controller's safe fall strategy. . . 24
4.4 Diagrams of human-exoskeleton model position at specific instants in the fall. Representation of the positions used to create the $\mathcal{M}_{xy}$ reference for the model. 26
4.5 An example of different resulting $\mathcal{M}_x$ and $\mathcal{M}_y$ references for different combinations of xSlope and ySlope values. 27
4.6 Reference signals used to execute the squat response strategy. 29
4.7 Illustrative diagram for the process involved in assessing the performance score for every simulation. 32
4.8 An example of the model's poor reference execution due to the use of higher xSlope and ySlope values. 34

5.1 Comparison of $\mathcal{M}_y$, $\mathcal{M}_x$ and θ_{hip} values, between reference and simulation values. 38
5.2 Diagrams of the human-exoskeleton model's position throughout two simulations. 39
5.3 Values of the $\mathcal{M}_{xy}$ Score for different combinations of xSlope and ySlope values. 42
5.4 Values of the θ_{hip} scores for different combinations of xSlope and ySlope values. 43

5.5 Diagrams of the human-exoskeleton model's position throughout simulations using lower slope parameter values. 44
5.6 Diagrams of the human-exoskeleton model's position throughout simulations using higher slope parameter values. 45
5.7 Values of the average torque integral for different combinations of xSlope and ySlope values. 46
5.8 Values of the normalized hip vertical impact velocity for different combinations of xSlope and ySlope values. 47
5.9 Values of the performance score for different combinations of xSlope and ySlope values. 48

B.1 Values of the $\mathcal{M}_{xy}$ Score for different combinations of xSlope and ySlope values. 65

C.1 Values of the θ_{hip} Score for different combinations of xSlope and ySlope values. 71

D.1 Values of the average joint torque integral for different combinations of xSlope and ySlope values. 77

E.1 Values of the normalized hip vertical velocity for different combinations of xSlope and ySlope values. 83

F.1 Values of the performance score for different combinations of xSlope and ySlope values. 89

List of Tables

4.1 Coordinates for the CoM and inertias for each part of the WE2. 23
4.2 Complete set of values used in simulation to test the proposed safe fall strategy. 35

A.1 Diagrams of the human-exoskeleton model's initial positions, and their respective joint angles. 64

Acronyms, Initialisms and Abbreviations

CM	Centroidal Momentum.
CoM	Center of Mass.
CoP	Center of Pressure.
DoF	Degrees of Freedom.
FD	Forward Dynamics.
FDA	Food and Drug Administration.
FSF	Full State Feedback.
IMU	Inertial Measurement Unit.
LLE	Lower Limb Exoskeletons.
MBC	Momentum Based Control.
NSCISC	National Spinal Cord Injury Statistical Center.
ODE	Ordinary Differential Equation.
PD	Proportional Derivative.
PGain	Proportional Derivative Controller's Proportional Term.
SCI	Spinal Cord Injury.

Chapter 1

Introduction

A Spinal Cord Injury (SCI) is, as the name indicates, an injury to the spinal cord, as a result of trauma, disease or infection. When this injury is in the cervical region of the spine, it is referred to as tetraplegia. An injury of this nature results in full paralysis of the lower limbs, and partial paralysis of the trunk and arms. If the injury is in the trunk or lumbar region, it is referred to as paraplegia. In this case, the legs are completely paralyzed, there is partial paralysis of the trunk, but the arms are fully functional [1].

Loss of mobility is among the most impactful consequences of sustaining a SCI, as it prevents individuals from performing daily activities, house-hold chores, and interact with an outside community [2]. In short, it strips people of their autonomy [3]. As such, much attention has been given to the issue of restoring mobility to these individuals as much as possible.

The most common mobility option for individuals with SCI is the wheelchair. Manual or powered wheelchairs provide a considerable degree of mobility to their users, allowing them to perform some daily activities. However, they are not without their shortcomings. Shoulder pain and shoulder injuries are common among wheelchair users, due to high loads on this joint that result from manual wheeling and transferring out of bed and onto the chair in the morning [4, 5], or even postural changes overtime [6]. Pressure ulcers are also prevalent among people with SCI, due to long periods of time spent in wheelchairs. A prolonged seating position is not beneficial, but it remains necessary for full engagement in daily activities on the part of wheelchair users [7].

To contrast, the standing position provides a number of benefits to individuals with SCI. These include preventing lower limbs contractures, improving renal function, stimulation of circulation, and beneficial effects on femur bone mass density [8–10].

For these reasons, assistive devices such as walkers, crutches and canes, have been prescribed to SCI individuals. While capitalizing on the positive effects of standing, these

technologies have not replaced the use of wheelchairs. A big reason behind this is the fact that they demand a large energy cost from their users. Reports of exhaustion and high loads on the upper limb joints are major complaints in relation to these devices [9, 11–13], and users often end up going back to the wheelchair for regular use.

In recent decades, advancements in robotics, actuators, sensors and control systems have allowed for the development of powered Lower Limb Exoskeletons (LLE), to improve mobility of people with SCI [14]. The use of external power to achieve movement has made it possible for users to walk and move for longer periods of time, without feelings of exhaustion or considerable upper body pain.

Research involving these new devices has been promising. Results point to positive effects in regards to gait rehabilitation, along with all the benefits of the standing position previously mentioned. Improvements in pain, bowel and bladder function and spasticity have been reported [15–17]. Additionally, the ability to provide a walking experience has often been associated with an improvement on user motivation and participation in the therapeutic process, which in turn can lead to improved results [18].

In addition to these positive effects, the apparent potential for LLE to be used without physical assistance during daily activities is evident for both users and therapists. Unfortunately, there exist still some obstacles that prevent this from being a reality: device weight, portability and issues associated with assembly are all aspects that still need to see development [18]. Human help is often required to install and make these devices operable for users [2], which to some extent is due to the fact that many LLE are initially designed to be used only within the context of supervised therapy. Also, one of the main barriers to the adoption of LLE in everyday life is instability, loss of balance, and falls.

Current LLE do not fully ensure balance during standing and walking conditions, and users still need crutches to maintain equilibrium. Balance control is key for these devices to be adopted in the context of daily activities, and implemented controllers need to be safe and robust enough to be accepted by stakeholders [19, 20]. Before considering daily use, scenarios of external perturbations have to be taken into account, as well as a wide range of walking surfaces.

Additionally, in the event of unavoidable falls, LLE should have a control strategy to maximize user safety and minimize chances of injury. This is particularly important when considering the increased safety risk in the event of a fall, in relation to wheelchairs. Falling while using a LLE not only means falling from higher up, but also the device itself restricts the users' movements and eventual efforts to catch themselves [18]. It is in this context that this work was developed.

The goal of this thesis is to investigate safe fall strategies to reduce the severity of the impact in case of a loss of balance with a LLE. As a first step, the backwards fall scenario is examined, and a fall strategy is implemented in a simulation environment, to test its effectiveness and assess the results. The conclusions of this work can be used to develop safe fall strategies in real exoskeletons in the future.

The safe fall strategy presented here is based on human-like falls. This choice was

made for two reasons: first, there is a large amount of research to draw from on the development of safe fall strategies for healthy individuals. The same cannot be said for research concerning the human-exoskeleton system. The other reason is that, from the perspective of a smoother human-machine interaction, a strategy that better mimics more natural responses of its users is expected to result in a safer outcome.

When discussing fall scenarios, it's important to differentiate between types of falls. One way of doing this is by classifying falls into three categories in regards to fall direction: forward, backwards and sideways [21]. This thesis covers backwards falls. This scenario was chosen for two reasons: it is a type of fall where upper limb influence is less relevant to ensure safety (in contrast to forward falls), which is important to consider as the exoskeleton in question does not have upper limb control. Plus, an established backwards fall strategy can prove useful when designing a sideways fall in the future, as some research has pointed to the positive effects of rotating backwards during a sideways fall for avoiding hip impact or reducing hip impact force [22, 23].

The next chapters will detail the investigation on the effectiveness of a backwards fall strategy in a simulation environment, as well as the results on its impact on user safety during the fall.

Chapter 2

Concepts

2.1 Spinal Cord Injury

Spinal Cord Injury (SCI) is defined as a neurological disturbance as a consequence of trauma, disease, vascular compromise, or congenital neural tube defect, with manifestations of this injury depending on location and severity of the damage to the spinal cord [24, 25].

An injury of this nature is commonly associated with a fracture involving vertebral dislocation or subluxation, being caused by ischaemia, traction or direct compression of the spinal cord [24].

Cases of loss of motor and/or sensory function stemming from damage to the cervical segments of the spinal cord are referred to as tetraplegia, whereas paraplegia refers to losses of this nature to the thoracic, lumbar, or sacral segments. Function in the upper extremities, lower extremities and trunk in the event of tetraplegia, while in the case of paraplegia, depending on the injury, function is impairs in the trunk and/or lower extremities [24, 26].

According to the most recent data by the National Spinal Cord Injury Statistical Center (NSCISC), the leading causes of SCI are vehicle crashes and falls. Traumatic SCIs are associated with fractures, loss of consciousness, traumatic pneumothorax or hemothorax, head injuries, skull and facial fractures, limb fractures and intra-abdominal injuries to the liver, spleen and kidneys [27].

In the United States, an estimated 294,000 people with SCI exist, and the annual incidence is approximately 54 cases per million, or 17810 new cases per year [27]. There is no effective measure to cure SCI [28]. After an injury of this nature, rehabilitation starts in the hospital setting, with the goal of preventing complications and maximize long-term functional recovery. SCI patients can experience severe problems in many

aspects of their lives, including daily living, physical well being and self-care, mobility, social interaction, accommodation, employment, family support, sexual function and psychological well being. As such, to improve quality of life for SCI patients', rehabilitation programmes require the involvement and collaboration of a multidisciplinary team of medical professionals [25, 28].

2.2 Exoskeletons

The Food and Drug Administration (FDA) defines a powered exoskeleton as "a prescription device that is composed of an external, powered, motorized orthosis used for medical purposes that is placed over a person's paralyzed or weakened limbs for the purpose of providing ambulation" [29]. Systems of actuators and sensors are used in order to achieve movements [20]. Exoskeletons are designed to move in parallel with their users' skeletons, so that no additional degrees of freedom are needed, to follow the user's motions [30]. Lower Limb Exoskeletons (LLE) in particular have seen development recently, to meet demands of greater rehabilitation goals for people with lower limb impairments [31]. Currently, their use is mainly limited to supervised clinical settings, for rehabilitation or health purposes, but the end goal for these devices is daily use as functional mobility aids [20].

2.3 Falls

A fall can be defined as "an unexpected event in which the participant comes to rest on the ground, floor, or lower level" [32]. In the US, falls are the leading cause for both non-fatal injuries among almost all age groups, and fatal injuries among people aged 65 or older [33]. Falls don't often cause death, but head injuries or fractures are common. As such, they have a considerable impact on the health and quality of life for older adults [34]. Additionally, the financial costs of falls are also notable. A recent study estimated that, in 2015, the direct medical costs of non-fatal falls were $31.3 billion [35]. As such, interventions to prevent falls have been studied, developed, tested and summarized in systematic reviews and meta-analysis. Exercise interventions are the most effective in reducing fall rates and fall risk. With that said, participants of these exercise programs still fall [36].

Besides fall prevention, methods for falling and minimizing injury risk have also been investigated. The assumption behind this research is that there exist protective movements which when executed enable a safe landing during fall events [37]. Injury risk has been quantified by biomechanical parameters such as force and velocity, which reflect the magnitude of loads applied to the body at impact. A recent review on safe landing strategies reported that a multitude of strategies have had significant effects on reducing impact severity in fall scenarios [21]. This incorporated techniques based on falling direction, like squatting during backwards falls [38, 39], and elbow flexion during forward

falls [40, 41]. Strategies for sideways falls included forward and backward rotation [22], stepping [42], falling while relaxing the muscles [43, 44], and also techniques associated with martial arts [23, 45–47]. The review concludes by pointing out a need to verify the effectiveness and suitability for these strategies to be applied by at-risk populations.

2.3.1 Falls and Exoskeletons

In the context of LLE exoskeletons, the risk of falls remains a considerable limitation to the adoption of these technologies outside of a clinical or rehabilitation setting. The FDA identified "instability, falls, and associated injuries" as one of the risks to health associated with "powered lower extremity exoskeletons" [29]. External perturbations to the user while wearing the exoskeleton might lead the destabilization and fall of the system. In this case, the impact velocity when hitting the ground can be large enough to cause head injuries or fractures. Addressing this safety risk is thus a top priority in the development of these devices, if they are expected to be adopted by their users to perform activities of daily living independently [31].

2.4 Inverted Pendulum Model

In the field of biomechanics, optimal control theory is used to study the human body and its dynamics as a system. Optimal control has been used to find muscle excitations in musculoskeletal models while performing tasks such as jumping [48–51], gait [52, 53], rising from a chair [54] or cycling [55]. For these studies, very detailed models are used, including multiple degrees of freedom and muscle actuators for human limbs. This level of detail makes the associated numerical problems very computationally intensive. To mitigate this, new approaches were developed to provide accurate representations of the system, while avoiding these numerical problems. As a result, it is common to represent the dynamics of the human body with a model of an inverted pendulum [54].

In the inverted pendulum model, it "is assumed that the two legs are simulated and move identically, and the body consists of four segments (i.e., foot, shank, thigh, and trunk and head)" [56]. Each segment's Center of Mass (CoM) is assumed to be located on the line which connects the two adjacent joints, and the foot "is assumed to be flat on the ground throughout the motion".

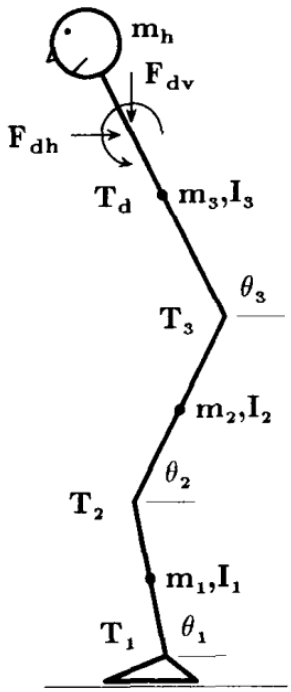

Figure 2.1: Inverted pendulum model used for skeletal dynamics, as described in [56]. Each segment is assumed to be rigid, and its center of mass is located on the straight line connecting the adjacent joints. $I_i (i = 1, 2, 3)$ is the moment of inertia regarding the center of mass of the ith segment. The masses of the head and segments are represented by m_h and $m_i (i = 1, 2, 3)$, respectively. T_i's $(i = 1, 2, 3)$ are the joint torques produced at the ankle, knee and hip joints, respectively. The net forces and torque resulting from arm movement, which is modeled as an external disturbance to the model, are represented by $F_d h$, $F_d v$ and T_d. θ_i's represent segmental angles.

Chapter 3

Literature Review

3.1 Balance Controllers in Exoskeletons

In the context of Lower Limb Exoskeletons (LLE), balance controllers are developed with the goal of creating a more robust and stable gait performance. A loss of sensory information for users leads to less precise foot placement [57], and as individuals with SCI have lost or impaired control of their lower limbs, an external way of monitoring and maintaining a balanced walk is needed.

A robust walk process is crucial, but it is also one of the biggest current challenges in the field. Most exoskeletons cannot detect or react to perturbations which may lead to a fall. This is something noted by Gardner, Potgieter and Noble [58] in their recent review of commercially available exoskeletons and their abilities. Among the four exoskeletons reviewed in [58], which the authors considered the market leaders, only the Indigo reported a method for fall detection and correction. This method is not yet publicly available. To my and the authors' knowledge at the time, it is only mentioned in the 510k device summary report submitted to the FDA for approval [59].

Besides this, there have been other efforts to develop systems for maintaining user balance and stability. S. Wang *et al.* [60], for instance, set out to develop a powered LLE to support SCI paraplegics in walking, while maintaining postural stability. The result was the MINDWALKER. During the design process, the exoskeleton's Degrees of Freedom (DoF) and joint range of motion were specified in accordance to human anatomy and joint range of motion, and made to allow sitting, standing and walking. Gait assistance is provided through a finite-state machine based controller. The stability condition for the controller is based on the concept of an "Extrapolated Center of Mass" (XCoM), previously applied in human balance control analysis [61].

The XCoM concept is based on the modeling of bipedal gait in single stance as a linear

inverted pendulum, that is, a concentrated mass kept at a constant height by a massless extendable leg. A gait pattern can be considered statically stable if this XCoM lies within the area of the supporting polygon.

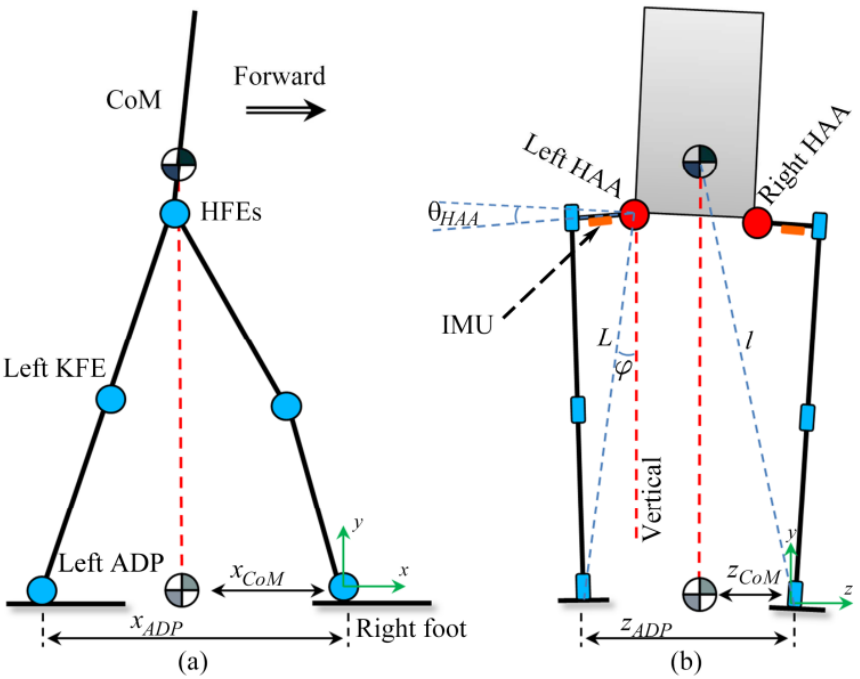

Figure 3.1: Sketch of how CoM position is estimated in the MINDWALKER. The sagittal plane is represented in (a) and the frontal plane is represented in (b). The distances between CoM ground projection and the leading foot are represented by x_{CoM} and z_{CoM} for the sagittal and frontal plane, respectively. Step length and step width are represented by x_{ADP} and z_{ADP}, respectively, and L is the distance between the swing HAA and foot. Finally, φ is the angle between L and gravity, and l is the pendulum length. Image reproduced from [60].

The MINDWALKER exoskeleton was tested on both healthy subjects and paraplegics, with large perturbations only applied to tests with healthy subjects. The authors report that the algorithm reacted with wider steps in response to large changes in XCoM position, effectively counteracting disturbances. Among users, some reported that the use of this algorithm made their walk more stable. However, the authors did not feel comfortable making a consistent conclusion regarding the effectiveness of this approach, citing limitations in accurate foot placement and XCoM estimation, as well as variability between user perception.

The need for an indicator of system stability in this context was something that Jung, Gutiérrez and Veneman [62] saw as valuable. They postulated that the Centroidal Momentum (CM), composed of the angular and linear momentum at the Center of Mass (CoM), could be used as a Stability Index to detect perturbations and losses of balance.

To examine how this CM would behave in scenarios of perturbed walking, Jung and Veneman tested it in a follow-up study [63]. Here, the CM real time computation was

tested in the context of a healthy subject walking in the LOPES II, a treadmill-based robotic gait training exoskeleton for lower limb rehabilitation developed by Twente University. Unexpected pelvic perturbations were applied during walking, and resulting changes in CM were investigated. The authors reported significant differences in the subject's CM behavior when comparing unperturbed and perturbed walking, which reinforces the potential for the use of CM to monitor the state of balance in the exoskeleton.

On the topic of developing balance controllers, it is a challenge shared also by the field of humanoid robot locomotion. In both of these fields, physical constraints such as torque limits or joint speeds have to be considered, and model stability is a shared goal. However, the field of humanoid robots has seen greater development in control technology, and model-based feedback controllers for dynamic and robust locomotion have had promising results [64–66]. This was something that Harib *et al.* [67] took note of, and sought to replicate. More specifically, they considered that, in order to achieve dynamic and hands-free exoskeleton mobility, a new framework of control design was needed. To this end, a system of virtual constraints was designed as an alternative to the pendulum models for limb coordination. This system was tested in an experimental environment, using the ATALANTE exoskeleton, a fully-actuated LLE intended for rehabilitation use. This exoskeleton, shown in Figure 3.2, includes twelve actuated joints, three inertial measurement units and force sensors to detect ground contact. Preliminary experimental results reported very slow but stable walking on the order of 0.1 m/s. Simulation results suggest than higher speeds can be achieved with current hardware, and the authors are optimistic regarding the prospect of extending their optimization methods to tackle other tasks beyond walking, such as transitioning from sitting to standing.

Human behavior is also a source of inspiration for designing balance controllers in the context of LLE. Humans naturally sense situations of imbalance, and reflexively re-position their body to restore a stable position when possible, in large part through adjustments to their joint angles. Building off of this, Baud, Fasola, Vouga *et al.* [68] decided to implement a balance controller based on strategies employed by healthy individuals. To this end, subjects were constrained in a passive exoskeleton, CAPTUR (Figure 3.3 (a)), which limited subjects' DoF to hip and knee flexion and extension. This forced subjects to employ compensatory movements, and the resulting strategies were then studied. Following these experiments, a strategy based on the knee joint angle's influence on the CoM position was developed. This strategy was tested first in a simulation environment, and then on the TWICE exoskeleton, shown in Figure 3.3, operated without a user through the balance controller. Results showed that the controller could maintain a standing position and resist CoM excursions of up to 50 mm to the back and 61 mm to the front, with minimal sensing (an Inertial Measurement Unit (IMU) in the trunk and the joint encoders). While this is promising, the authors are wary of unexpected behaviors between user and exoskeleton, and so they point to tests including users as a necessary next step.

Bayón, Emmens, Afschrift *et al.* [70] also set out to develop a human-like balance

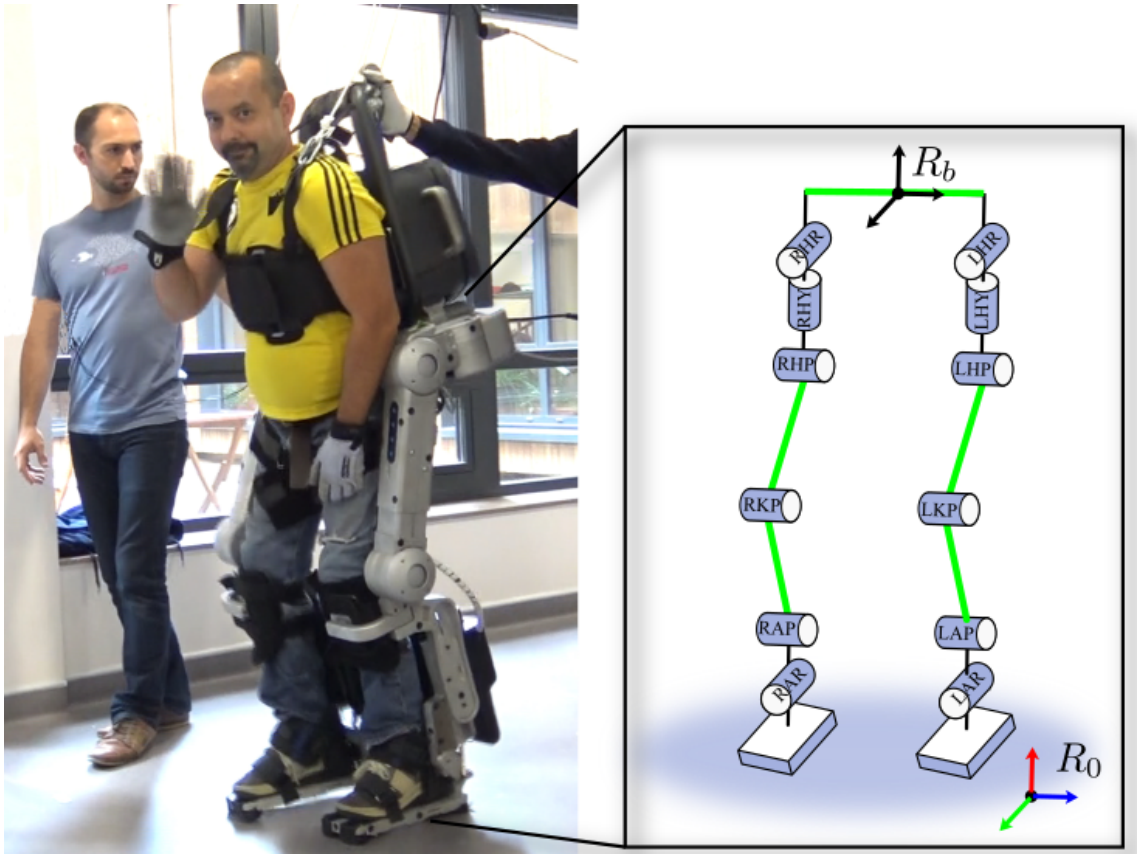

Figure 3.2: A diagram of the ATALANTE human-exoskeleton system. Each cylinder represents one of the actuated joints. Three joints control the spherical motion of each hip, and in each leg, a single joint actuates each knee, and two joints manage each ankle's rotation in the sagittal and frontal planes. The patient is secured to the exoskeleton by means of fasteners located at the ankle, the shin, the thigh, the abdomen, and the torso. The lengths of links highlighted in green are adjustable. Image reproduced from [67].

control strategy to be applied in the human-exoskeleton system. To this end, the application of Momentum Based Control (MBC) in the field of humanoid robots was taken into consideration. The MBC generates joint accelerations and contact wrenches to reach an intended whole-body momentum, one which corresponds to a balanced state. It was considered suitable for implementation due to its promising results balancing humanoids in standing experiments, and due to the nature of the approach, which could be extended to balance walking. The authors hypothesized that MBC would perform better at generating human-like responses to perturbations than Full State Feedback (FSF) laws, which generate joint angles and velocities based on the model's CoM position.

To investigate this, joint angle data was collected from experiments involving real subjects, focused on perturbing the standing position. Subjects stood on a moving platform, and were instructed to maintain balance as the platform moved backwards. Afterwards, the collected data was used to recreate these unbalanced scenarios in a simulation environment, using a three-link pendulum model. The simulation's joint torques were

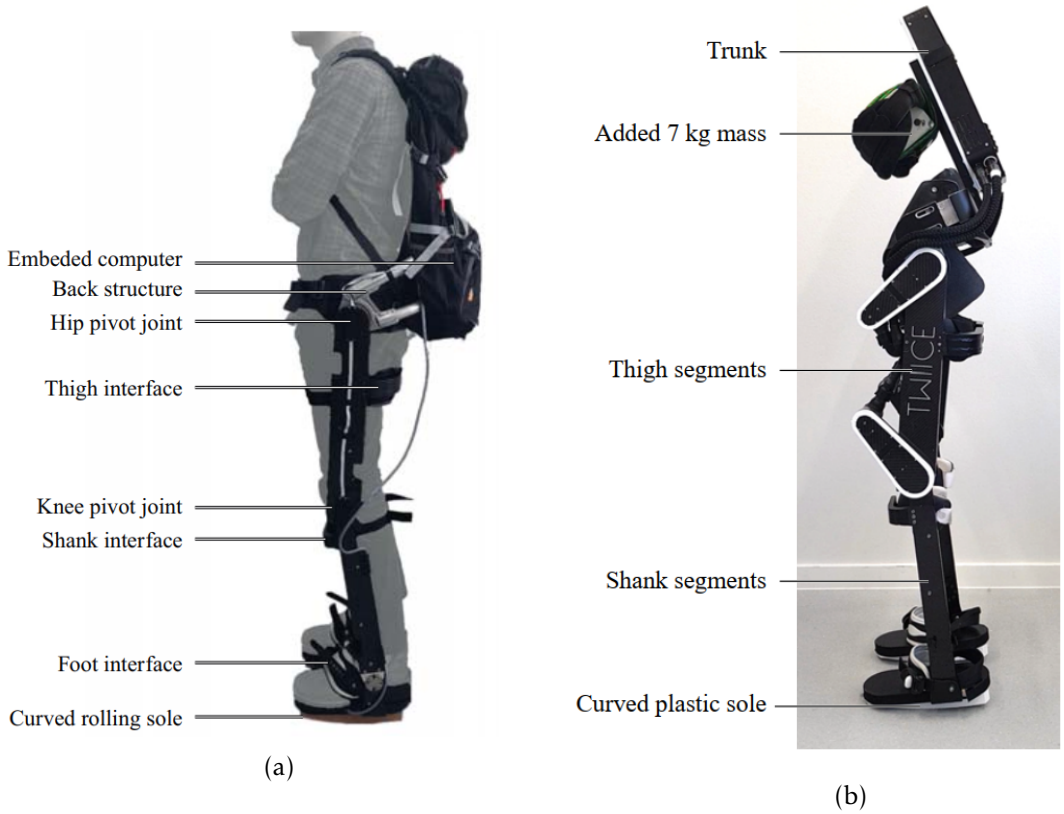

(a) (b)

Figure 3.3: (a) The passive exoskeleton, CAPTUR, was used to constrain ankle dorsiflexion and lateral legs' movement while standing. (b) TWICE 2016 standing, including an added 7 kg mass, to shift the exoskeleton's CoM forward. Images reproduced from [69] and [68], respectively.

generated using the MBC and FSF, and the respective performances were assessed. This optimization procedure is illustrated in Figure 3.4. Both controllers provided stable responses to perturbations, although often not human-like. More specifically, the MBC was not very effective in applying a hip strategy in situations where an ankle strategy is not sufficient. In the end, the authors conclude that is it not obvious whether the MBC is more suitable than the FSF in terms of performance.

3.2 Safe-fall Controllers in Exoskeletons

Despite the fact that the studies covered so far are obviously important steps in the direction of providing balance and postural stabilization for LLE, focus has not yet been on developing strategies to ensure the safety of the user against falling. Safety is a primary concern for both therapists and individuals with mobility impairments in relation to the possibility of a more general adoption of these technologies [20, 71].

This research gap was acknowledged and tackled by Khalili, Borisoff and Loos [72], who set out to develop a control strategy to improve user safety in the event of a human-exoskeleton backwards fall. The backwards fall was chosen due to its association with

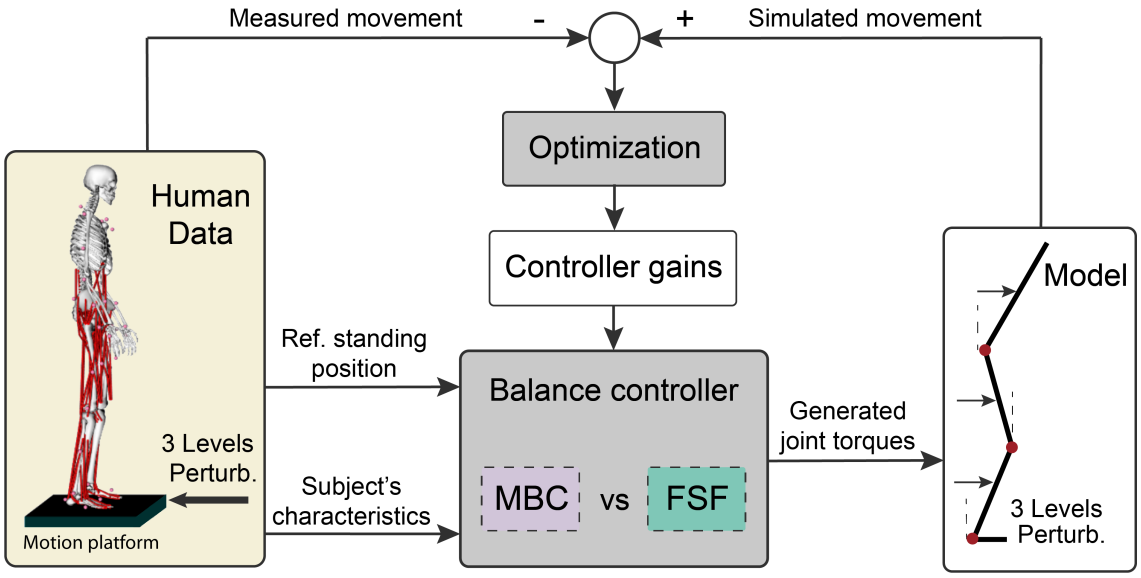

Figure 3.4: Optimization procedure for the MBC and FSF to fit human balance responses. Image reproduced from [70].

risk of head impact, as well as its high prevalence among healthy individuals. A three-link model of an inverted pendulum was created to present the dynamics of the fall (Figure 3.5 (a)).

Among other assumptions, the authors assumed that the falls were symmetrical and studied in the sagittal plane, and that both feet remained in contact with the ground throughout. The model's equations of motion were then derived and used to simulate the falls, with the established main goals of avoiding head impact and minimizing hip impact velocity, both of which were correlated with the values of the angular velocity of the trunk and hip, respectively. Additionally, the characteristics of a hypothetical exoskeleton were added, including mass, center of mass, length of each segment, mass moment of inertia, and actuators' specifications. For this model, it was assumed that the actuators would govern the kinematic and dynamic characteristics of the knee and hip joints during the fall.

The resulting optimal fall strategies were similar between the models (one example is shown Figure 3.5 (b)). A squat motion was performed, followed by an extension of the knee joint at the last stage of the fall, whilst keeping the trunk upright. The quick squat motion led to a rapid reduction of existing potential energy that otherwise would have been converted to kinetic energy at the moment of impact. The knee extension led to the conversion of vertical kinetic energy to horizontal kinetic energy (parallel to the ground).

A follow-up study by the same authors extended the application of these optimization techniques to study different fall scenarios, within a range of different fall duration values and coefficients of friction, with the goal of simulating more realistic fall conditions [73]. In regards to fall duration, it was observed that there exists an optimal fall duration for specific optimization conditions, which the authors postulate could prove to be useful in

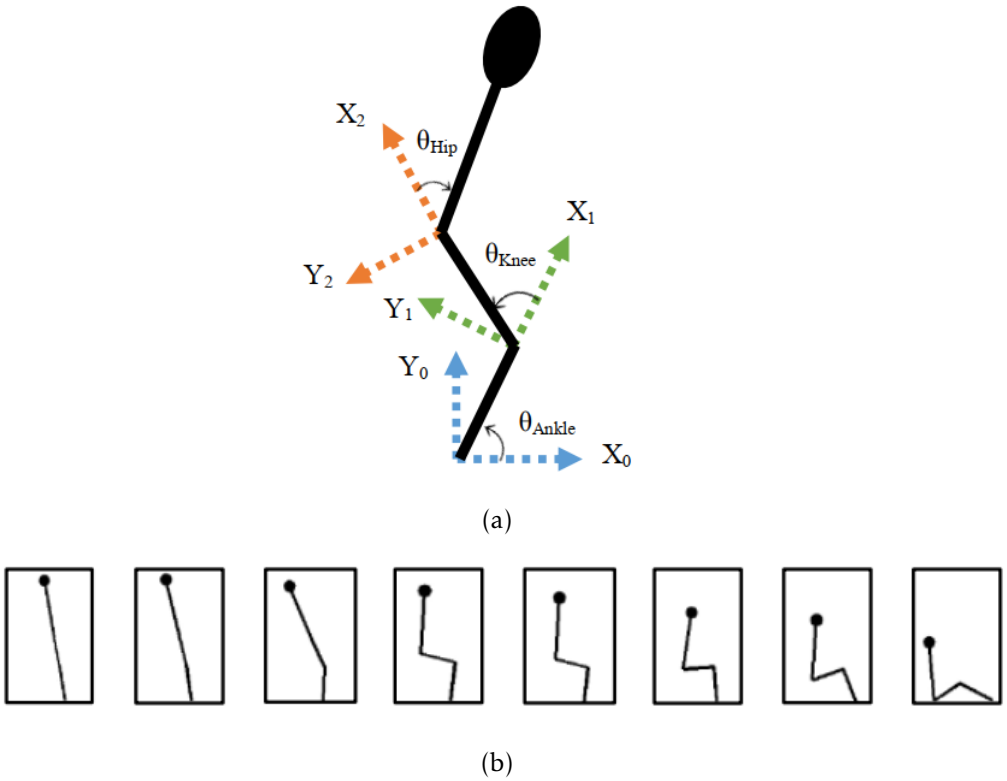

(a)

(b)

Figure 3.5: (a) Three-link model created to represent the dynamics of a human and human-exoskeleton fall. (b) Representations of the human-exoskeleton model's position at specific instants in throughout the fall (0.00, 0.10, 0.20, 0.30, 0.40, 0.50, 0.60, 0.74 sec) while optimal torques were applied at the joints. Images reproduced from [72].

determining control mode transitions, for performance optimization. As for coefficients of friction, predictably it was shown that the severity of fall is higher on slipperier floors.

Despite dealing mostly with simulation, these studies show promising results for the implementation of safe fall strategies in the context of LLE, and their impact on ensuring users' safety. However, for a better human-exoskeleton interaction, it would be desirable to investigate human-like safe-fall strategies. In that sense, the next section details some results associated with research in human falls.

3.3 Safe Falls in Healthy Individuals

In healthy individuals, landing strategies to reduce the impact severity of falls have been considerably investigated, including the specific influence of factors like location of impact, direction of falling, and magnitude of loads applied to the body [21]. For the purposes of this review, the focus will be on research dealing with backward falls, for as stated before, in these falls the use of the upper limbs is less important in ensuring safety, and also the development of a safe fall strategy for backward falls can be useful in the future when designing for sideways falls.

At the turn of the century, Robinovitch *et al.* [74] set out to identify which factors separate injurious falls from non injurious falls, for the purposes of developing exercise-based therapies that would enhance safe-landing abilities. More specifically, the authors postulated that impact severity would increase with increases to both vertical descent distance and distance from the center-of-gravity to the ankles during backward descents.

This was tested through self-initiated backwards descents from standing to pelvis impact at either knee (SIT) or ground (FALL) level, and at a horizontal distance from the ankles of either 33% or 66% of lower extremity length (Figure 3.6). The subjects' body segments' 3D position were measured through a 6-camera motion analysis system, and reaction forces were acquired through the use of a force platform.

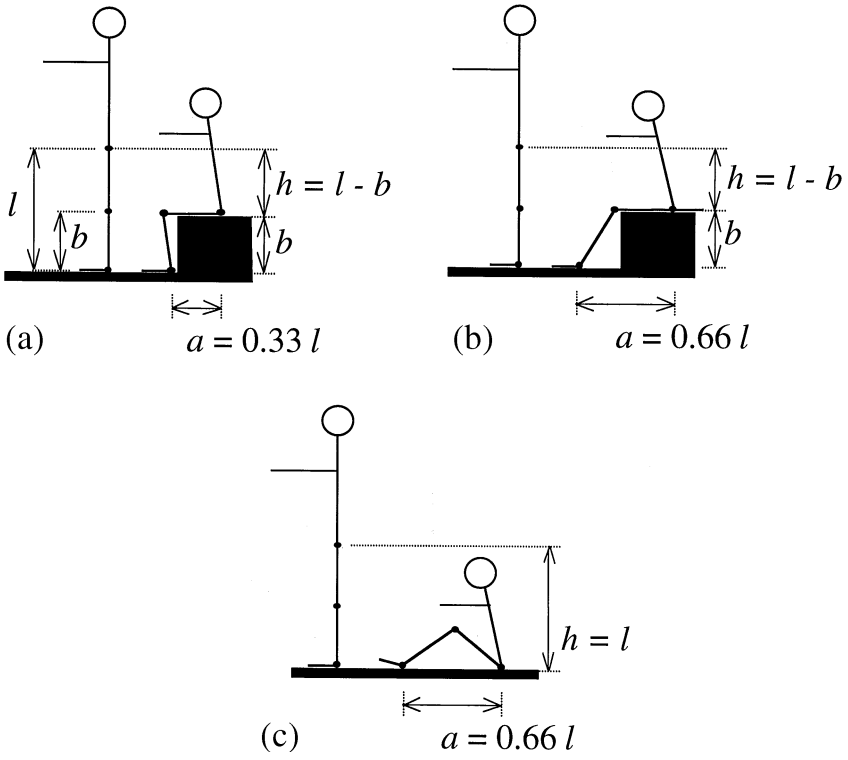

Figure 3.6: Schematic of (a) 33% SIT trials; (b) 66% SIT trials; and (c) 66% FALL trials. Image reproduced from [74].

The results showed that subjects generated eccentric extensor torques at the hip and knees to decrease downward acceleration, with substantially reduced impact velocities and kinetic energy throughout descents. The authors conclude that sitting movements represent reasonable models of backwards falling.

With this in mind, Sandler and Robinovitch [75] set out to examine the theoretical effect on fall severity that lower extremity muscle contractions have during backward descents. This study was restricted to two-dimensional models of backward falls. The complex, out-of-plane motions present in sideways falls excluded them from study, and forward falls often involve impact to the hands and not the pelvis [37, 44, 76]. A one-link, two-link and three-link inverted pendulum models of backward falls from standing

height were developed, which assumed movement strictly in the sagittal plane and stationary feet position in contact with the ground (Figure 3.7).

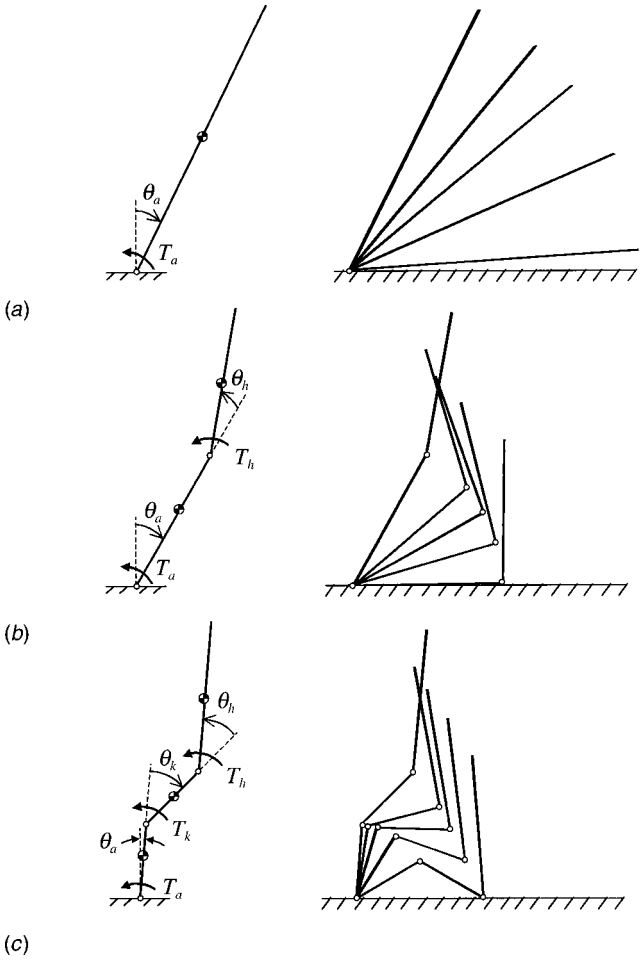

Figure 3.7: Descent kinematics associated with: (a) one-link model, (b) two-link model, and (c) three-link model (T_a = ankle torque; T_k = knee torque; T_h = hip torque; θ_a = ankle rotation; θ_k = knee rotation; θ_k = hip rotation). Image reproduced from [75].

The one-link model served to simulate a fall where the knees and hips remained extended throughout descent, while rotation and energy absorption occurred at the ankles. The two-link model simulated a fall where the knees are extended, with rotation and energy absorption occurring at the ankles and hips. The three-link model simulated a fall where rotation and energy absorption occurred in all three joints. Each of these models was simulated to release from an initial configuration where the center-of-gravity was posterior to the ankle joint. Each simulation proceeded until impact, which was signified by the vertical position of the pelvis dropping below the ankles.

For analysis, impact severity was represented by the vertical components of both the model's kinetic energy, as well as the velocity of the pelvis at the instant of contact. The descent of the one-link model with zero ankle torque applied to it was used as a source of comparison as a worst-case scenario.

Results showed that torque generation at each joint influenced fall severity, but also

that "technique" is at least as important as strength, as considerable decrements in kinetic energy were achieved with small peak joint torques. The authors suggest that "relaxed" falls (when properly executed) should minimize risk when compared to rigid falls with minimal joint flexion.

A key limitation present in the previous studies is their use of exclusively self-initiated falls, while most falls are caused by sudden losses of balance or stability. To address this, Robinovitch, Brumer and Maurer [39] set out to test the previously studied squat response during a backwards fall caused by sudden loss of balance. A falling experiment took place, where subjects were positioned resting on a wooden block on top of a force platform, and fell backwards onto a gymnastic mat (represented in Figure 3.8). Foot contact forces and three-dimensional positions were measured across five series of falling trials. Subjects voluntarily initiated their descent from a standing position in two of these trials: one while utilizing squatting and one while inhibiting squatting throughout the descent. In the remaining three trials, the fall was initiated by the sudden release of the subject through a tether and electromagnet. These trials served to simulate a fall due to a sudden loss of balance. Across these series the initial lean angles was manipulated by adjusting the length of the tether, to control the stage during the descent when the squat response was initiated. The three initial lean angles which were tested were 2°, 5° and 12°.

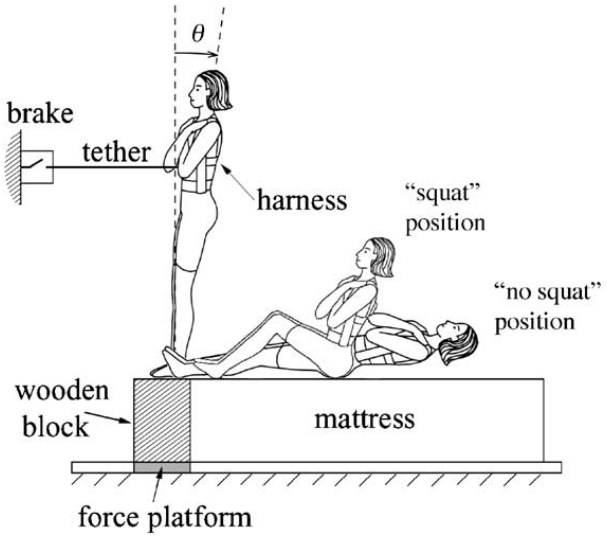

Figure 3.8: Representation of the tether-release falling experiment, where θ represents the lean angle at release. Image reproduced from [39].

Results spoke to the effect that the squat response can have on injury risk during falls. Comparing falls when the squat response was utilized as opposed to inhibited with an initial lean angle of 5°, the average magnitudes of impact energy were 43% lower, and the average magnitudes of impact velocity was 18% lower. However, increases in this initial lean angle did lead to a reduction in joint energy absorption and an increase in impact energy, which suggests that the protective quality of the squat response is dependent on how quickly one can initiate the response. Additionally, when comparing these results

with the self-initiated falls results, it is evident that the squat response was less effective in reducing impact velocity for falls caused by sudden losses of balance.

One notable aspect of the squat response employed was the influence of the trunk position during descent. Subjects tended to maintain the trunk in a forwardly flexed position throughout the descent, impacting the ground with the trunk in an almost vertical position. The authors consider this beneficial for a few reasons, including the fact that impacting the ground with the trunk upright allows for avoiding head impact, and reduces how far the center of gravity moves away from the ankles horizontally.

3.4 Conclusion on literature review

The field of Lower Limb Exoskeletons (LLE) has seen promising progress in the development of balance controllers. Stable gaits have been reported, and, thanks to improvements to device technology, hands-free walking for exoskeleton systems is starting to become a reality. However, one key limitation frequently mentioned is unexpected behaviors and perturbations. Perturbation detection is rarely considered, and the controller strategies that are being developed are relatively untested and unrefined. To add to this, there is a noted research gap pertaining to strategies to maximize safety in the event of falls caused by large imbalance or external perturbations. Strategies based on healthy human safe fall options have seen validation in their own field, and there have been signs of their potential to be replicated in the context of LLE. This makes them a prime candidate for adaptation and integration through balance controller technology. It is in this context that this work was developed. The goal was then to develop and implement a safe fall strategy for a human-exoskeleton system, for backwards falls.

In the following chapter, the concept of the controller is detailed, and the design of the strategy is described. Adapting the reference strategy to the system's height at the time of fall detection is also covered, as well as the process of testing and evaluation in the simulation environment.

Chapter 4

Methods

4.1 Purpose of the controller

The main objective of this thesis is to develop a controller for exoskeletons to execute a strategy for maximizing safety, upon the detection of an imminent and unpreventable backwards fall. The controller was not designed to prevent falls by counteracting unbalances, nor to detect the falls themselves. It was conceptualized to be one part of a larger control system, already capable of detecting situations of unbalance reliably, where correction strategies are no longer viable, and a fall is inevitable. This system is not yet developed, but the assumption of its existence in the near future and its functionality was based on the existing research focused on sensor based fall detection or gait instability detection. Some examples that showed promising results in identifying situations of instability in healthy humans, take into account individuals' Center of Mass (CoM) and/or Center of Pressure (CoP) [77–79], or just accelerometer and gyroscope data [80]. Given the fact that most exoskeletons already have access to accelerometer and gyroscope data, and estimate their system's CoM and CoP, it is not a stretch to assume that similar developments in fall detection or imbalanced gait detection can be made in the field of Lower Limb Exoskeletons (LLE).

In this work, the developed strategy and the simulation environment both operate in the sagittal plane, as is was assumed that body movements were primarily made in this plane. Moreover, for a backwards fall, movements were assumed to be symmetric for both legs in the sagittal plane. Assumptions of this nature were commonly made in previous research involving backward falls [39, 72, 74]. At this point, the nomenclature for this chapter should be defined. $\mathcal{M}_{xy}$ is the CoM for the system or segment in question. $\mathcal{M}_x$ and $\mathcal{M}_y$ are $\mathcal{M}_{xy}$'s horizontal and vertical component, respectively. Later, θ_{hip} is used to refer to the model's hip angle, in degrees. Positive values are associated with this

joint's extension, and negative values are associated with its flexion.

A three-link model of an inverted pendulum was used, with one added two-link attached at shoulder height, to represent the mass and inertia of an upper limb. The controller did not have access to this upper limb, just as the exoskeleton does not control the user's upper limbs. A human of 1.76 m of height and 58 kg of body mass was considered for the model. The individual segments' masses, lengths, inertias and CoM location in respect to the joints were then derived from the mass and height, through approximation, as described by Winter in [81] (see Figure 4.1).

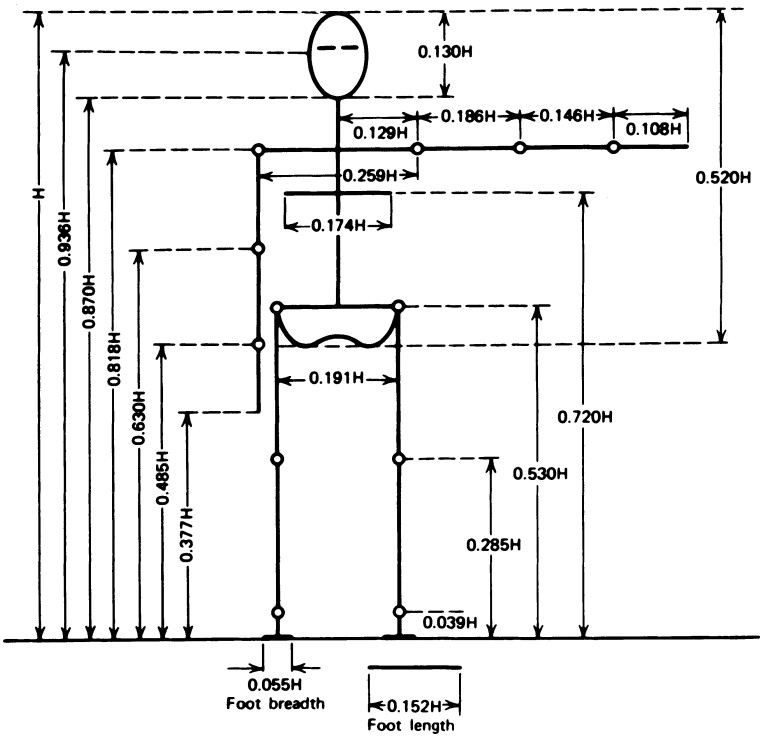

Figure 4.1: Body segment lengths expressed as a fraction of body height H, as described by Winter. Image reproduced from [81].

On top of this, to accurately represent the human-exoskeleton system, specifications associated with the Symbitron+ wearable exoskeleton WE2 (represented in Figure 4.2) were added. These included the masses, and the coordinates for the CoM, $\mathcal{M}_{xy}$, and inertias for each segment. Table 4.1 contains these values. For the $\mathcal{M}_{xy}$ values shown, they are presented in relation to each segments' respective lower joint. This means that the shanks' coordinates are expressed in relation to the ankle joints' position, the thighs' coordinates are in relation to the knee joint, and the trunk's coordinates are in relation to the hip joint. The exoskeleton includes three modules, for the hip, knee and ankle joints. These govern six degrees of freedom: hip endo/exorotation, abduction/adduction and flexion/extension, knee flexion/extension, ankle inversion/eversion and dorsiflexion/plantarflexion.

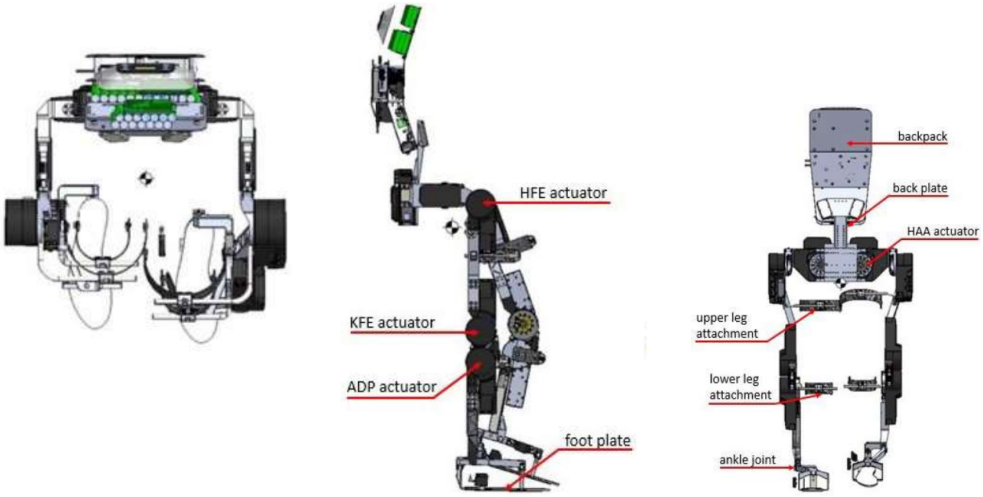

(a) Top View (b) Lateral View (c) Frontal View

Figure 4.2: Design features of the WE2 exoskeleton. The design includes hip, knee and ankle module, which govern 6 degrees of freedom: hip endo/exorotation, abduction/adduction and flexion/extension (HFE), knee flexion/extension (KFE), ankle inversion/eversion and dorsiflexion/plantarflexion (ADP).

The process of execution for the controller's strategy is represented in the block diagram shown in Figure 4.3. This model was simulated in a 2D space (considering the sagittal plane), and changes to its segments' positions and velocities were described through the use of Forward Dynamics (FD), in accordance to the applied torques and segments' weight. In a similar fashion as reported in [72], several assumptions were made for these simulations:

- Both feet remain in contact with the ground throughout the fall.
- Available torques at the joints could be applied instantaneously with no time delay.

Segment	Mass (kg)	Center of Mass (m)	Moment of Inertia (kg*m^2)
Shanks	6.5477	$\mathcal{M}_x$ = 0.0062 $\mathcal{M}_y$ = 0.3216	0.7542
Thighs	7.7400	$\mathcal{M}_x$ = 0.0098 $\mathcal{M}_y$ = 0.2201	0.6065
Trunk	18.098	$\mathcal{M}_x$ = -0.1823 $\mathcal{M}_y$ = 0.1981	2.5743

Table 4.1: Coordinates for the CoM and inertias for each part of the WE2. For each segment, the $\mathcal{M}_{xy}$ coordinates are expressed in relation to their respective lower joint. The shank coordinates are thus in respect to the ankle joint, the thigh coordinates in respect to the knee joint, and the trunk coordinates are in respect to the hip joint. The values for the moment of inertia are associated with both legs of the exoskeleton, as in this work they are assumed to move together in the sagittal plane.

- The hip is considered the only contact point to the ground at impact.

- The bilateral segments (both legs and arms) move together in the sagittal plane.

Throughout the simulation, the model's $\mathcal{M}_{xy}$ was estimated using the FD's resulting positional and inertial data. This was done to replicate how the actual exoskeleton would assess the human-exoskeleton system's state and estimate its $\mathcal{M}_{xy}$ in real-time. For this same reason, this $\mathcal{M}_{xy}$ value was used by the controller throughout the fall to execute the strategy.

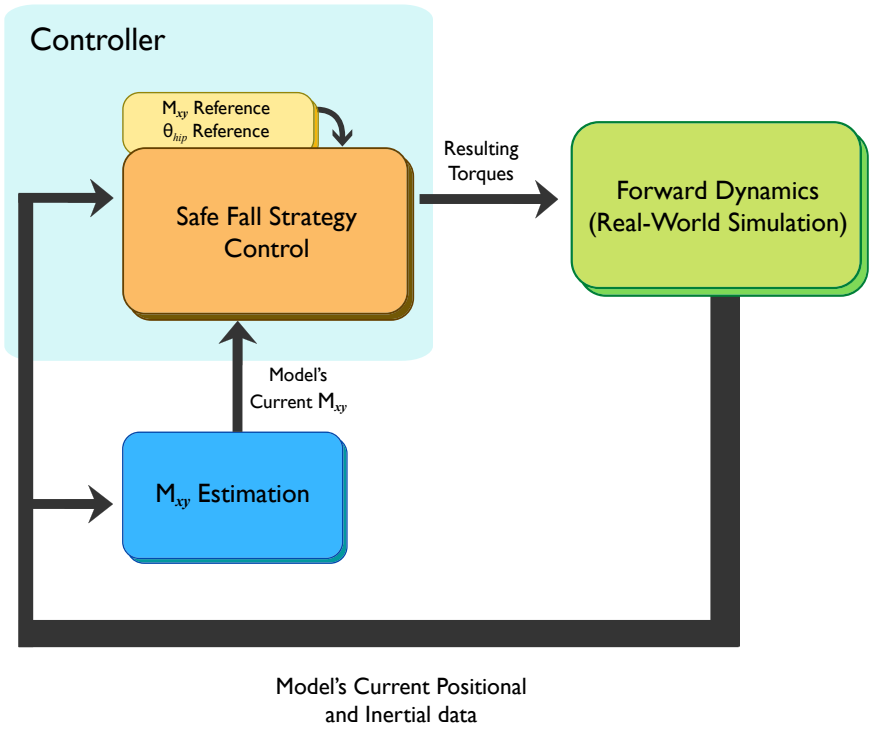

Figure 4.3: Overview of the process of execution for the controller's safe fall strategy. Throughout the simulation, the human-exoskeleton system's positional and inertial data is collected and used to estimate its $\mathcal{M}_{xy}$. This includes joint angles, model data (segment masses and inertias), and joint damping. Next, the safe fall controller uses this data to estimate the necessary torques for the system to execute the strategy.

Lastly, the safe fall strategy controller generated the appropriate torques, using the FD's positional and inertial data, the estimated current $\mathcal{M}_{xy}$ and θ_{hip}, and their respective references.

4.2 Reference trajectory for the Center of Mass

The safe fall controller was designed to emulate the squat protective response presented in the previous chapter [39, 75]. As mentioned before, this strategy was tested in healthy individuals with promising results in reducing the risk of injury in backward falls.

For the controller to execute a strategy similar to this one, the first step was to choose some type of reference that would translate well into the desired squat protective response. Throughout this process of deliberation, references which would be able to be followed using relatively low computational power were better valued. Specifically, the goal was to be able to execute the strategy through the use of Proportional Derivative (PD) controllers for joint actuation. In the case of the fall strategy explored in [72], using optimization methodology, the resulting joint kinematic data was considerably non linear in character, and pointed to a need for intricate coordination between joints, in order to maximize user safety. The presence of strong non-linearities in particular is something that PD controllers have difficulties handling [82–84]. This discouraged the use of torque or joint angle profiles for each joint as reference, as these would often be rapid-changing. Preliminary testing using these type of references was also shown to cause very unstable behavior in the model, presumably for this reason. Focus was then turned to adapting a squat response through a $\mathcal{M}_{xy}$ reference for the model to follow.

Since there was no $\mathcal{M}_{xy}$ reference present in the literature, it was decided that the best way to build a strategy was to recreate key model positions that were apart of a squat protective response, get the corresponding $\mathcal{M}_{xy}$ values in the simulation environment, and through regression obtain a continuous $\mathcal{M}_{xy}$ reference for the model. Joint torques would then be produced through a PD controller, taking into account differences between the reference $\mathcal{M}_{xy}$ and the actual $\mathcal{M}_{xy}$ values, as well as the system's current jacobian values.

Analyzing the diagrams for the human-exoskeleton position reported in [72] (shown in Figure 4.4 (a)), three notable poses were chosen to be replicated (see Figure 4.4 (b)): the initial standing position, in which both the knee and the hip joint are nearly fully extended (0.00 sec); the squat position, where the $\mathcal{M}_{xy}$ position is vertically lowered, and horizontally there has been relatively little translation (0.50 sec); and the final position now after an extension of the knee joint (0.74 sec). These three positions were recreated in the simulation environment through experimentation, setting joint angle values for the model.

Based on these key positions, the corresponding $\mathcal{M}_{xy}$ kinematic data was then collected and used as following: first, the $\mathcal{M}_{xy}$'s vertical component was normalized in relation to its value for the standing position (for simplicity, from now on $\mathcal{M}_y$ will refer to the normalized value). By doing this, the strategy was not dependent with the subject's height. Second, a temporal relation was established between this $\mathcal{M}_y$ and the $\mathcal{M}_{xy}$'s horizontal component ($\mathcal{M}_x$). This was used to set a representative fall duration, and also an appropriate time interval between the standing position and the squat position. The

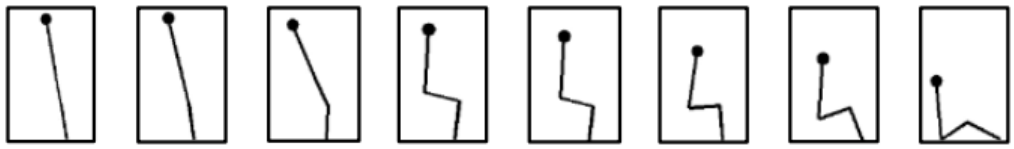

(a)

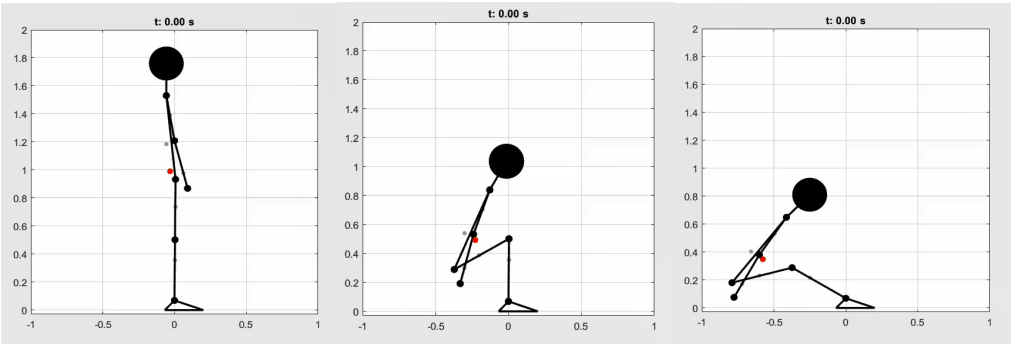

(b)

Figure 4.4: (a) Diagrams of human-exoskeleton model position at specific instants in the fall (0.00, 0.10, 0.20, 0.30, 0.40, 0.50, 0.60, 0.74 sec) while optimal torques are applied at the joints. Reproduced from [72]. (b) Representations of the three positions used to create the $\mathcal{M}_{xy}$ reference for the model.

time chosen for the fall duration was based on the work done by Choi, Wakeling and Robinovitch [85], where kinematic analysis was collected from real-life falls experienced by older adults in long-term care facilities. Based on this study, an average duration of 1271 ms was reported. This value was used as the duration for the squat response reference. The interval of time for the squat was not reported in [72], which left only room for gross estimation based on the shown diagrams. The value decided on was 0.20 ms.

During testing, it became clear that using a relation obtained only through the three reference positions' $\mathcal{M}_{xy}$ values resulted in a very sudden change in the $\mathcal{M}_x$ reference, especially in the beginning of the fall. To counteract this issue and ensure that $\mathcal{M}_x$ reference would not change considerably before the model would complete the squat motion, a fourth $\mathcal{M}_{xy}$ reference was added exclusively to maintain this relation between $\mathcal{M}_x$ and $\mathcal{M}_y$. This reference point shares the $\mathcal{M}_x$ value with the starting position, and has a (normalized) $\mathcal{M}_y$ value of 0.8.

With these positions and a fall duration value as reference, a template for the general safe fall strategy was made. The next step now was to enable finer tuning of the strategy, both with respect to the projected duration of the safe fall, as well as to the rate of horizontal translation in relation to vertical translation. To this end, two parameters were included, to be multiplied to both $\mathcal{M}_y$ and $\mathcal{M}_x$ reference values. The first of which, which will be referred to from now on as ySlope, adjusts how fast the reference $\mathcal{M}_y$ value changes, and consequently how long the fall takes. The latter, to be referred to as xSlope, adjusts the rate of horizontal translation in relation to the current $\mathcal{M}_y$ reference value.

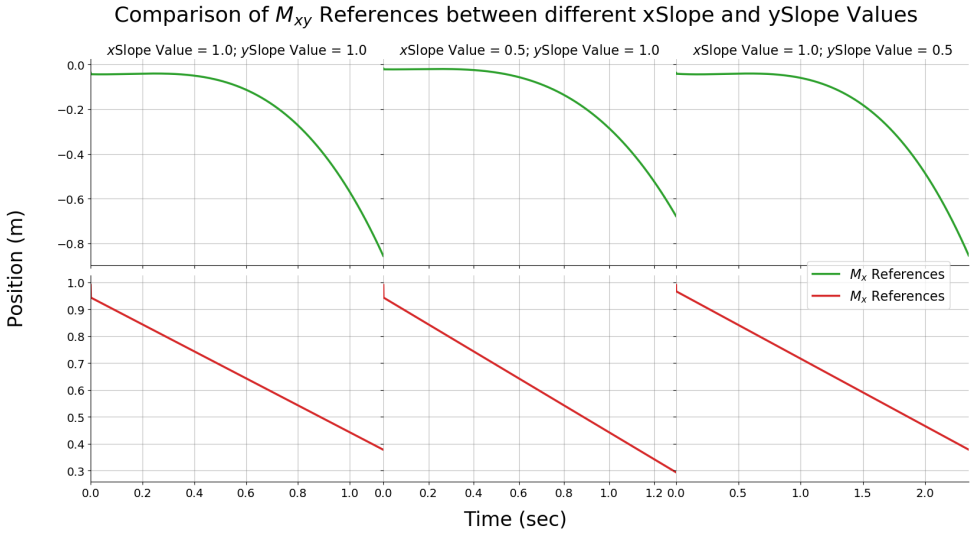

Figure 4.5: An example of different resulting $\mathcal{M}_x$ and $\mathcal{M}_y$ references for different combinations of xSlope and ySlope values. For $\mathcal{M}_x$, the positive direction refers to forward motion, and the negative direction to backwards motion. For $\mathcal{M}_y$, the positive direction refers to upwards motion, and the negative direction to downwards motion. Fall duration increased with larger values for both xSlope in (b), and ySlope in (c).

Figure 4.5 illustrates how these parameters had an effect on the $\mathcal{M}_{xy}$ references provided to the model. In testing, a range of values were used throughout the simulations, to ensure a degree of flexibility within these relations (more on this in Section 4.8).

4.2.1 Adapting the Center of Mass Reference

Having obtained a $\mathcal{M}_{xy}$ reference for a squat response strategy, the next question was: how can this strategy be adapted to the initial position of the model at the time of the fall detection? After all, it would be highly ineffective for the controller to, upon the detection of a fall, output a $\mathcal{M}_{xy}$ reference associated with a standing position if the subject is already in a lower position, for example. As such, to ensure a good execution of the strategy in a wide range of fall scenarios, the controller had to accommodate the $\mathcal{M}_{xy}$ reference to the subject's current $\mathcal{M}_{xy}$ at the fall onset.

This accommodation was accomplished as follows: when a fall is detected, the controller checks what the current $\mathcal{M}_y$ for the model and obtains a corresponding time through the $\mathcal{M}_y$ vs fall time reference signal. This time value is then used to obtain the corresponding reference $\mathcal{M}_y$ and $\mathcal{M}_x$ values. Having done this, the model proceeds to execute the strategy as starting from that $\mathcal{M}_{xy}$ position in the reference, and not from the value associated with the initial position. In other words, the model "skips ahead" of its reference in accordance to its' $\mathcal{M}_y$ value.

4.3 Hip Actuation

When testing the CoM-based strategy in simulations, an unexpected behavior was observed: despite the fact that the references were being followed fairly well by the model, they was not ensuring a good trunk flexion when squatting. Instead, the model followed the reference $\mathcal{M}_{xy}$ values by moving the trunk backwards through application of an extension torque. This resulted in a very unsafe fall strategy for the model as it did not protect the head of the user, and in fact had the opposite effect than the one intended for the squat safe strategy. There was therefore a need to further ensure that the trunk was safely kept flexed throughout the fall.

To address this issue, it was decided that the hip joint would not be actuated through the outputs resulting from the provided $\mathcal{M}_{xy}$ reference. Instead, this joint would be actuated through a controller based on an angle reference for hip flexion/extension. From this point on, for simplicity, this hip joint angle will be referred to as θ_{hip}. It is also worth reminding that the flexion was the negative direction for the joint motion, and the extension the positive direction. In other words, a larger θ_{hip} value corresponds to an extended hip joint, which in turn means the model's trunk is leaned backwards, and vice-versa.

This θ_{hip} reference was made dependent on the current $\mathcal{M}_y$ value. More specifically, the current $\mathcal{M}_y$ value is the base of a power that is then saturated in such a way that the maximum and minimum values that the reference θ_{hip} can take are 0 and -130 degrees, respectively. As previously mentioned, this was done to ensure that the trunk is prevented from extending during the fall.

The resulting θ_{hip} reference is used to produce the model's hip joint torque through a second PD controller. The final three described references are presented in Figure 4.6.

4.4 Center of Mass and Hip Angle Reference Tracking

After designing the references, the next step was to track the model's performance in following these references throughout the simulation. To this end, the $\mathcal{M}_{xy}$ and θ_{hip} references were compared with the model's values at each timestep (every 0.001 seconds), and a "penalty scoring system" was created to grade the model's performance. A score of 0 would mean a perfect tracking and worse tracking performances resulted in larger scores.

In the case of θ_{hip}, a difference of 5 degrees or less was deemed acceptable, and in these instances the score was not increased. A difference between 5 and 20 degrees would lead to an increase of the score by 1 point. A difference between 20 and 60 degrees would yield an increase of 2 points, and for more than 60 degrees the score would increase 3 points. At the end of the fall, a final normalized score was produced by dividing the resulting by the worst possible score, of 3 points per timestep.

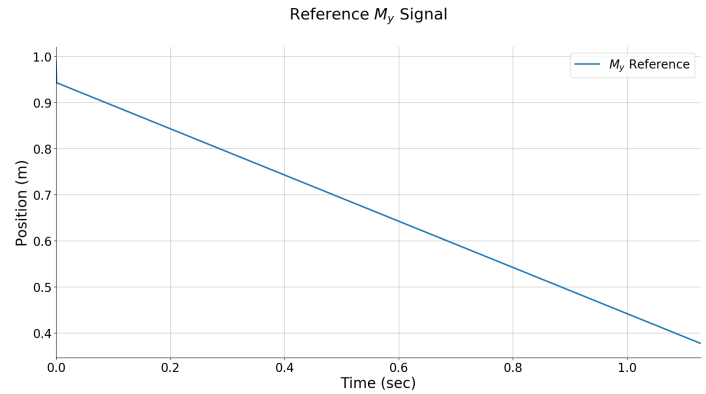

(a)

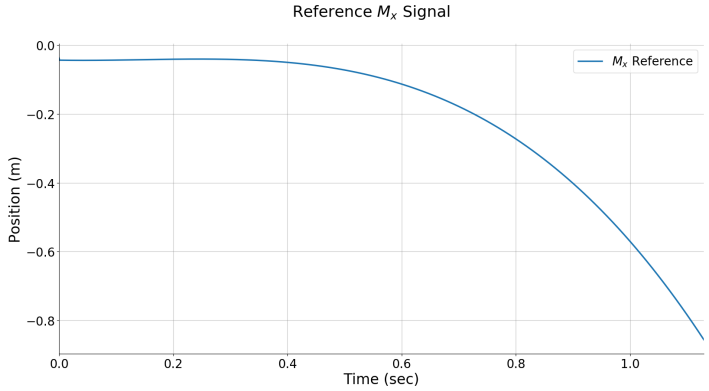

(b)

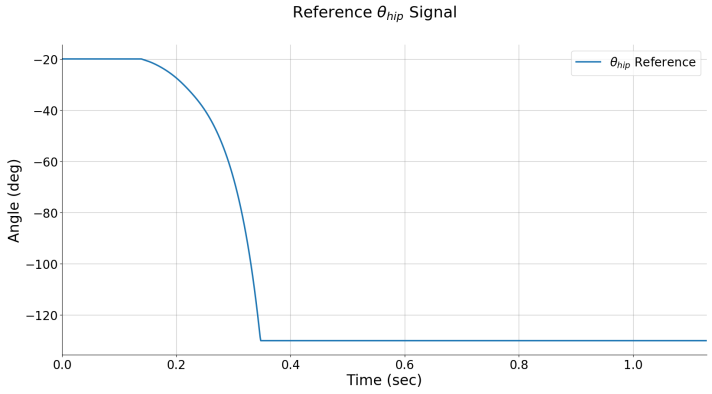

(c)

Figure 4.6: Reference signals for (a) $\mathcal{M}_y$ position, (b) $\mathcal{M}_x$ position, and (c) θ_{hip}, used to execute the squat response strategy. The initial $\mathcal{M}_y$ reference value is dependent on the model's $\mathcal{M}_y$ value at the beginning of the fall, which in turn affects the initial $\mathcal{M}_x$ reference value. In a similar fashion, the initial θ_{hip} reference value is adapted to the model's initial θ_{hip} value.

When it came to $\mathcal{M}_{xy}$, both $\mathcal{M}_x$ and $\mathcal{M}_y$ were compared to their respective references separately, and only one threshold was chosen. When $\mathcal{M}_x$ or $\mathcal{M}_y$ were off from their respective reference by 0.1 m or more, their respective score would increase by 0.1 points. Any difference lower than 0.1 m would yield an increase equal to the difference itself. Once again, at the end of the fall, these sums were divided by a "worst-case scenario" score (0.1 points for every simulation timestep, or 0.001 seconds), and averaged to produce one final score value.

4.5 Integral Joint Torques

Besides measuring the model's ability to closely follow its references, it was also deemed important to get a sense of how demanding the strategy's execution was for the system. The main concern was ensuring that the angles would not prove too fast-changing for the system, and not cause the system to spend most of the simulation exerting maximum torques (simulations of this nature were reported during development and testing). If this was shown to be the case, then it could be a sign that the strategy was too unreliable, from a stability point-of-view, for the system's limitations. As such, to verify this, the torques for each joint were collected at every instant throughout the simulation, and divided by the maximum torque value that each joint motor could provide (220 Nm for the hip and ankle joints, and 165 Nm for the knee joints). In this way, for each joint, the final value was between 0 and 1. The average value for all three joint values was then computed and passed to the cost function. In this way, the final value acted as an indicator of how much relative torque (taking into account all three joints) was necessary to perform the strategy.

4.6 Studying Fall Safety

Along with the references for the model to follow, it was necessary to evaluate the strategy in its ability generate safe backwards falls for the human-exoskeleton system. To this end, and based on previous research involving safe backwards falls [72], it was decided that the two goals for the strategy were to minimize hip vertical impact velocity and avoid head impact. In the case of the hip vertical impact velocity, this was able to be directly tracked within the simulation environment. For the head impact avoidance, it was assumed that the possibility of head impact was correlated with the angular velocity of the trunk, meaning the angular velocity for the hip joint. As such, the maximum value for the hip angular velocity reached throughout the fall was tracked, and used as an indicator of the trunk's stability. A lower maximum was considered to be synonymous with a smoother fall. These two criteria were both included during the performance score tracking (detailed next in Section 4.7), but only the hip impact velocity was chosen for separate analysis. This was due to the lack of a reference value for the maximum hip angular velocity, which discouraged qualifying the resulting values separately as associated with unsafe or safe falls. For the hip impact velocity, the chosen reference

value for a "worst-case" fall was 3.22 m/s, as reported by Sandler and Robinovitch in [75]. In their work, the authors used a one-link model to represent a "worst-case fall" source of comparison, and measured vertical (downward) velocity of the pelvis at the instant of contact. The fall was simulated by releasing the one-link model from a configuration involving 27 degrees of plantar-flexion at the ankles. Now, it should be noted that this value did not serve as an exact measure for judging what a worst-case fall would translate to for our developed model. For one, the model developed in [75] was representative of a subject of height 1.6 m and body mass 53.7 kg, while our model was simulated with a height of 1.76 m and body mass 58 kg. Nevertheless, given the lack of a reference for a worst-case fall applied to the context of our model, this value allowed for a preliminary qualitative analysis of the reported vertical impact velocities.

4.7 Performance Tracking

Lastly, the goal of this work was both to have the model execute the proposed strategy, but also have that strategy show good results in maximizing user safety. Thus, more than tracking these two aspects separately, it was necessary to track something that would represent how the model performed in both aspects simultaneously.

To this end, a performance score function was developed to quantify both of these aspects during the simulations. Figure 4.7 shows an illustrative diagram for how the performance score is calculated. This score took into account the hip linear vertical velocity at the moment of impact with the ground, the maximum value for the hip angular velocity reached throughout the fall, the integral torque for all three joints, and finally the $\mathcal{M}_{xy}$ and θ_{hip} tracking scores. The performance function included weight factors for each of these elements. The final values used for the weight factors were chosen through experimentation, to ensure that the final value was representative of all of its criteria. Following in line with each of its elements, the performance score value is lower for falls where both strategy execution and safety are found to be better, and vice-versa. Scores were collected for each simulation performed with the assumption that, if the performance score values were to behave similarly than the $\mathcal{M}_{xy}$ and θ_{hip} scores, then that would mean that the hip impact velocity and maximum hip angular velocity values were low, and associated with safe falls. This, in turn, would point to the conclusion that the designed strategy results in safer falls.

4.8 Testing Protocol

Seven initial positions of the model were considered to test the controller in simulation, each representing unbalanced states that will lead to a fall. MATLAB's Simulink was used to setup to execute the simulations. Simulink is a block diagram environment, which supports a simulation engine with fixed-step and variable-step Ordinary Differential Equation (ODE) solvers. In this work, a fixed-step solver was used, with a step size of

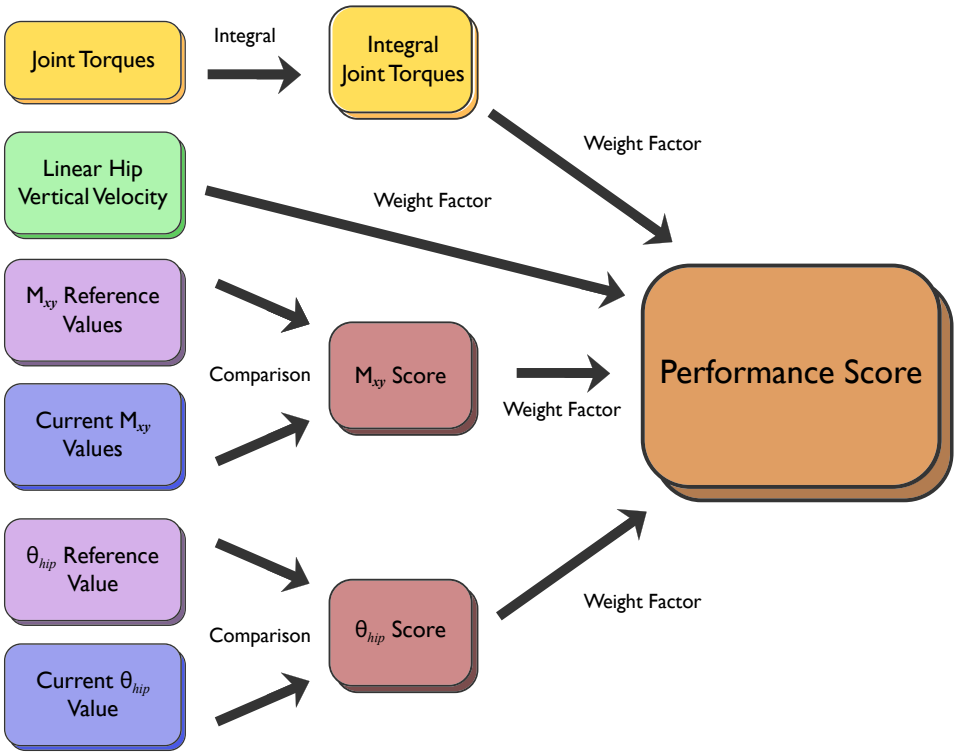

Figure 4.7: Illustrative diagram for the process involved in assessing the performance score for every simulation. The weight factors ensured that any given element was neither over nor underrepresented in the final value for the simulation performance.

0.001 seconds. Each simulation was ran with the assumption that an imminent fall is detected at the first instant, and so the strategy comes into effect from the start, and lasts through the entirety of the simulation.

Aiming to test several variations of the strategy, values for several fields involved in the simulation were changed. The Proportional Derivative Controller's Proportional Term (PGain) was one such case: in order to test for different magnitudes of changes in output for changes in error, a range of values was used, that varied from 27000 and 80000, for a total of 18 different values. These were set after testing: it was observed that for lower PGain values the model behaved in a very unresponsive way, and for higher values the controller's responses led to fast, unstable and unsafe movements. Values for the ySlope and xSlope, previously mentioned in Section 4.2, were also tested in a range, both varying from 0.10 to 1.25, for a total of 24 different values. Higher values for these parameters were also tested, but ultimately excluded from analysis, as the references they produced were shown to be too fast-changing for the controller to follow. This is illustrated in the example shown in Figure 4.8, where both xSlope and ySlope took the value of 2.0, and a PGain value of 64000 was used. The higher values for the slope parameters resulted in a faster rate of change for $\mathcal{M}_{xy}$ references. This made the model continuously overshoot

its position, and fail in the tracking of its references, affecting even the *hipq* tracking. Generally speaking this is to be expected, due to the previously mentioned difficulty of PD controllers and PID controllers in general in managing systems with high rates of change, or unstable systems [82–84]. In this sense, it is logical to view the references created from the higher ySlope and xSlope values as leading to a more unstable system, and thus harder to execute for the controller.

The full set of parameters changed in simulation to test the strategy is shown in Table 4.2. For each of the seven initial position, 10368 simulations were then ran, for a total of 72576 simulations. The combinations of joint angles associated with each initial position can be consulted in the Appendix A.

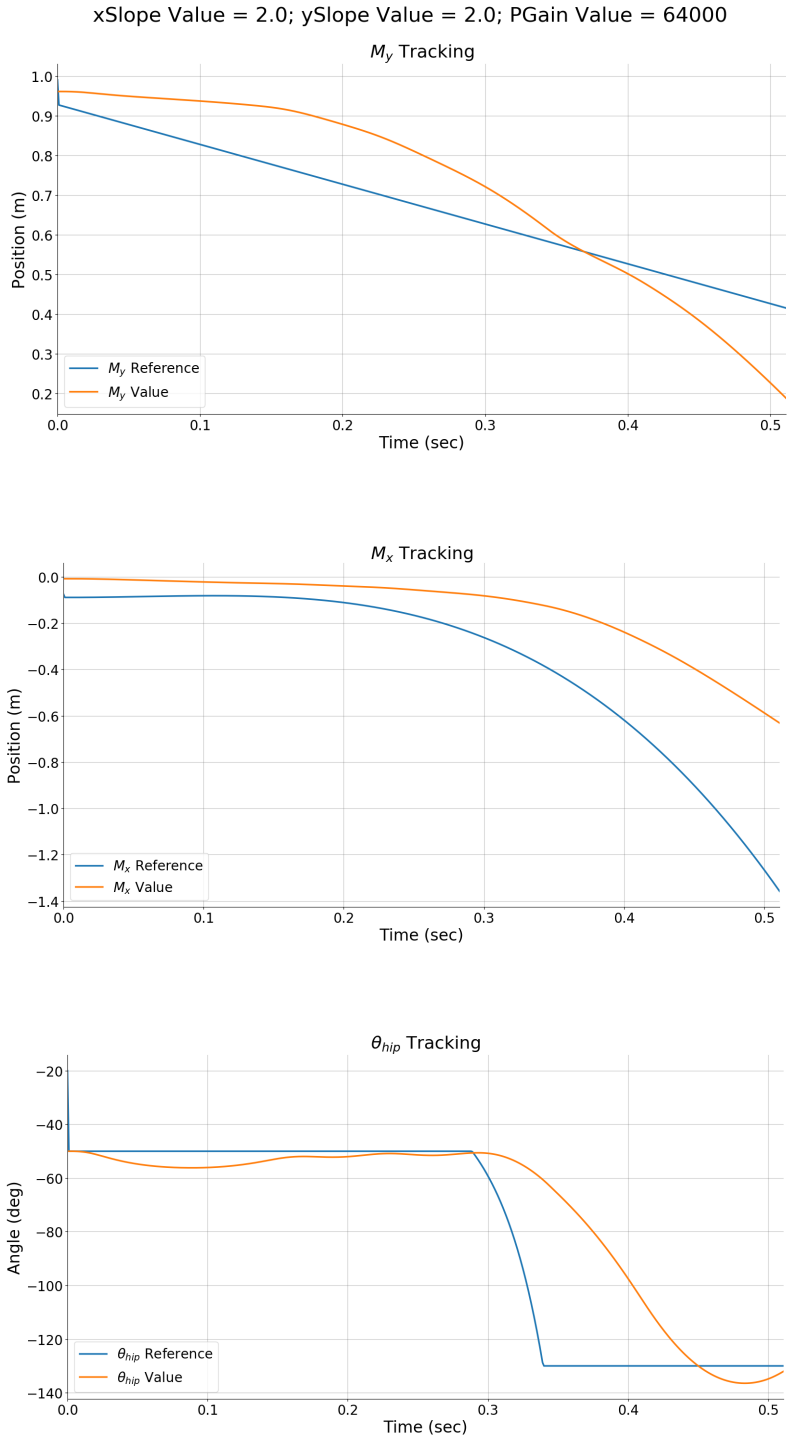

Figure 4.8: An example of the model's poor reference execution due to the use of higher xSlope and ySlope values. The value for both in this simulation was 2.0, and a value of 64000 was used for the PGain. The faster rate of change in $\mathcal{M}_{xy}$ references resulted in position overshooting and overall poor model performance.

Initial Position	PGain Value	xSlope Value	ySlope Value
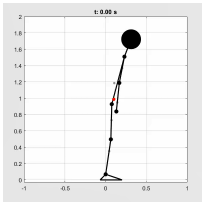	27000	0.1000	0.1000
		0.1500	0.1500
	30000	0.2000	0.2000
	33000	0.2500	0.2500
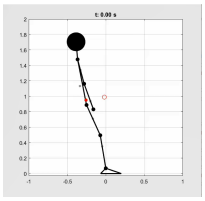	36000	0.3000	0.3000
		0.3500	0.3500
	39000	0.4000	0.4000
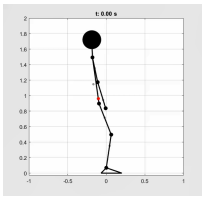	42000	0.4500	0.4500
	45000	0.5000	0.5000
		0.5500	0.5500
	48000	0.6000	0.6000
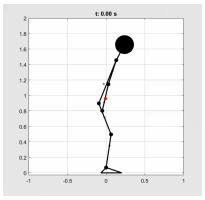	51000	0.6500	0.6500
	54000	0.7000	0.7000
		0.7500	0.7500
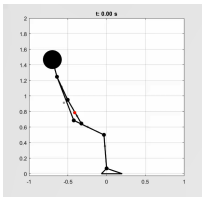	57000	0.8000	0.8000
	60000	0.8500	0.8500
	63000	0.9000	0.9000
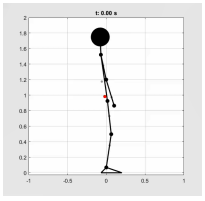	66000	0.9500	0.9500
		1.0000	1.0000
	69000	1.0500	1.0500
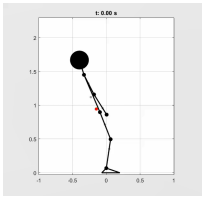	72000	1.1000	1.1000
		1.1500	1.1500
	75000	1.2000	1.2000
	78000	1.2500	1.2500

Table 4.2: Complete set of values used in simulation to test the proposed safe fall strategy. Each position is defined by its combination of ankle, knee and hip joint angles.

Chapter 5

Results

5.1 Reference Tracking and Strategy Execution

To represent the tracking of the $\mathcal{M}_{xy}$ and θ_{hip} references, two simulations are presented as examples. Figure 5.1 shows the model's tracking of the $\mathcal{M}_{xy}$ and θ_{hip} references throughout the simulations. In both instances, the initial position of the model at the onset of the fall was the same. The first simulation was run with a Proportional Derivative Controller's Proportional Term (PGain) value of 33000, an xSlope value of 0.3, and a ySlope value of 0.2. Tracking from this simulation is presented in (a), (c) and (e) of Figure 5.1. Aside from brief adjustment periods, the model was able to follow both $\mathcal{M}_{xy}$ and θ_{hip} references throughout the fall. In the second simulation (Figure 5.1 (b), (d), (f)), the xSlope and ySlope values were both 1.0. The increased ySlope value resulted in a considerably shorter fall, as the second simulation had a fall duration of 1.270 seconds, while the first one lasted for 7.709 seconds. In the shorter fall, the model performed slightly worse, particularly in relation to the $\mathcal{M}_y$ tracking, as shown in (b). The $\mathcal{M}_x$ and θ_{hip} tracking, shown in (d) and (f), were less unstable by comparison.

Figure 5.2 includes several diagrams of the model's position throughout these same simulations. In both cases, the model was successful in performing the fall in the two intended main steps: a transition from the standing position to the squat position without considerable horizontal movement, observable in (b), (c), (f) and (g); and afterwards the knee extension while maintaining an upright posture, shown through (d) and (h). Comparing the two simulations, the notable difference is the head position in throughout both these steps. In the longer fall, the model's head is kept in line or ahead of the hip joint during the squat motion, but by the end of the knee extension, it is behind the hip. This is contrary to the intended safe upright position, and most likely due to the long fall time interval defined by the smaller slope values. In Simulation 2, conversely, the model's

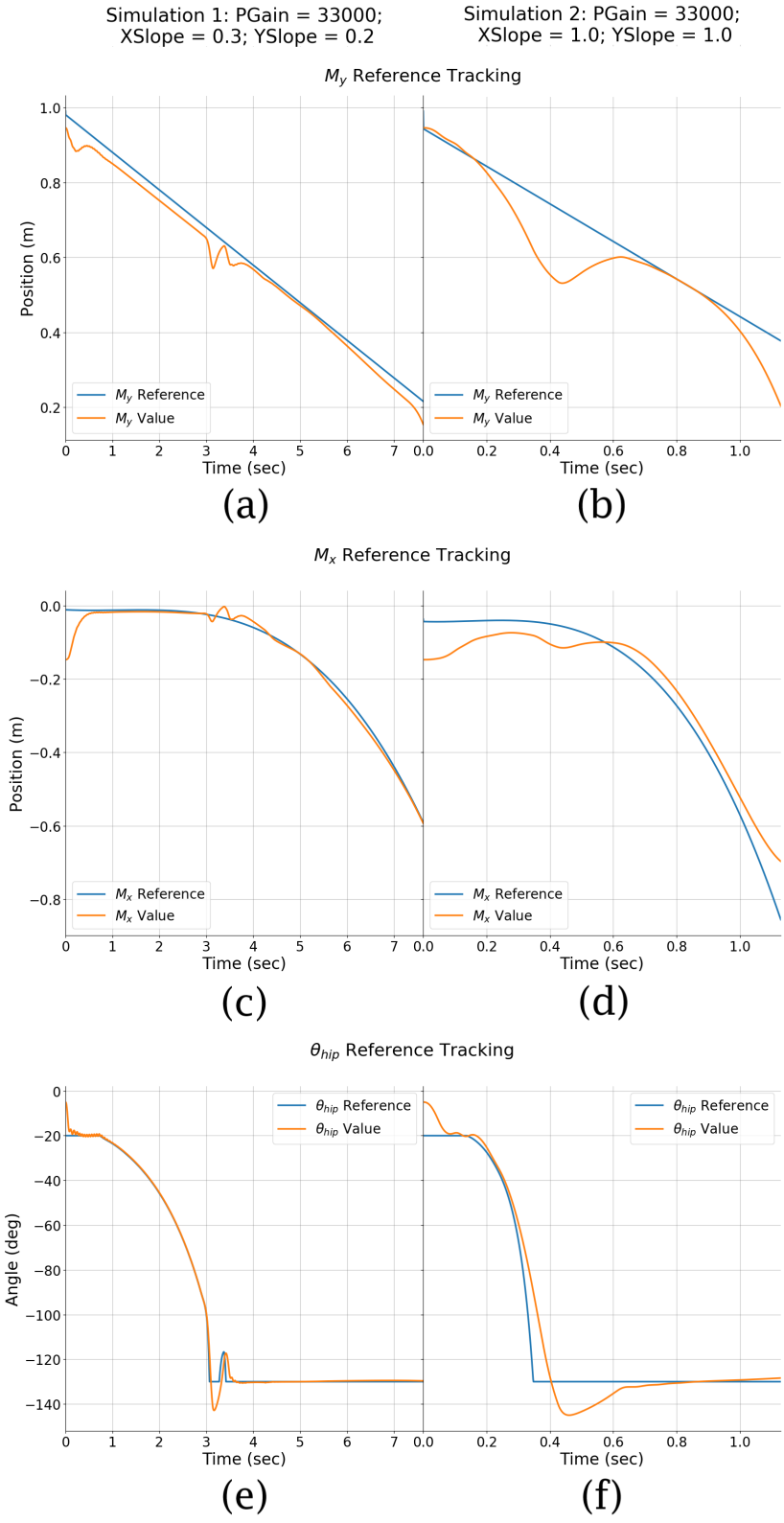

Figure 5.1: Comparison of $\mathcal{M}_y$, $\mathcal{M}_x$ and θ_{hip} values, between reference and simulation values. Sub-figures (a), (b), (c) and (d) refer to the $\mathcal{M}_{xy}$'s relative distance to the feet position, which stayed fixed throughout the simulation.

head is initially behind the hip during the squat motion (see (f)), but by the end of the fall it is found safely ahead the same joint (see (h)).

Simulation 1: PGain = 33000; xSlope = 0.3; ySlope = 0.2

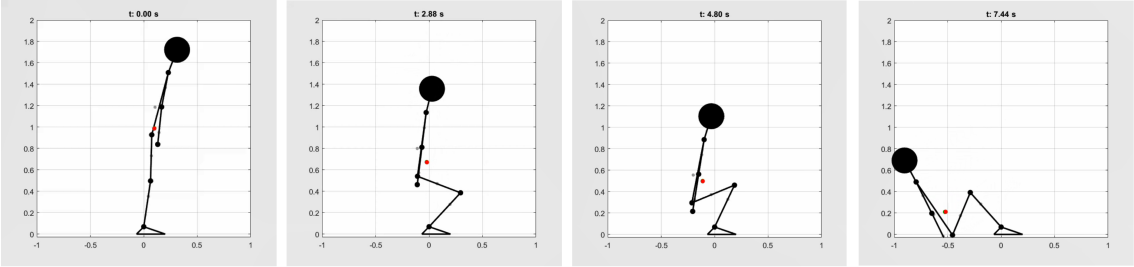

(a) t = 0.00 s (b) t = 2.88 s (c) t = 4.80 s (d) t = 7.44 s

Simulation 2: PGain = 33000; xSlope = 1.0; ySlope = 1.0

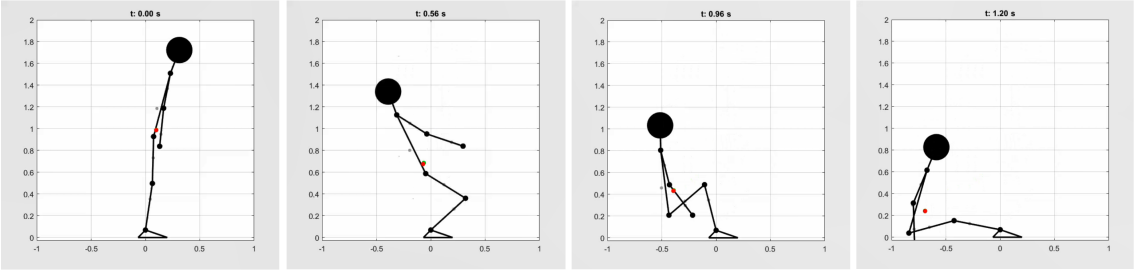

(e) t = 0.00 s (f) t = 0.56 s (g) t = 0.96 s (h) t = 1.20 s

Figure 5.2: Diagrams of the human-exoskeleton model's position throughout two simulations. The fall's duration, conditioned by the different slope parameters, influences how the model executes the squat response and knee extension.

5.1.1 Center of Mass and Hip Angle Score Tracking

Besides these two previous examples, the fall strategy was tested over a large set of simulations, where different initial positions, PGain values and xSlope and ySlope coefficient values were used. Due to the large number of performed simulations, only a selection is presented in this chapter. A larger selection can be consulted in the Appendixes B and C [1]. The simulations reviewed in this section were chosen based on how representative they were of their respective larger set of results. Figures 5.3 and 5.4 show $\mathcal{M}_{xy}$ and θ_{hip} score values, respectively, for one of the eighteen different PGain values (48000), over three of the seven initial positions tested. For simplicity, throughout this chapter the initial positions are indicated as per their respective joint angles. For a visual representation, the combinations of joint angles associated with each initial position can be consulted in the Appendix A. In both cases, lower scores were consistently associated with lower values for both the xSlope and ySlope. Changes in the ySlope value were shown to have a greater influence on the $\mathcal{M}_{xy}$ score, with closer score values found across most xSlope

[1] The full set of results from the simulations described in this dissertation will not be included in this manuscript. Please contact the author of this work to have access to any results that were omitted.

values. Looking at θ_{hip} scores in particular, frequent jumps in θ_{hip} score value between lower and higher ySlope values can be noted.

To better assess how these score values represent the model's ability to follow the references and perform the intended strategy, individual simulations were chosen for closer analysis. Specifically, six simulations in total, two for each of these initial positions, were chosen. Three of them were chosen to reflect simulations which used lower values for both slope parameters, and resulted in lower scores for both $\mathcal{M}_{xy}$ and θ_{hip} tracking. Diagrams of the model's position during these simulations are shown in Figure 5.5. The other three simulations used higher values for the slope parameters, which resulted in higher tracking scores. Their respective diagrams are shown in Figure 5.6. The scores for these simulations are highlighted in Figures 5.3 and 5.4. For each set, the simulation with the lower score is highlighted in blue, and the simulation with the higher score is highlighted in red, with their respective scores also shown.

Looking at these simulation diagrams, a few things are notable: first, for all simulations, the model visibly performs its fall strategy by first executing a squat motion (without much horizontal translation), and then a knee extension, causing the $\mathcal{M}_{xy}$ to move backwards. This is illustrative of the model's ability to execute the proposed strategy with a good degree of accuracy, for both the best and worst cases of tracking tested. The model was also able to perform the strategy between the different initial positions, with minimal changes to the reference scores. This is also a positive sign of this strategy's potential to be dynamically adapted to a variety of backwards fall scenarios. Lastly, comparing the knee extension movement between simulations with the better tracking scores (illustrated in 5.5 (d), (h) and (l)), and the simulations with worse tracking scores (shown in 5.6 (d), (h) and (l)), a difference in execution is notable. Contrarily to what the better score values would suggest, the model performs only a partial knee extension in simulations with lower slope parameters. In the simulations with worse tracking, the knee extension is much closer to the intended strategy, and as a result the head ends up in a safer position by the end of the fall.

5.1.2 Joint Torque Involved in the Safe Fall Strategy

As one other way of measuring how comfortable the system is when executing the strategy throughout the simulations, the integral joint torques were analyzed separately. Figure 5.7 shows results for the same simulation sets shown in Figures 5.3 and 5.4, with the maximum values for each set highlighted in red. An extended set of results can be consulted in the Appendix D.

For the most part, the average joint integral values follow similar trends to the tracking scores: smaller slope parameter values resulted overall in lower integral torque values, and changes in ySlope values had more impact in general, when compared with changes to xSlope values. Looking at the values themselves, they remained within reasonable

intervals, which points to the system's ability to execute the proposed strategy within reasonable demand on the available joint torques. The acceptable maximum values reported, representative of the worst executions, reflect that even in these scenarios the strategy is still performed at an acceptable level.

5.2 Fall Safety and Vertical Hip Impact Velocity

Figure 5.8 shows values for the hip vertical impact velocities, in relation to (divided by) the reference value presented in [75] of 3.22 m/s. For each set, the simulations that resulted in the highest value are highlighted in red, and the simulations that resulted in the lowest value are highlighted in blue. A larger set of these results is available in the Appendix E.

In general, values were found to be low across different initial positions, xSlope and ySlope values. This points to the strategy's ability to increase fall safety, even for worse executions. Lower velocity values were associated with very slow and more controlled falls, defined by the lower Slope parameter values, in a similar fashion to the relations noted in Figure 5.3, for the $\mathcal{M}_{xy}$ tracking scores. For each simulation set, these lower values reported show that the model was able to essentially stop fall momentum before impact, due to the long fall times (see 5.5 (d), (h) and (l)).

5.3 Performance Score

After analyzing the simulation results on the model's reference tracking and impact on fall safety individually, the performance score results would clarify if these two aspects shared a correlation, or if they opposed each other.

Figure 5.9 shows performance score values, for one of the eighteen different PGain values (48000), over three of the seven initial positions tested. A larger set of results can be consulted in the Appendix F. Comparing these results with the performance score's individual components presented in Figures 5.3, 5.4 and 5.8, the performance score's values generally followed similar trends to the tracking scores values. Lower combinations of xSlope and ySlope values resulted in lower values for the performance score. Juxtaposing the values in Figures 5.3 (a), (b), 5.4 (a), (b) and 5.8 (a), (b), these even share a clear split in values for a ySlope value of higher or lower than 0.6. Overall, these results point to a congruence between the strategy tracking scores and the criteria chosen to represent fall safety.

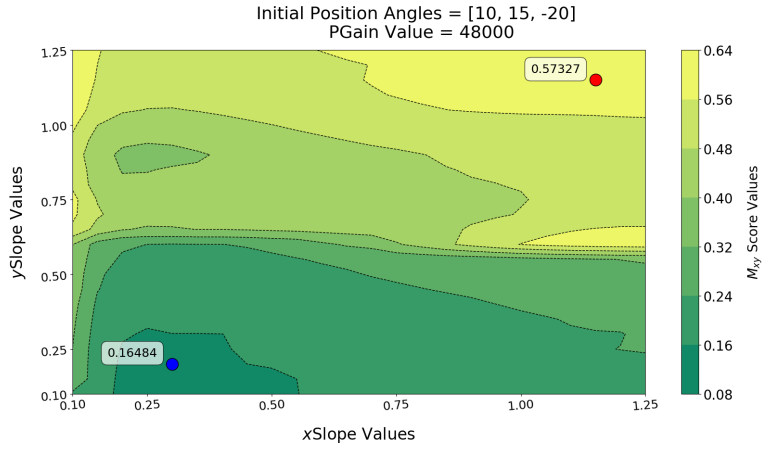

(a)

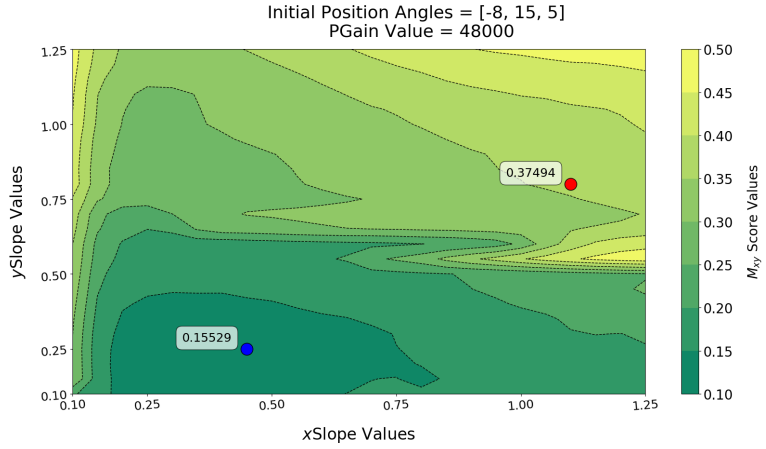

(b)

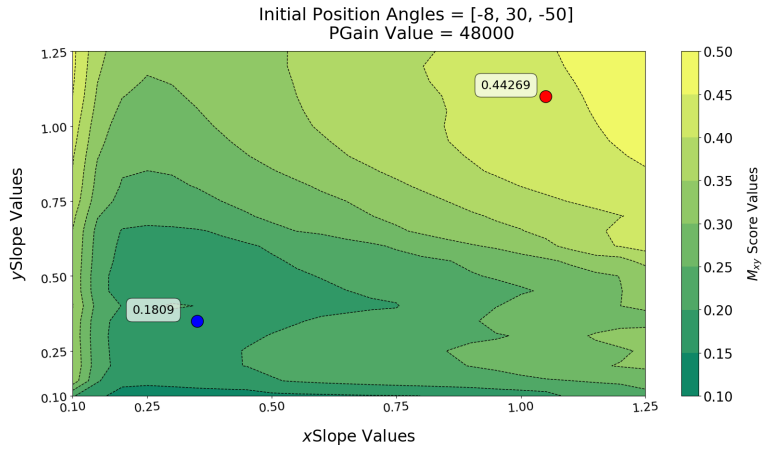

(c)

Figure 5.3: Values of the $\mathcal{M}_{xy}$ Score for different combinations of xSlope and ySlope values. The initial positions are defined by the initial angle values for the ankle, knee and hip joints. The PGain value used in all three simulation sets was 48000. The contour lines indicate similar values, and determine the difference in colors between regions. Each color map is set for its own plot, which makes it so that similar colors between plots may not correspond to the same values. The highlighted value in blue corresponds to the better result used for analysis, and the value in red corresponds to the worse score.

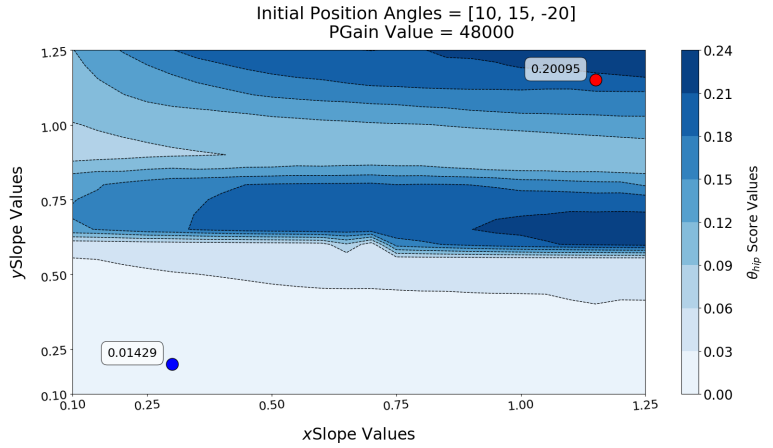

(a)

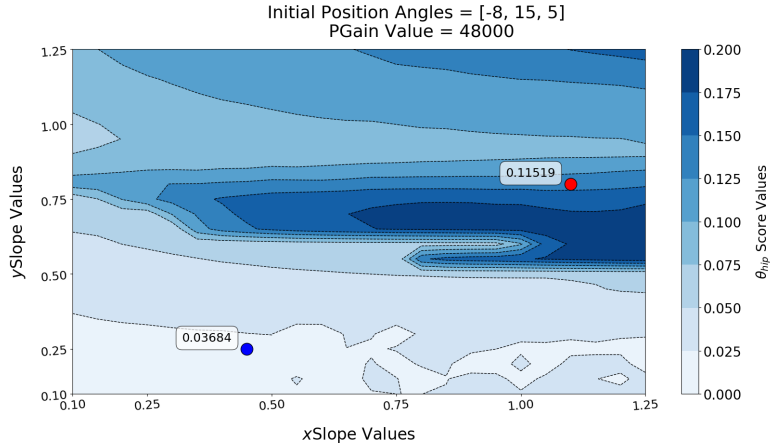

(b)

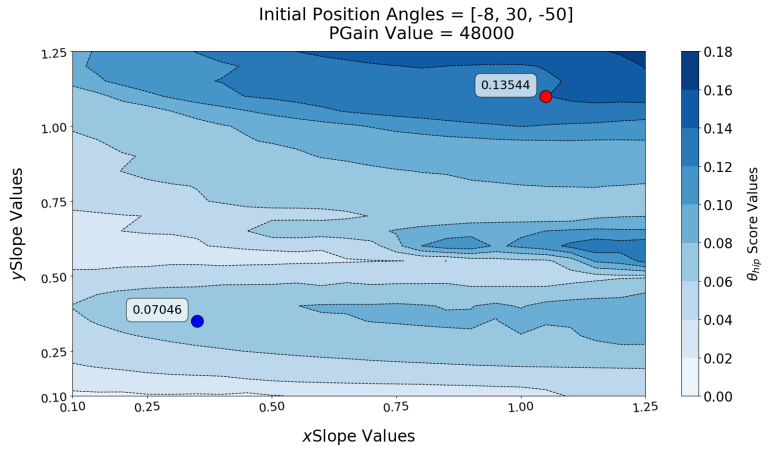

(c)

Figure 5.4: Values of the θ_{hip} scores for different combinations of xSlope and ySlope values. The initial position is defined by the initial angle values for the ankle, knee and hip joints. The PGain value used in all three simulation sets was 48000. The contour lines indicate similar values, and determine the difference in colors between regions. Each color map is set for its own plot, which makes it so that similar colors between plots may not correspond to the same values. The annotated values correspond to the scores of the highlighted simulations, used for closer analysis.

Initial Position Angles = [10, 15, -20]
PGain = 48000; xSlope = 0.30; ySlope = 0.20

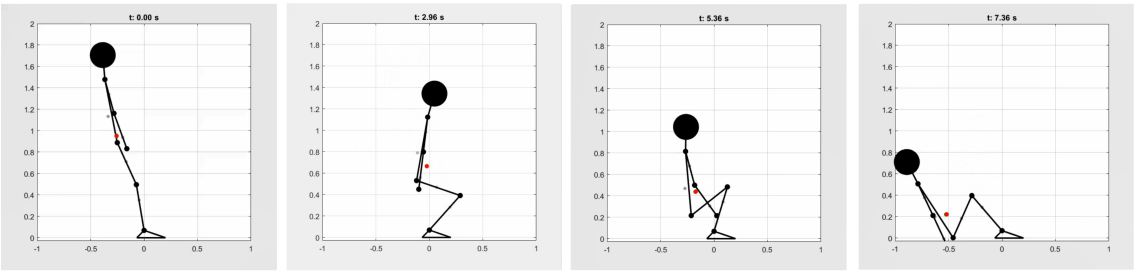

(a) t = 0.00 s (b) t = 2.96 s (c) t = 5.36 s (d) t = 7.36 s

Initial Position Angles = [-8, 15, 5]
PGain = 48000; xSlope = 0.45; ySlope = 0.25

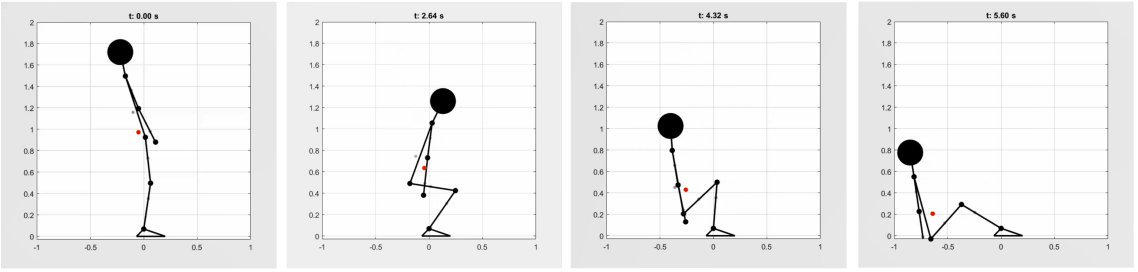

(e) t = 0.00 s (f) t = 2.64 s (g) t = 4.32 s (h) t = 5.60 s

Initial Position Angles = [-8, 30, -50]
PGain = 48000; xSlope = 0.35; ySlope = 0.35

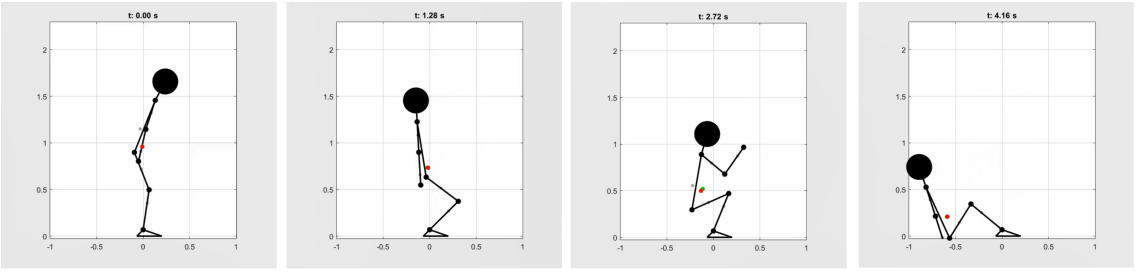

(i) t = 0.00 s (j) t = 1.28 s (k) t = 2.72 s (l) t = 4.16 s

Figure 5.5: Diagrams of the human-exoskeleton model's position throughout simulations using lower slope parameter values. The fall's duration, conditioned by the different slope parameters, influences how the model executes the squat response and knee extension. Each intermediate instant shown was chosen manually, with the purpose of reflecting the two main steps involved in the strategy: the squat motion without backwards movement, and the following knee extension.

Initial Position Angles = [10, 15, -20]
PGain = 48000; xSlope = 1.15; ySlope = 1.15

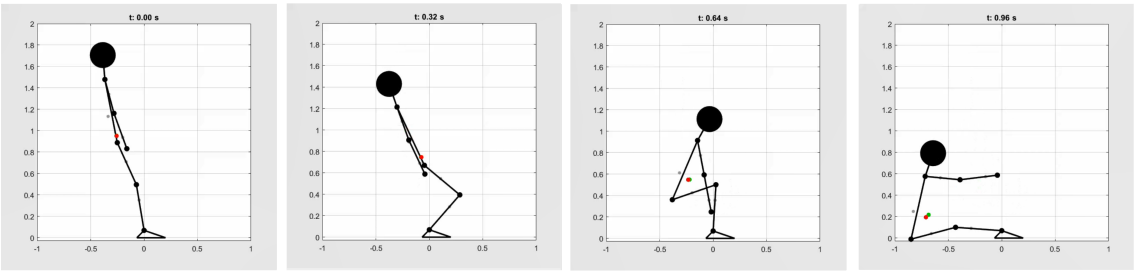

(a) $t = 0.00\ s$ (b) $t = 0.32\ s$ (c) $t = 0.64\ s$ (d) $t = 0.96\ s$

Initial Position Angles = [-8, 15, 5]
PGain = 48000; xSlope = 1.10; ySlope = 0.80

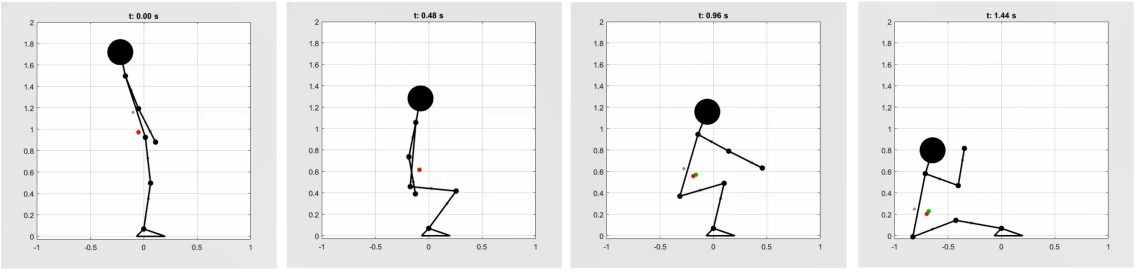

(e) $t = 0.00\ s$ (f) $t = 0.48\ s$ (g) $t = 0.96\ s$ (h) $t = 1.44\ s$

Initial Position Angles = [-8, 30, -50]
PGain = 48000; xSlope =1.05 ; ySlope =1.10

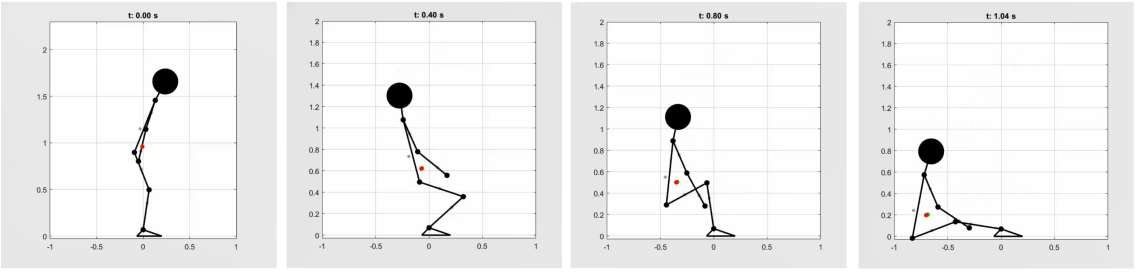

(i) $t = 0.00\ s$ (j) $t = 0.40\ s$ (k) $t = 0.80\ s$ (l) $t = 1.04\ s$

Figure 5.6: Diagrams of the human-exoskeleton model's position throughout simulations using higher slope parameter values. The fall's duration, conditioned by the different slope parameters, influences how the model executes the squat response and knee extension. Each intermediate instant shown was chosen manually, with the purpose of reflecting the two main steps involved in the strategy: the squat motion without backwards movement, and the following knee extension.

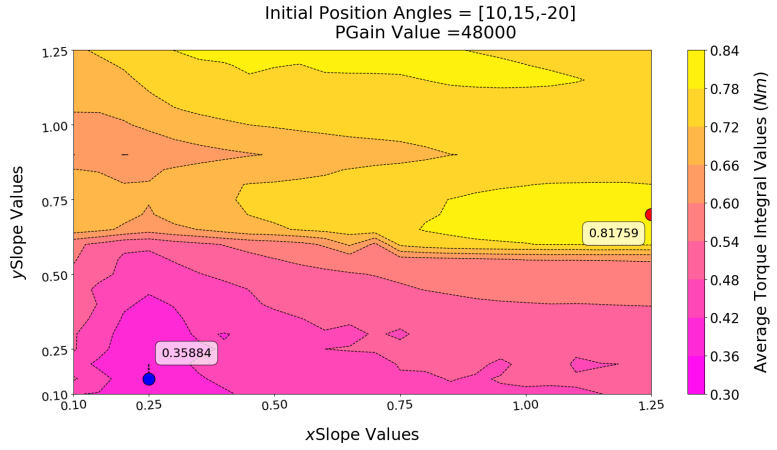

(a)

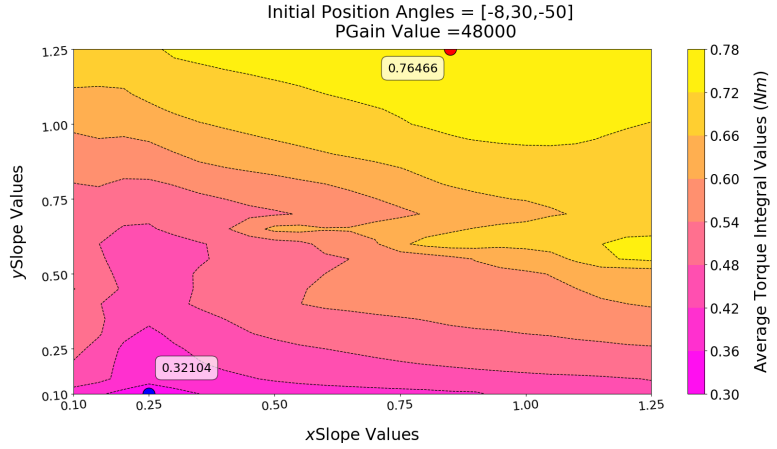

(b)

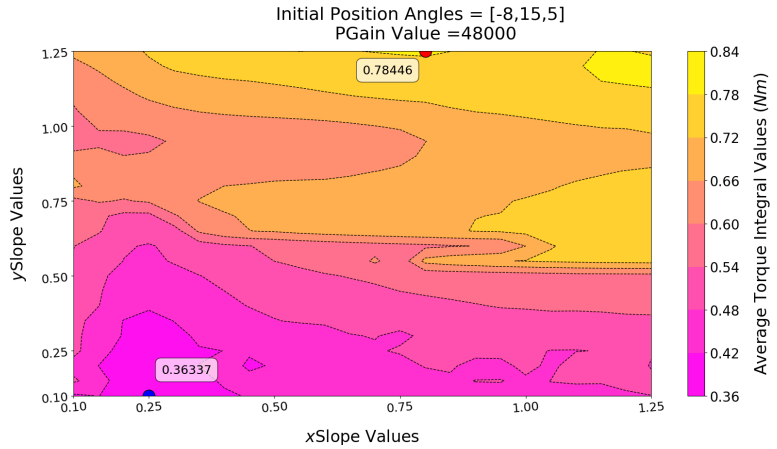

(c)

Figure 5.7: Values of the average torque integral for different combinations of xSlope and ySlope values. The initial position is defined by the initial angle values for the ankle, knee and hip joints. The PGain value used in all three simulation sets was 48000. The contour lines indicate similar values, and determine the difference in colors between regions. Each color map is set for its own plot, which makes it so that similar colors between plots may not correspond to the same values. The annotated values correspond to the highest (red) and lowest (blue) values.

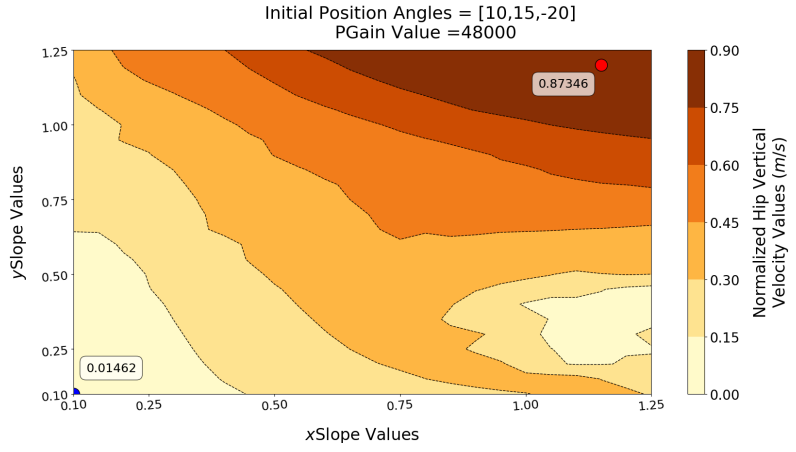

(a)

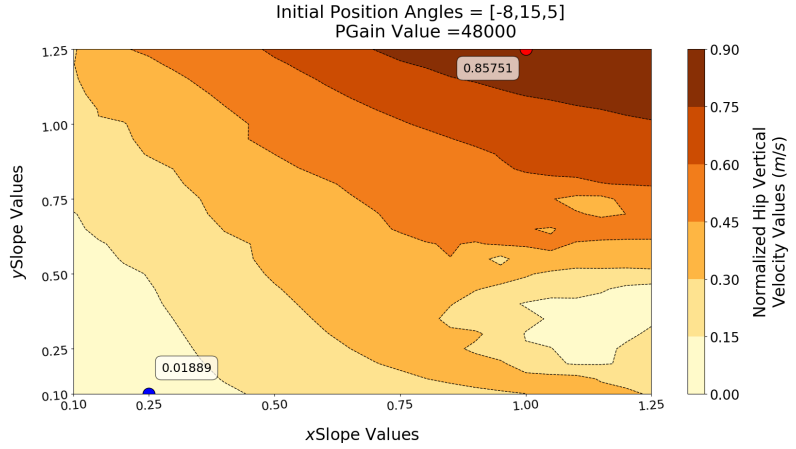

(b)

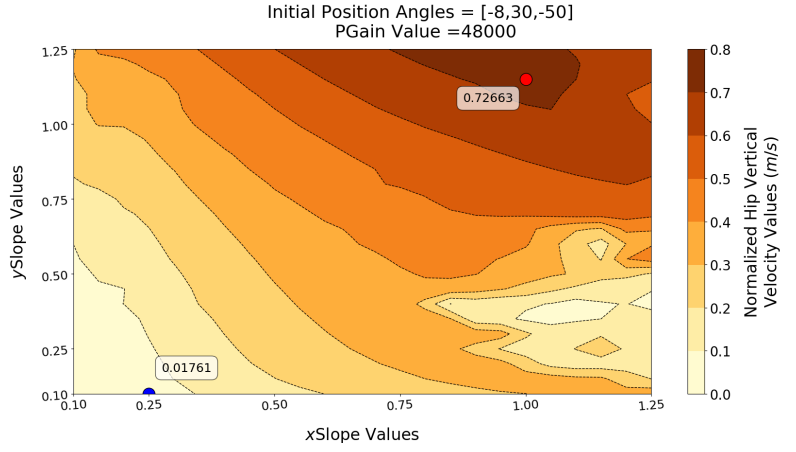

(c)

Figure 5.8: Values of the normalized hip vertical impact velocity for different combinations of xSlope and ySlope values. Resulting hip vertical impact velocity values were divided by the reference value (3.22 m/s) reported in [75], to better reflect the improvement in safety between executions. The annotated values correspond to the highest (red) and lowest (blue) values.

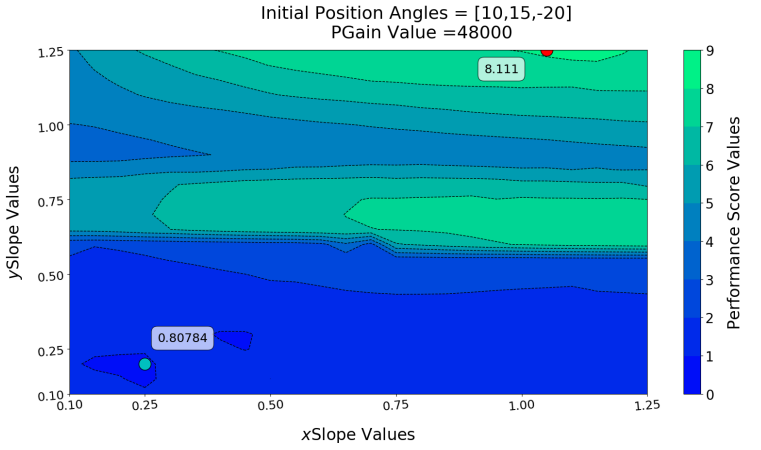

(a)

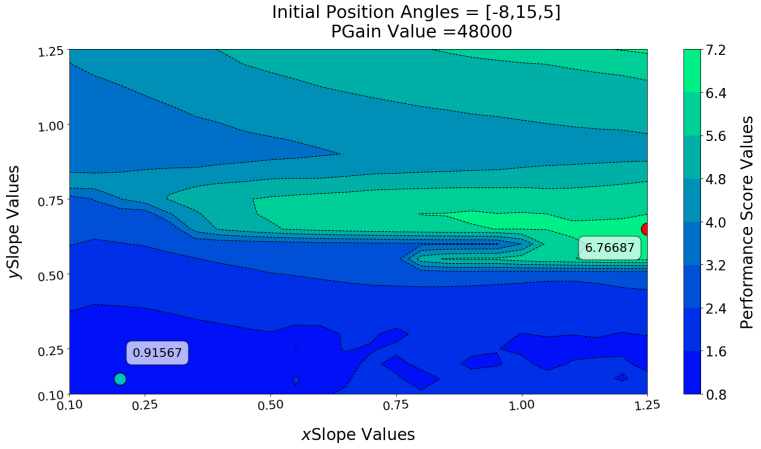

(b)

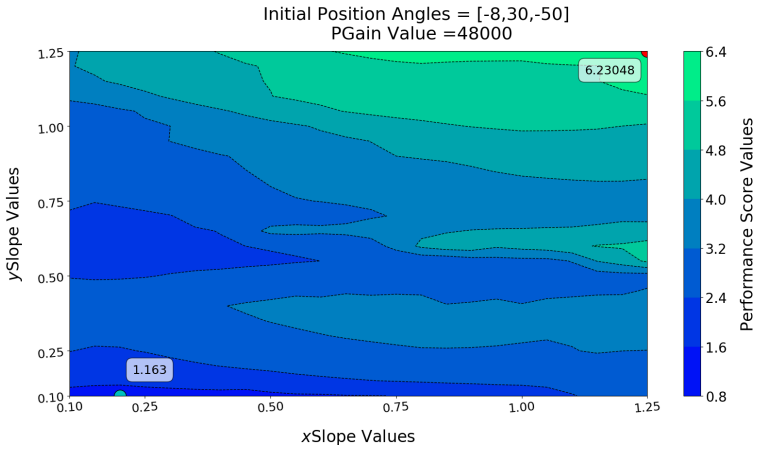

(c)

Figure 5.9: Values of the performance score for different combinations of xSlope and ySlope values. The PGain value used in all shown simulations was 48000. The contour lines indicate similar values, and determine the difference in colors between regions. Each color map is set for its own plot, which makes it so that similar colors between plots may not correspond to the same values. The annotated values correspond to the highest (red) and lowest (cyan) values.

Chapter 6

Discussion

The purpose of this work was to implement and evaluate the squat response strategy for a human-exoskeleton system in the context of a backwards fall. To accomplish this, a Center of Mass (CoM) reference was designed to mimic the movement associated with a squat response. This reference was then complemented by a hip angle reference, to ensure safe trunk positioning throughout the fall.

The resulting strategy was tested using seven initial positions, with varying combinations of Proportional Derivative Controller's Proportional Term (PGain) values, as well as the ySlope and xSlope parameter values. In total, 10368 simulations for each initial position were computed. To judge how well the model could follow its references, the $\mathcal{M}_{xy}$ and θ_{hip} references were compared with the model's values throughout the simulation, and their differences were aggregated in score values.

Results showed that the model was able to execute the strategy incorporating both references. The model's $\mathcal{M}_{xy}$ and θ_{hip} values were closely tracked throughout most of the falls' duration, showing no signs of clashing as a result of providing references of different nature. This is a promising outcome, as it suggests potential in combining these types of, as a way of designing safe fall strategies for human-exoskeleton systems. The references were followed more closely by the model in the case of longer falls, as determined by the ySlope value used in the simulations. Performance was overall better for combinations of lower values for these two parameters, across initial positions and controller proportional gain values. This result is to be expected, as longer falls provide more time for the controller to follow its references.

When evaluating individual simulations, and the model's position throughout, it was noted that the model was able to execute the strategy performing the two intended movements: the squat response used to lower the $\mathcal{M}_y$, and the knee extension while maintaining an upright posture. This points to the hypothesis that using key positions

involved in complex movements (in this instance, the squat response for safe backwards falls) as reference is a valid way of designing references and strategies for this system.

Despite the fact that the two part execution was present in all of the simulations shown, the difference in the knee extension between longer and shorter falls is notable. During simulations featuring higher values for the Slope parameters, which were for the most part associated with worse tracking scores when compared to simulations with lower Slope values, the knee extension was executed closer to the intended motion, and was more effective in keeping the head in front of the hip joint while falling. This difference can be attributed to the longer and slower-changing reference in the simulations with lower Slope values. The transition between the squat position and the extended knee position can only happen smoothly is performed in one swift and continuous motion through the extension at the knee. In these cases, the $\mathcal{M}_{xy}$ reference was too slow moving to represent this strategy, and so the model's resulting response was a slow backwards movement, that failed to incorporate knee extension as intended. The better tracking scores associated with these slow responses serve as evidence that the references themselves are the cause. In future implementations, a relation between knee angle and $\mathcal{M}_y$ value in a similar fashion to the established relation between $\mathcal{M}_y$ and θ_{hip} might be worth exploring to tackle this issue. Just as the trunk was maintained upright as intended through the use of the θ_{hip} reference, the knee might be made to extend at the proper time (or $\mathcal{M}_y$ value) through a knee angle reference.

To evaluate how successful the strategy was in ensuring the user's safety, the model's hip joint impact velocity throughout the simulations was collected. Using the reference value reported in [75] as a guideline for an unsafe, "worst-case fall", the obtained values were shown to be consistently lower, even in cases with worse execution. These results are a promising sign of the potential effectiveness of this strategy in the context of human-exoskeleton systems. With that said, it is necessary to further validate this effectiveness, using references specific to the system to better compare fall safety outcomes between this strategy, and a representative "bad" or "worst-case" fall (as it stands now, there is no such reference for this model).

Looking at the simulations associated with the lower hip impact velocities, the obtained values reflect the model's ability to effectively stop its momentum. This is a sign that, in these cases, these fall scenarios are too lenient with the model's balance, and are not accurate representations of an unavoidable fall. Keeping this in mind, in the future it might prove useful to investigate how to better create these unavoidable fall scenarios in a simulation environments. This could be accomplished by perhaps simulating external perturbations to the system, like a push. For a realistic demonstration, this would require that the model would also be able react to these perturbations. Developing a reactive fall detection controller of this nature remains a separate challenge on its own [77, 78, 86–90].

Lastly, in an effort to evaluate the strategy's effectiveness in ensuring safety during the

simulation, a performance score function was designed. This function's output incorporated not only on the reference tracking scores for the model, and joint torque integrals, but also the model's hip impact velocity, and maximum hip angular velocity throughout the fall. It was presumed that the strategy would prove effective if its values presented similar behavior to the reference tracking scores. This would indicate that better tracking scores led to lower (and less expressive) values for the hip impact velocity and maximum angular velocity, meaning safer falls.

Results showed that the performance score values followed similar trends as the reference tracking scores, in relation to changes with higher and lower Slope parameter values, and across initial positions. The lower costs were consistently associated with simulations with better tracking scores, and vice-versa. This is in line with the initial hypothesis and indicates that the strategy's execution is directly correlated with safer falls, as measured by both the hip vertical impact velocity, the maximum value for the hip angular velocity, and their impact on the performance score function. However, due to the observations made in regards to strategy execution in the simulations associated with the lowest scores, a conclusion regarding the optimal combination of values for the strategy can not be made.

It is important to consider the limitations of this work, with focus on why the simulated falls may differ from real-life falls. First, the strategy was developed to be executed in reaction to a situation of instability. As of now, the WE2+ exoskeleton is not yet capable of reliably detect imminent backward falls. As such, before the strategy studied in this work can be implemented in the exoskeleton, developing systems for posture estimation and/or gait analysis is necessary. As previously mentioned, promising results have been reported involving sensor data [80], and derived Center of Mass (CoM) and Center of Pressure (CoP) information [77–79]. Similar developments for the human-exoskeleton system should be investigated.

The process of designing the strategy involved a few choices which could be further explored in the future. This includes the value chosen as reference for the fall duration, of 1271 ms, and also the estimated duration for the squat phase of the strategy, of 0.20 ms. Both of these choices surely impacted the obtained results, and in both cases the chosen values were not based on the model's specifications. In the future, real-life trials with the exoskeleton could be performed, and values more suitable for this system could be obtained.

Regarding the simulations, the model's feet were restrained and maintained contact with the ground throughout descent, which is often not the case for backward falls. Furthermore, this neglects situations where slips occur, and both feet may lose contact with the ground during descent. The impact velocity may be particularly severe for these cases, so proper attention is warranted. Falls were also considered to be symmetric in the sagittal plane, and only the backward fall scenario was considered. Ideally, the safe fall strategy should be extended to maximize user safety in the event of sideways and forward falls. Previous research in sideways falls has suggested that rotating backward during

descent can be effective in avoiding hip impact for subjects [22]. A similar approach could potentially be taken for the human-exoskeleton system. Specifically, in the event of a sideways fall, the system could rotate backward and transition into the backward fall strategy.

6.1 Conclusion

This thesis presented the development of a safe fall strategy for human-exoskeleton backwards falls. The strategy was designed based on strategies studied in healthy humans, and applied through a combination of Center of Mass (CoM) and hip joint angle reference signals. The motivation for this work is to ultimately improve Lower Limb Exoskeletons (LLE) users' safety, and allow them to be used outside of a hospital setting, and in daily living activities. For this thesis, the main goal was to mitigate the injury risk by minimizing the hip impact velocity and maintaining an upright posture, thus avoiding head impact.

The results verified the model's ability to execute the proposed strategy, and its effectiveness in providing safer falls. The reference tracking scores results showed that the model could follow its references simultaneously, and the performance scores pointed to a causal relation between the references and safer falls. Similar trends were for the most part noted throughout the seven different initial positions, which points to the validity of the strategy to be useful in different backwards fall scenarios.

Despite this, the strategy should be improved to ensure that the intended knee extension at the end of the fall is consistently performed. There is also room for improving the criteria for evaluating fall safety in the simulation environment. Beyond the simulations, research should be done on testing this strategy in real-life scenarios, and developing strategies for other fall scenarios, like sideways and front-facing falls. Until safe fall strategies that can protect LLE users' safety are developed and validated in all of these situations, LLE's utility cannot be extended past the clinical setting.

Bibliography

[1] S. A. Sisto, G. Forrest, and P. Faghri. "Technology for mobility and quality of life in spinal cord injury: Analyzing a series of options available." In: *IEEE Engineering in Medicine and Biology Magazine* 27.2 (2008), pp. 56–68. ISSN: 07395175. DOI: 10.1109/EMB.2007.907398.

[2] V. Lajeunesse, C. Vincent, F. Routhier, E. Careau, and F. Michaud. "Exoskeletons' design and usefulness evidence according to a systematic review of lower limb exoskeletons used for functional mobility by people with spinal cord injury." In: *Disability and Rehabilitation: Assistive Technology* 11.7 (2016), pp. 535–547. ISSN: 17483115. DOI: 10.3109/17483107.2015.1080766.

[3] M. L. Lund, A. Nordlund, L. Nygård, J. Lexell, and B. Bernspång. "Perceptions of participation and predictors of perceived problems with participation in persons with spinal cord injury." In: *Journal of Rehabilitation Medicine* 37.1 (2005), pp. 3–8. ISSN: 16501977. DOI: 10.1080/16501970410031246.

[4] W. E. Pentland and L. T. Twomey. "Upper limb function in persons with long term paraplegia and implications for independence: Part i." In: *Paraplegia* 32.4 (1994), pp. 211–218. ISSN: 00311758. DOI: 10.1038/sc.1994.40.

[5] W. E. Pentland and L. T. Twomey. "Upper limb function in persons with long term paraplegia and implications for independence: Part ii." In: *Paraplegia* 32.4 (1994), pp. 219–224. ISSN: 00311758. DOI: 10.1038/sc.1994.41.

[6] K. A. Cratsenberg, C. E. Deitrick, T. K. Harrington, N. R. Kopecky, B. D. Matthews, L. M. Ott, and R. R. Coeytaux. "Effectiveness of exercise programs for management of shoulder pain in manual wheelchair users with spinal cord injury." In: *Journal of Neurologic Physical Therapy* 39.4 (2015), pp. 197–203. ISSN: 15570584. DOI: 10.1097/NPT.0000000000000103.

[7] D. Fogelberg, M. Atkins, E. Blanche, M. Carlson, and F. Clark. "Decisions and dilemmas in everyday life: Daily use of wheelchairs by individuals with spinal cord injury and the impact on pressure ulcer risk." In: *Topics in Spinal Cord Injury Rehabilitation* 15.2 (2009), pp. 16–32. ISSN: 10820744. DOI: 10.1310/sci1502-16.

[8] S. Goemaere, M. Van Laere, P. De Neve, and J. M. Kaufman. "Bone mineral status in paraplegic patients who do or do not perform standing." In: *Osteoporosis International* 4.3 (1994), pp. 138–143. ISSN: 0937941X. DOI: 10.1007/BF01623058.

[9] R. J. Jaeger, G. M. Yarkony, and E. J. Roth. *Rehabilitation technology for standing and walking after spinal cord injury*. 1989. DOI: 10.1097/00002060-198906000-00006.

[10] J. S. Walter, P. G. Sola, J. Sacks, Y. Lucero, E. Langbein, and F. Weaver. "Indications for a home standing program for individuals with spinal cord injury." In: *Journal of Spinal Cord Medicine* 22.3 (1999), pp. 152–158. ISSN: 10790268. DOI: 10.1080/10790268.1999.11719564.

[11] M. Arazpour, M. A. Bani, S. W. Hutchins, and R. K. Jones. "The physiological cost index of walking with mechanical and powered gait orthosis in patients with spinal cord injury." In: *Spinal Cord* 51.5 (2013), pp. 356–359. ISSN: 13624393. DOI: 10.1038/sc.2012.162.

[12] L. Noreau, C. L. Richards, F. Comeau, and D. Tardif. "Biomechanical analysis of swing-through gait in paraplegic and non-disabled individuals." In: *Journal of Biomechanics* 28.6 (1995), pp. 689–700. ISSN: 00219290. DOI: 10.1016/0021-9290(94)00118-N.

[13] E. Melis, R Torres-Moreno, H Barbeau, and E. Lemaire. "Analysis of assisted-gait characteristics in persons with incomplete spinal cord injury." In: *Spinal Cord* 37.6 (1999), pp. 430–439. ISSN: 1362-4393. DOI: 10.1038/sj.sc.3100850. URL: http://ovidsp.ovid.com/ovidweb.cgi?T=JS{\&}PAGE=reference{\&}D=emed4{\&}NEWS=N{\&}AN=1999237591http://www.nature.com/articles/3100850.

[14] T. N. Bryce, M. P. Dijkers, and A. J. Kozlowski. "Framework for assessment of the usability of lower-extremity robotic exoskeletal orthoses." In: *American Journal of Physical Medicine and Rehabilitation* 94.11 (2015), pp. 1000–1014. ISSN: 15377385. DOI: 10.1097/PHM.0000000000000321.

[15] J. Kressler, C. K. Thomas, E. C. Field-Fote, J. Sanchez, E. Widerström-Noga, D. C. Cilien, K. Gant, K. Ginnety, H. Gonzalez, A. Martinez, K. D. Anderson, and M. S. Nash. "Understanding therapeutic benefits of overground bionic ambulation: Exploratory case series in persons with chronic, complete spinal cord injury." In: *Archives of Physical Medicine and Rehabilitation* 95.10 (2014), 1878–1887.e4. ISSN: 1532821X. DOI: 10.1016/j.apmr.2014.04.026. URL: http://dx.doi.org/10.1016/j.apmr.2014.04.026.

[16] A. Esquenazi, M. Talaty, A. Packel, and M. Saulino. "The Rewalk powered exoskeleton to restore ambulatory function to individuals with thoracic-level motor-complete spinal cord injury." In: *American Journal of Physical Medicine and Rehabilitation* 91.11 (2012), pp. 911–921. ISSN: 08949115. DOI: 10.1097/PHM.0b013e318269d9a3.

[17] A. Wall, J. Borg, and S. Palmcrantz. "Clinical application of the hybrid assistive limb (Hal) for gait training – A systematic review." In: *Frontiers in Systems Neuroscience* 9.MAR (2015). ISSN: 16625137. DOI: 10.3389/fnsys.2015.00048.

[18] H. Fritz, D. Patzer, and S. S. Galen. "Robotic exoskeletons for reengaging in everyday activities: promises, pitfalls, and opportunities." In: *Disability and Rehabilitation* 41.5 (2019), pp. 560–563. ISSN: 14645165. DOI: 10.1080/09638288.2017.1398786. URL: https://doi.org/10.1080/09638288.2017.1398786.

[19] V. Huynh, C. Bidard, and C. Chevallereau. "Balance control for an active leg exoskeleton based on human balance strategies." In: *Mechanisms and Machine Science* 48 (2018), pp. 197–211. ISSN: 22110992. DOI: 10.1007/978-3-319-59972-4_15.

[20] T. Bhatnagar, W. Ben Mortensen, J. Mattie, J. Wolff, C. Parker, and J. Borisoff. "A survey of stakeholder perspectives on a proposed combined exoskeleton-wheelchair technology." In: *IEEE International Conference on Rehabilitation Robotics* (2017), pp. 1574–1579. ISSN: 19457901. DOI: 10.1109/ICORR.2017.8009472.

[21] Y. Moon and J. J. Sosnoff. "Safe Landing Strategies During a Fall: Systematic Review and Meta-Analysis." In: *Archives of Physical Medicine and Rehabilitation* 98.4 (2017), pp. 783–794. ISSN: 1532821X. DOI: 10.1016/j.apmr.2016.08.460. URL: http://dx.doi.org/10.1016/j.apmr.2016.08.460.

[22] S. N. Robinovitch, L. Inkster, J. Maurer, and B. Warnick. "Strategies for Avoiding Hip Impact During Sideways Falls." In: *Journal of Bone and Mineral Research* 18.7 (2003), pp. 1267–1273. ISSN: 08840431. DOI: 10.1359/jbmr.2003.18.7.1267. arXiv: arXiv:1011.1669v3.

[23] B. E. Groen, V. Weerdesteyn, and J. Duysens. "Martial arts fall techniques decrease the impact forces at the hip during sideways falling." In: *Journal of Biomechanics* 40.2 (2007), pp. 458–462. ISSN: 00219290. DOI: 10.1016/j.jbiomech.2005.12.014.

[24] D. A. Umphred, G. U. Burton, R. T. Lazaro, and M. L. Roller. *Umphred'S Neurological Rehabilitation*. Ed. by D. A. Umphred, G. U. Burton, R. T. Lazaro, and M. L. Roller. 6th. Elsevier, 2013, pp. 459–520. ISBN: 9780323075862.

[25] S. Darwish, A. I. Tsirikos, and S. Maguire. "Rehabilitation following spinal cord injury." In: *Orthopaedics and Trauma* 34.5 (2020), pp. 315–319. ISSN: 18771335. DOI: 10.1016/j.mporth.2020.06.009. URL: https://doi.org/10.1016/j.mporth.2020.06.009.

[26] S. C. Kirshblum, W. Waring, F. Biering-Sorensen, S. P. Burns, M. Johansen, M. Schmidt-Read, W. Donovan, D. Graves, A. Jha, L. Jones, M. J. Mulcahey, and A. Krassioukov. "International standards for neurological classification of spinal cord injury (Revised 2011)." In: *Journal of Spinal Cord Medicine* 34.6 (2011), pp. 535–546. ISSN: 10790268. DOI: 10.1179/107902611X13186000420242.

[27] National Spinal Cord Injury Statistical Center. "Spinal Cord Injury Facts and Figures at a Glance." In: *National Spinal Cord Injury Statistical Center* (2020). URL: https://www.nscisc.uab.edu/Public/FactsandFigures-2021.pdf.

[28] Y. Kang, H. Ding, H. Zhou, Z. Wei, L. Liu, D. Pan, and S. Feng. "Epidemiology of worldwide spinal cord injury: a literature review." In: *Journal of Neurorestoratology* Volume 6 (2018), pp. 1–9. ISSN: 2324-2426. DOI: 10.2147/jn.s143236.

[29] H. Food and Drug Administration. "Medical devices; physical medicine devices; classification of the powered lower extremity exoskeleton; republication. Final order; republication." In: *Federal register* 80.85 (2015), pp. 25226–30. ISSN: 0097-6326. URL: http://www.ncbi.nlm.nih.gov/pubmed/25985478.

[30] H. Van Der Kooij, J. Veneman, and R. Ekkelenkamp. "Design of a compliantly actuated exo-skeleton for an impedance controlled gait trainer robot." In: *Annual International Conference of the IEEE Engineering in Medicine and Biology - Proceedings* (2006), pp. 189–193. ISSN: 05891019. DOI: 10.1109/IEMBS.2006.259397.

[31] M. Khalili, J. F. Borisoff, and M. H. V. Der. "The Importance Of Studying Safe-Fall Strategies For Lower Limb Exoskeletons Institute of Technology." In: *Resna* (2017), pp. 1–5.

[32] S. E. Lamb, E. C. Jørstad-Stein, K. Hauer, and C. Becker. "Development of a common outcome data set for fall injury prevention trials: The Prevention of Falls Network Europe consensus." In: *Journal of the American Geriatrics Society* 53.9 (2005), pp. 1618–1622. ISSN: 00028614. DOI: 10.1111/j.1532-5415.2005.53455.x.

[33] National Center for Injurty Prevention and Control. *10 Leading Causes of Nonfatal Injuries, United States*. 2019. URL: http://www.cdc.gov/injury/wisqars/LeadingCauses.html (visited on 12/05/2020).

[34] S. Deandrea, E. Lucenteforte, F. Bravi, R. Foschi, C. La Vecchia, and E. Negri. "Risk factors for falls in community-dwelling older people: A systematic review and meta-analysis." In: *Epidemiology* 21.5 (2010), pp. 658–668. ISSN: 10443983. DOI: 10.1097/EDE.0b013e3181e89905.

[35] E. R. Burns, J. A. Stevens, and R. Lee. "The direct costs of fatal and non-fatal falls among older adults — United States." In: *Journal of Safety Research* 58 (2016), pp. 99–103. DOI: 10.1016/j.jsr.2016.05.001..

[36] B. Stubbs, S. Brefka, and M. D. Denkinger. "What works to prevent falls in community-dwelling older adults? Umbrella review of meta-analyses of randomized controlled trials." In: *Physical Therapy* 95.8 (2015), pp. 1095–1110. ISSN: 15386724. DOI: 10.2522/ptj.20140461.

[37] E. T. Hsiao and S. N. Robinovitch. "Common protective movements govern unexpected falls from standing height." In: *Journal of Biomechanics* 31.1 (1997), pp. 1–9. ISSN: 00219290. DOI: 10.1016/S0021-9290(97)00114-0.

[38] J. S. Tan, J. J. Eng, S. N. Robinovitch, and B. Warnick. "Wrist impact velocities are smaller in forward falls than backward falls from standing." In: *Journal of Biomechanics* 39.10 (2006), pp. 1804–1811. ISSN: 00219290. DOI: 10.1016/j.jbiomech.2005.05.016.

[39] S. N. Robinovitch, R. Brumer, and J. Maurer. "Effect of the "squat protective response"on impact velocity during backward falls." In: *Journal of Biomechanics* 37.9 (2004), pp. 1329–1337. ISSN: 00219290. DOI: 10.1016/j.jbiomech.2003.12.015.

[40] P. H. Chou, Y. L. Chou, C. J. Lin, F. C. Su, S. Z. Lou, C. F. Lin, and G. F. Huang. "Effect of elbow flexion on upper extremity impact forces during a fall." In: *Clinical Biomechanics* 16.10 (2001), pp. 888–894. ISSN: 02680033. DOI: 10.1016/S0268-0033(01)00086-9.

[41] J. Lo, G. N. McCabe, K. M. DeGoede, H. Okuizumi, and J. A. Ashton-Miller. "On reducing hand impact force in forward falls: Results of a brief intervention in young males." In: *Clinical Biomechanics* 18.8 (2003), pp. 730–736. ISSN: 02680033. DOI: 10.1016/S0268-0033(03)00124-4.

[42] F. Feldman and S. N. Robinovitch. "Reducing hip fracture risk during sideways falls : Evidence in young adults of the protective effects of impact to the hands and stepping." In: *Journal of Biomechanics* 40 (2007), pp. 2612–2618. DOI: 10.1016/j.jbiomech.2007.01.019.

[43] M. Sabick, J. Hay, V. Goel, and S. Banks. "Active responses decrease impact forces at the hip and shoulder in falls to the side." In: *Journal of Biomechanics* 32.9 (1999), pp. 993–998. ISSN: 00219290. DOI: 10.1016/S0021-9290(99)00079-2. URL: https://linkinghub.elsevier.com/retrieve/pii/S0021929099000792.

[44] A. J. van den Kroonenberg, W. C. Hayes, and T. A. McMahon. "Hip Impact Velocities and Body Configurations for Voluntary Falls from Standing Height." In: *Journal of Biomechanics* 29.6 (1996), pp. 807–811.

[45] B. E. Groen, S. Maartenskliniek, E. Smulders, and D. de Kam. "Martial arts fall training to prevent hip fractures in the elderly." In: *Osteoporosis International* 21 (2010). DOI: 10.1007/s00198-009-0934-x.

[46] V Weerdesteyn, B. E. Groen, R van Swigchem, and J. Duysens. "Martial arts fall techniques reduce hip impact forces in naive subjects after a brief period of training." In: *Journal of Electromyography and Kinesiology* 18 (2008), pp. 235–242. DOI: 10.1016/j.jelekin.2007.06.010.

[47] A. M. V. D. Zijden, B. E. Groen, E Tanck, B Nienhuis, N Verdonschot, and V Weerdesteyn. "Can martial arts techniques reduce fall severity ? An in vivo study of femoral loading configurations in sideways falls." In: *Journal of Biomechanics* 45.9 (2012), pp. 1650–1655. ISSN: 0021-9290. DOI: 10.1016/j.jbiomech.2012.03.024. URL: http://dx.doi.org/10.1016/j.jbiomech.2012.03.024.

[48] F. C. Anderson and M. G. Pandy. "A dynamic optimization solution for vertical jumping in three dimensions." In: *Computer Methods in Biomechanics and Biomedical Engineering* 2.3 (1999), pp. 201–231. ISSN: 10255842. DOI: 10.1080/10255849908907988.

[49] M. G. Pandy and F. E. Zajac. "Optimal muscular coordination strategies for jumping." In: *Journal of Biomechanics* 24.1 (1991), pp. 1–10. ISSN: 00219290. DOI: 10.1016/0021-9290(91)90321-D.

[50] M. G. Pandy, F. E. Zajac, E. Sim, and W. S. Levine. "An optimal control model for maximum-height human jumping." In: *Journal of Biomechanics* 23.12 (1990), pp. 1185–1198. ISSN: 00219290. DOI: 10.1016/0021-9290(90)90376-E.

[51] T. Spägele, A. Kistner, and A. Gollhofer. "Modelling, simulation and optimisation of a human vertical jump." In: *Journal of Biomechanics* 32.5 (1999), pp. 521–530. ISSN: 00219290. DOI: 10.1016/S0021-9290(98)00145-6.

[52] F. C. Anderson and M. G. Pandy. "Static and dynamic optimization solutions for gait are practically equivalent." In: *Journal of Biomechanics* 34.2 (2001), pp. 153–161. ISSN: 00219290. DOI: 10.1016/S0021-9290(00)00155-X. URL: https://linkinghub.elsevier.com/retrieve/pii/S002192900000155X.

[53] G. T. Yamaguchi and F. E. Zajac. "Restoring Unassisted Natural Gait to Paraplegics Via Functional Neuromuscular Stimulation: A Computer Simulation Study." In: *IEEE Transactions on Biomedical Engineering* 37.9 (1990), pp. 886–902. ISSN: 15582531. DOI: 10.1109/10.58599.

[54] M. G. Pandy, B. A. Garner, and F. C. Anderson. "Optimal Control of Non-ballistic Muscular Movements: A constraint-based performance criterion for rising from a chair." In: *Journal of Biomechanical Engineering* 117.1 (1995), pp. 15–26. ISSN: 15288951. DOI: 10.1115/1.2792265.

[55] M. L. Kaplan and J. H. Heegaard. "Predictive algorithms for neuromuscular control of human locomotion." In: *Journal of Biomechanics* 34.8 (2001), pp. 1077–1083. ISSN: 00219290. DOI: 10.1016/S0021-9290(01)00057-4.

[56] G. Khang and F. Zajac. "Paraplegic standing controlled by functional neuromuscular stimulation. I. Computer model and control-system design." In: *IEEE Transactions on Biomedical Engineering* 36.9 (1989), pp. 873–884. ISSN: 00189294. DOI: 10.1109/10.35296. URL: http://ieeexplore.ieee.org/document/35296/.

[57] C. E. Bauby and A. D. Kuo. "Active control of lateral balance in human walking." In: *Journal of Biomechanics* 33.11 (2000), pp. 1433–1440. ISSN: 00219290. DOI: 10.1016/S0021-9290(00)00101-9.

[58] A. D. Gardner, J. Potgieter, and F. K. Noble. "A review of commercially available exoskeletons' capabilities." In: *2017 24th International Conference on Mechatronics and Machine Vision in Practice, M2VIP 2017* 2017-Decem (2017), pp. 1–5. DOI: 10.1109/M2VIP.2017.8211470.

[59] Food and Drug Administration. *510k Summary for the Indego exoskeleton*. Tech. rep. PSC Publishing Services, 2018. URL: https://www.accessdata.fda.gov/cdrh{_}docs/pdf17/K173530.pdf.

[60] S. Wang, L. Wang, C. Meijneke, E. Van Asseldonk, T. Hoellinger, G. Cheron, Y. Ivanenko, V. La Scaleia, F. Sylos-Labini, M. Molinari, F. Tamburella, I. Pisotta, F. Thorsteinsson, M. Ilzkovitz, J. Gancet, Y. Nevatia, R. Hauffe, F. Zanow, and H. Van Der Kooij. "Design and Control of the MINDWALKER Exoskeleton." In: *IEEE Transactions on Neural Systems and Rehabilitation Engineering* 23.2 (2015), pp. 277–286. ISSN: 15344320. DOI: 10.1109/TNSRE.2014.2365697.

[61] A. L. Hof. "The 'extrapolated center of mass' concept suggests a simple control of balance in walking." In: *Human Movement Science* 27.1 (2008), pp. 112–125. ISSN: 01679457. DOI: 10.1016/j.humov.2007.08.003.

[62] J. H. Jung, I. Gutiérrez, and J. Veneman. "The use of Centroidal Momentum Analysis for defining a Stability Index for walking with an exoskeleton." In: *TAR 2015: Technically Assisted Rehabilitation Conference*. 2015, pp. 1–4.

[63] J. H. Jung and J. F. Veneman. "Real time computation of Centroidal Momentum while human walking in the lower limbs rehabilitation exoskeleton: Preliminary trials." In: *IEEE International Conference on Rehabilitation Robotics* 2019-June (2019), pp. 721–726. ISSN: 19457901. DOI: 10.1109/ICORR.2019.8779441.

[64] B. Griffin and J. Grizzle. "Walking gait optimization for accommodation of unknown terrain height variations." In: *Proceedings of the American Control Conference* 2015-July (2015), pp. 4810–4817. ISSN: 07431619. DOI: 10.1109/ACC.2015.7172087.

[65] K. Galloway, K. Sreenath, A. D. Ames, and J. W. Grizzle. "Torque saturation in bipedal robotic walking through control Lyapunov function-based quadratic programs." In: *IEEE Access* 3 (2015), pp. 323–332. ISSN: 21693536. DOI: 10.1109/ACCESS.2015.2419630. arXiv: 1302.7314.

[66] Q. Nguyen and K. Sreenath. "Optimal robust control for bipedal robots through control lyapunov function based quadratic programs." In: *Robotics: Science and Systems* 11 (2015). ISSN: 2330765X. DOI: 10.15607/RSS.2015.XI.048.

[67] O. Harib, A. Hereid, A. Agrawal, T. Gurriet, S. Finet, G. Boéris, A. Duburcq, M. E. Mungai, M. Masselin, A. D. Ames, K. Sreenath, and J. W. Grizzle. "Feedback Control of an Exoskeleton for Paraplegics: Toward Robustly Stable, Hands-Free Dynamic Walking." In: *IEEE Control Systems* 38.6 (2018), pp. 61–87. ISSN: 1941000X. DOI: 10.1109/MCS.2018.2866604. arXiv: 1802.08322.

[68] R. Baud, J. Fasola, T. Vouga, A. Ijspeert, and M. Bouri. "Bio-inspired standing balance controller for a full-mobilization exoskeleton." In: *IEEE International Conference on Rehabilitation Robotics* 2019-June (2019), pp. 849–854. ISSN: 19457901. DOI: 10.1109/ICORR.2019.8779440.

[69] J. Fasola, T. Vouga, R. Baud, H. Bleuler, and M. Bouri. "Balance control strategies during standing in a locked-ankle passive exoskeleton." In: *IEEE International Conference on Rehabilitation Robotics* 2019-June.June (2019), pp. 593–598. ISSN: 19457901. DOI: 10.1109/ICORR.2019.8779500.

[70] C. Bayon, A. R. Emmens, M. Afschrift, T. Van Wouwe, A. Q. Keemink, H. Van Der Kooij, and E. H. Van Asseldonk. "Can Momentum-Based Control Predict Human Balance Recovery Strategies?" In: *IEEE Transactions on Neural Systems and Rehabilitation Engineering* 28.9 (2020), pp. 2015–2024. ISSN: 15580210. DOI: 10.1109/TNSRE.2020.3005455.

[71] S. Mohammed and Y. Amirat. "Towards intelligent lower limb wearable robots: Challenges and perspectives - state of the art." In: *2008 IEEE International Conference on Robotics and Biomimetics, ROBIO 2008* (2009), pp. 312–317. DOI: 10.1109/ROBIO.2009.4913022.

[72] M. Khalili, J. F. Borisoff, and H. F. Van Der Loos. "Developing safe fall strategies for lower limb exoskeletons." In: *IEEE International Conference on Rehabilitation Robotics* (2017), pp. 314–319. ISSN: 19457901. DOI: 10.1109/ICORR.2017.8009266.

[73] M. Khalili, H. F. Machiel Van Der Loos, and J. F. Borisoff. "Studies on practical applications of safe-fall control strategies for lower limb exoskeletons." In: *IEEE International Conference on Rehabilitation Robotics* 2019-June (2019), pp. 536–541. ISSN: 19457901. DOI: 10.1109/ICORR.2019.8779382.

[74] S. N. Robinovitch, J. Chiu, R. Sandler, and Q. Liu. "Impact severity in self-initiated sits and falls associates with center-of-gravity excursion during descent." In: *Journal of Biomechanics* 33.7 (2000), pp. 863–870. ISSN: 00219290. DOI: 10.1016/S0021-9290(00)00025-7.

[75] R. Sandler and S. Robinovitch. "An analysis of the effect of lower extremity strength on impact severity during a backward fall." In: *Journal of Biomechanical Engineering* 123.6 (2001), pp. 590–598. ISSN: 01480731. DOI: 10.1115/1.1408940.

[76] A. J. van den Kroonenberg, W. C. Hayes, and T. A. McMahon. "Dynamic models for sideways falls from standing height." In: *Journal of Biomechanical Engineering* 117.3 (1995), pp. 309–318. ISSN: 15288951. DOI: 10.1115/1.2794186.

[77] P. Di, J. Huang, S. Nakagawa, K. Sekiyama, and T. Fukuda. "Fall detection and prevention in the elderly based on the ZMP stability control." In: *Proceedings of IEEE Workshop on Advanced Robotics and its Social Impacts, ARSO* (2013), pp. 82–87. ISSN: 21627568. DOI: 10.1109/ARSO.2013.6705510.

[78] J. Huang, W. Xu, S. Mohammed, and Z. Shu. "Posture estimation and human support using wearable sensors and walking-aid robot." In: *Robotics and Autonomous Systems* 73 (2015), pp. 24–43. ISSN: 09218890. DOI: 10.1016/j.robot.2014.11.013. URL: http://dx.doi.org/10.1016/j.robot.2014.11.013.

[79] H. J. Lee and L. S. Chou. "Detection of gait instability using the center of mass and center of pressure inclination angles." In: *Archives of Physical Medicine and Rehabilitation* 87.4 (2006), pp. 569–575. ISSN: 00039993. DOI: 10.1016/j.apmr.2005.11.033.

[80] M. Zhou, S. Wang, Y. Chen, Z. Chen, and Z. Zhao. "An activity transition based fall detection model on mobile devices." In: *Lecture Notes in Electrical Engineering* 182 LNEE (2012), pp. 1–8. ISSN: 18761100. DOI: 10.1007/978-94-007-5086-9_1.

[81] D. A. Winter. *Biomechanics and Motor Control of Human Movement: Fourth Edition*. 4th. John Wiley & Sons, Inc, 2009, pp. 82–106. ISBN: 9780470398180. DOI: 10.1002/9780470549148.

[82] D. P. Atherton and S. Majhi. "Limitations of PID controllers." In: *Proceedings of the American Control Conference* 6.June (1999), pp. 3843–3847. ISSN: 07431619. DOI: 10.1109/acc.1999.786236.

[83] J. H. Park, S. W. Sung, and I. B. Lee. "An enhanced PID control strategy for unstable processes." In: *Automatica* 34.6 (1998), pp. 751–756. ISSN: 00051098. DOI: 10.1016/S0005-1098(97)00235-5.

[84] C. C. Valentine and M. Chidambaram. "PID control of unstable time delay systems." In: *Chemical Engineering Communications* 162.November 2014 (1997), pp. 63–74. ISSN: 00986445. DOI: 10.1080/00986449708936632.

[85] W. J. Choi, J. M. Wakeling, and S. N. Robinovitch. "Kinematic analysis of video-captured falls experienced by older adults in long-term care." In: *Journal of Biomechanics* 48.6 (2015), pp. 911–920. ISSN: 18732380. DOI: 10.1016/j.jbiomech.2015.02.025. URL: http://dx.doi.org/10.1016/j.jbiomech.2015.02.025.

[86] Q. Mascret, M. Bielmann, C. L. Fall, L. J. Bouyer, and B. Gosselin. "Real-Time Human Physical Activity Recognition with Low Latency Prediction Feedback Using Raw IMU Data." In: *Proceedings of the Annual International Conference of the IEEE Engineering in Medicine and Biology Society, EMBS* 2018-July (2018), pp. 239–242. ISSN: 1557170X. DOI: 10.1109/EMBC.2018.8512252.

[87] T. Muender and T. Röfer. "Model-Based Fall Detection and Fall Prevention for Humanoid Robots." In: *Lecture Notes in Computer Science*. Vol. 11175. Springer, Cham, 2018, pp. 312–324. ISBN: 9783030003081. DOI: 10.1007/978-3-030-00308-1_26. URL: http://link.springer.com/10.1007/978-3-030-00308-1{_}26.

[88] V. C. V. Kumar, S. Ha, G. Sawicki, and C. K. Liu. "Learning a Control Policy for Fall Prevention on an Assistive Walking Device." In: (2019). arXiv: 1909.10488. URL: http://arxiv.org/abs/1909.10488.

[89] Q. Yan, J. Huang, and Z. Luo. "Human-robot coordination stability for fall detection and prevention using cane robot." In: *2016 International Symposium on Micro-NanoMechatronics and Human Science, MHS 2016* 1 (2017). DOI: 10.1109/MHS.2016.7824171.

[90] M. Geravand, W. Rampeltshammer, and A. Peer. "Control of mobility assistive robot for human fall prevention." In: *IEEE International Conference on Rehabilitation Robotics* 2015-Septe (2015), pp. 882–887. ISSN: 19457901. DOI: 10.1109/ICORR.2015.7281314.

Appendix

Initial Positions and Joint Angles

Initial Position Diagram	Joint Angles (deg)
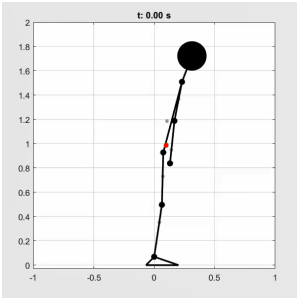	Ankle Joint: -8 Knee Joint: 7 Hip Joint: -20
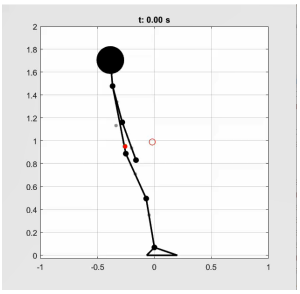	Ankle Joint: 10 Knee Joint: 15 Hip Joint: -20
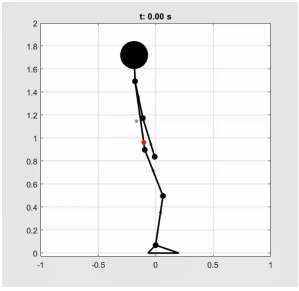	Ankle Joint: -8 Knee Joint: 30 Hip Joint: -20

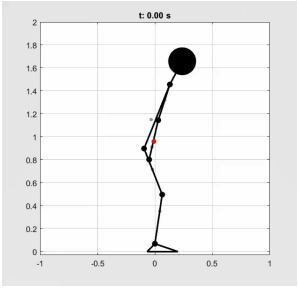	Ankle Joint: -8 Knee Joint: 30 Hip Joint: -50
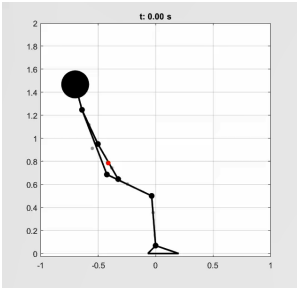	Ankle Joint: 5 Knee Joint: 60 Hip Joint: -50
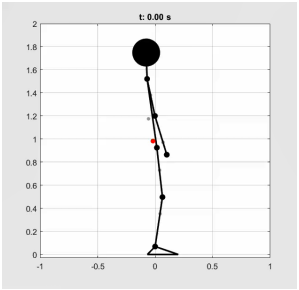	Ankle Joint: -8 Knee Joint: 15 Hip Joint: 5
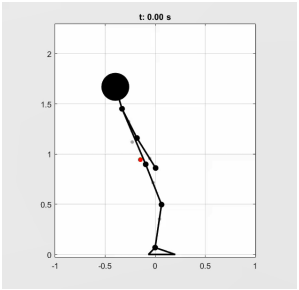	Ankle Joint: -8 Knee Joint: 30 Hip Joint: 5

Table A.1: Diagrams of the human-exoskeleton model's initial positions, and their respective joint angles.

APPENDIX B

Center of Mass Reference Tracking Results

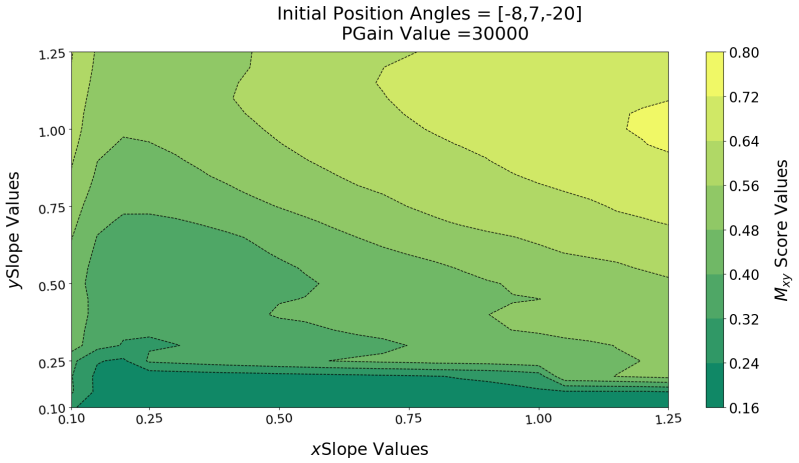

(a)

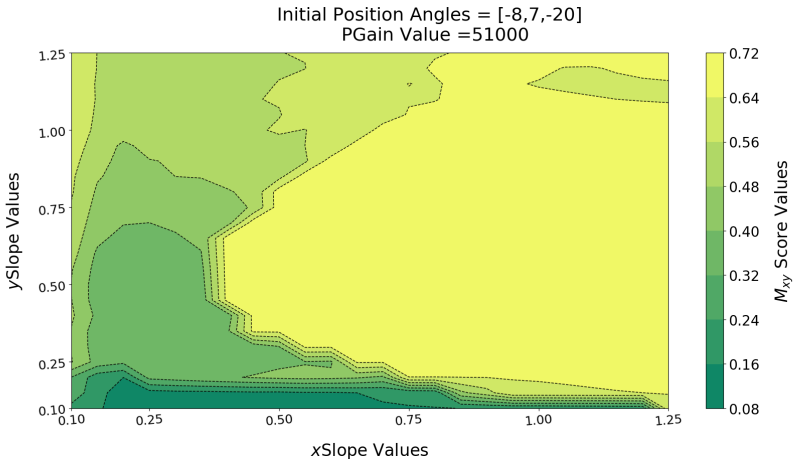

(b)

Figure B.1: Values of the $\mathcal{M}_{xy}$ Score for different combinations of xSlope and ySlope values.

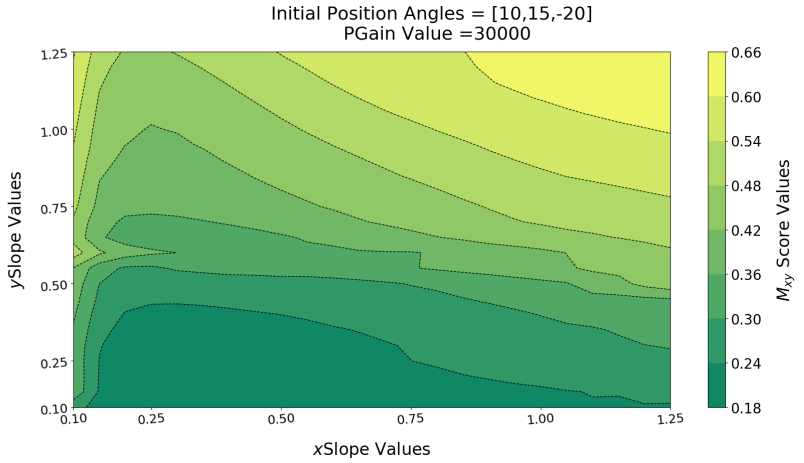

(c)

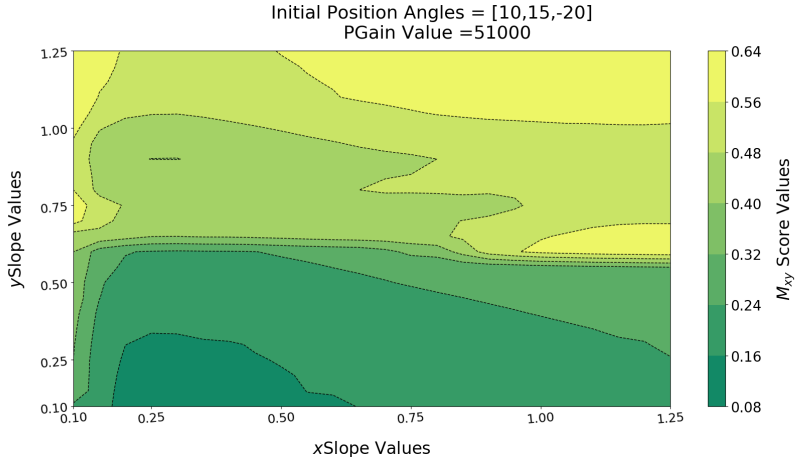

(d)

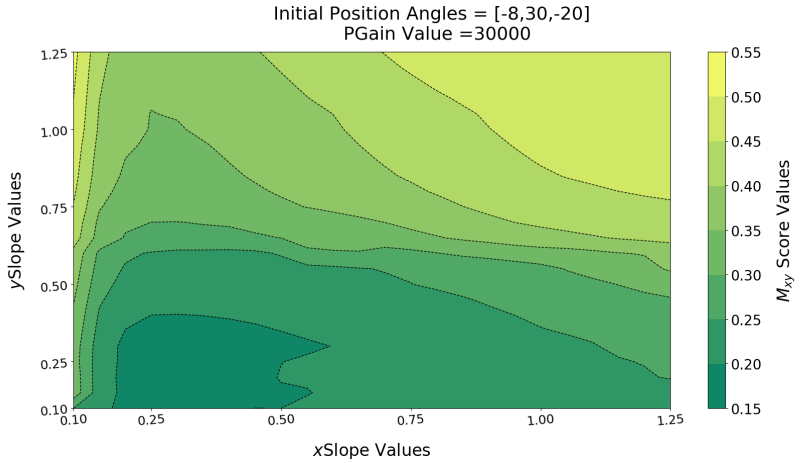

(e)

Figure B.1: Values of the $\mathcal{M}_{xy}$ Score for different combinations of xSlope and ySlope values.

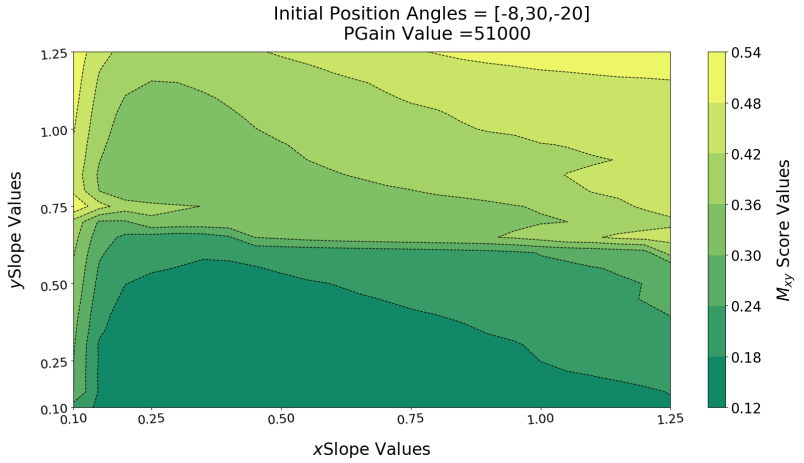

(f)

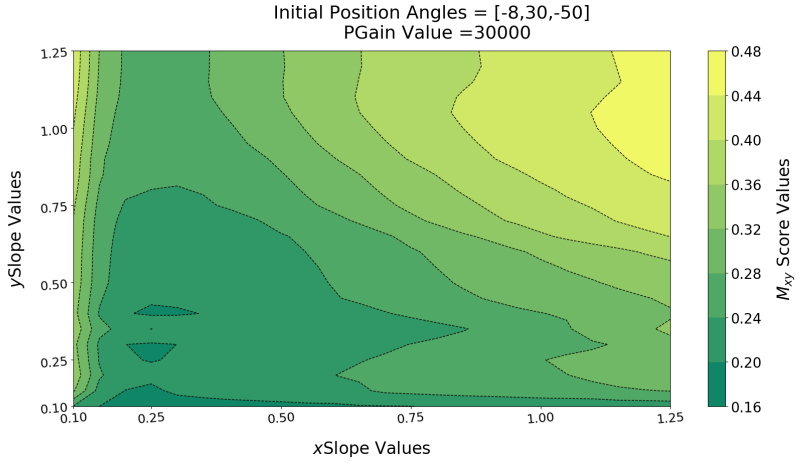

(g)

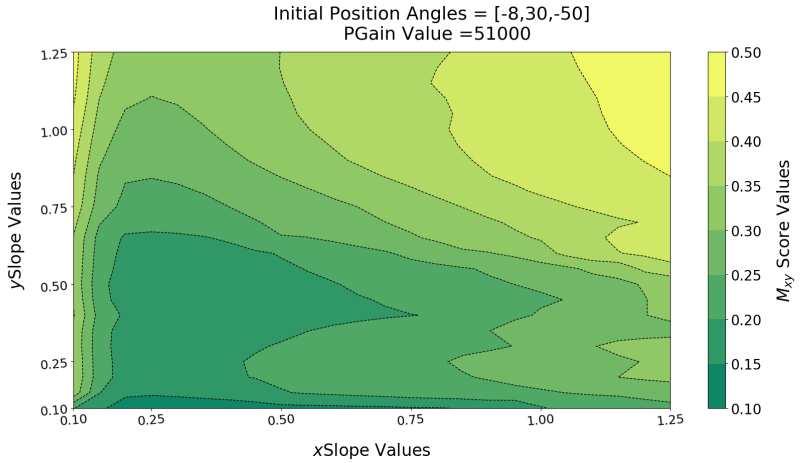

(h)

Figure B.1: Values of the $\mathcal{M}_{xy}$ Score for different combinations of xSlope and ySlope values.

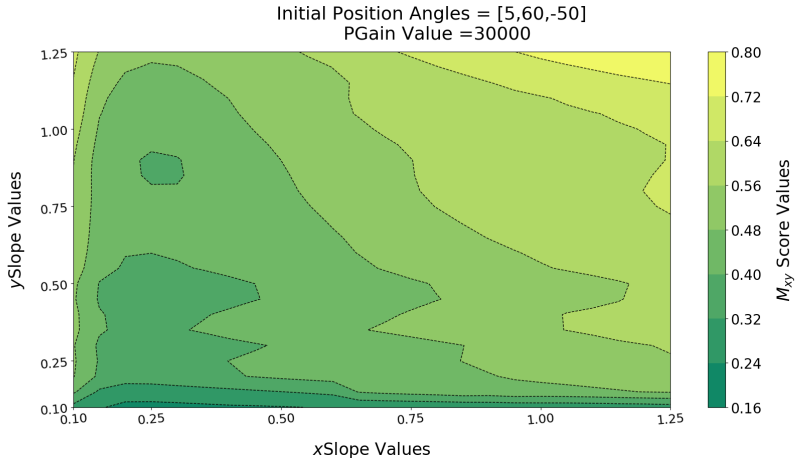

(i)

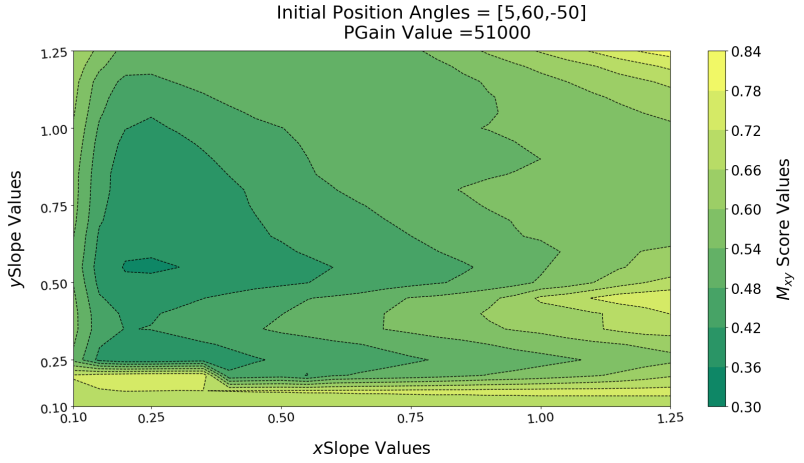

(j)

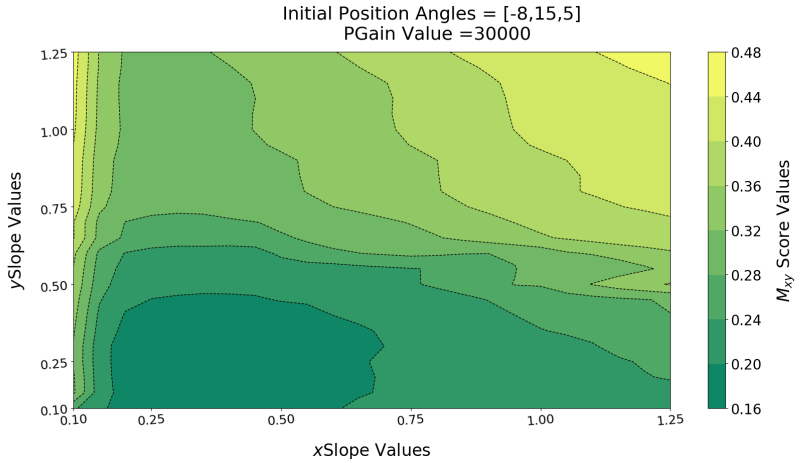

(k)

Figure B.1: Values of the $\mathcal{M}_{xy}$ Score for different combinations of xSlope and ySlope values.

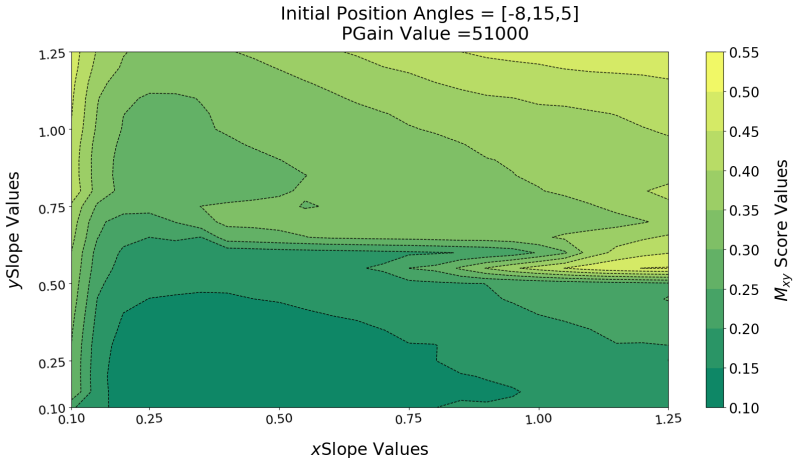

(l)

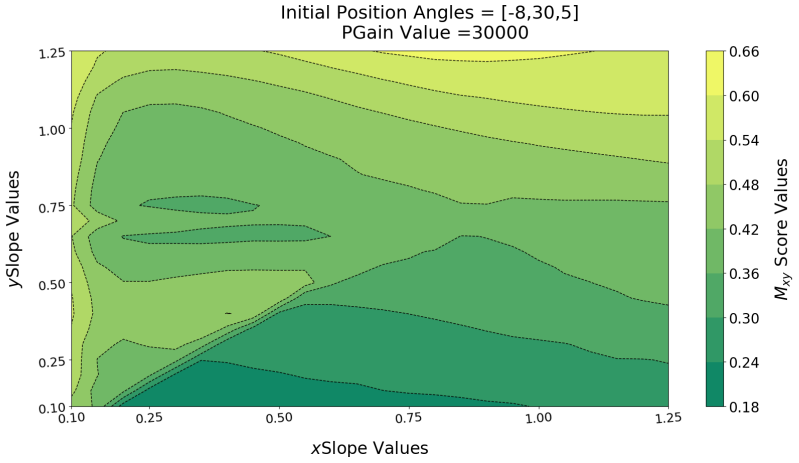

(m)

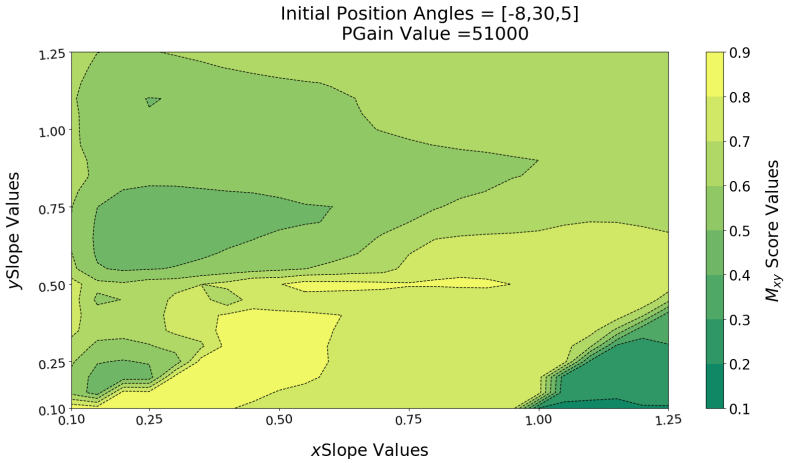

(n)

Figure B.1: Values of the $\mathcal{M}_{xy}$ Score for different combinations of xSlope and ySlope values.

APPENDIX C

Hip Joint Angle Reference Tracking Results

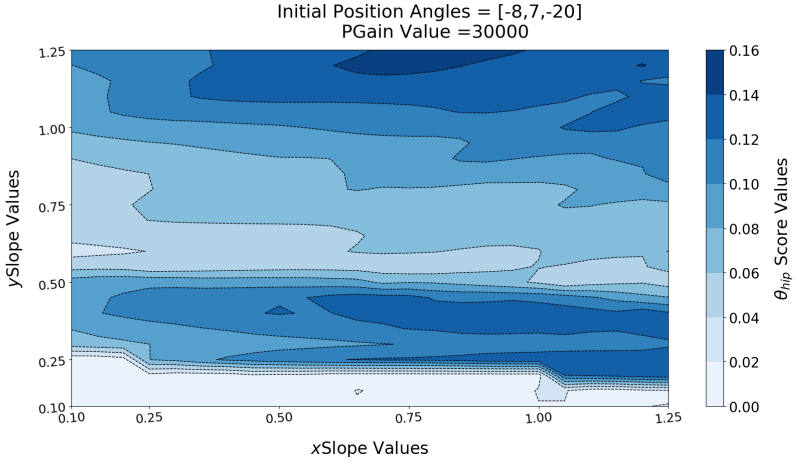

(a)

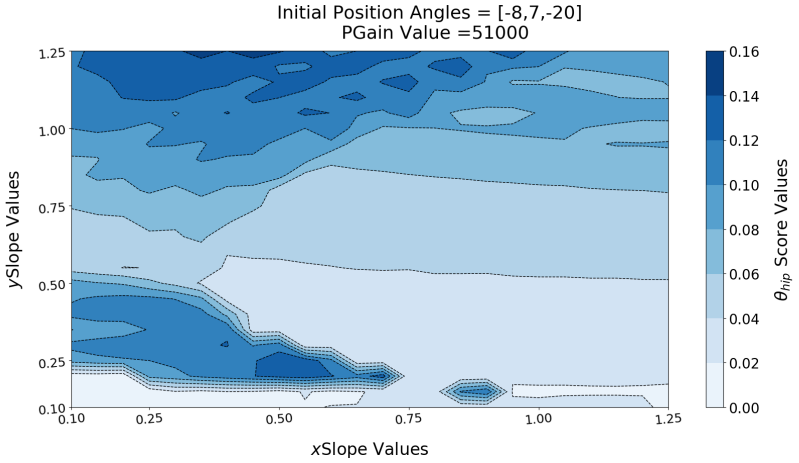

(b)

Figure C.1: Values of the θ_{hip} Score for different combinations of xSlope and ySlope values.

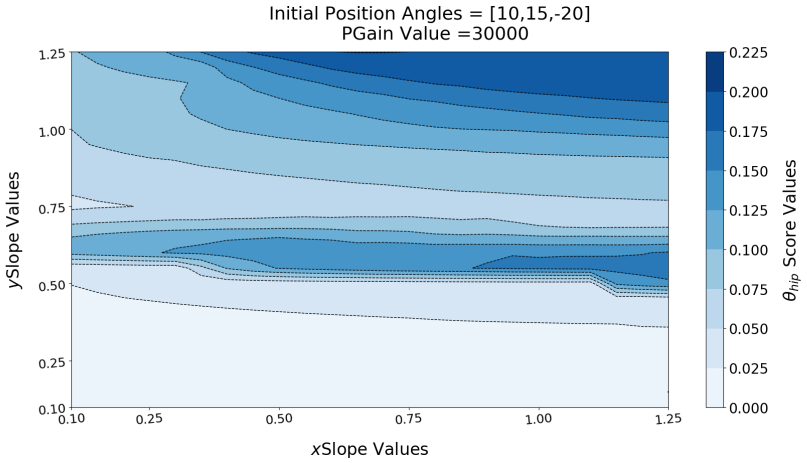

(c)

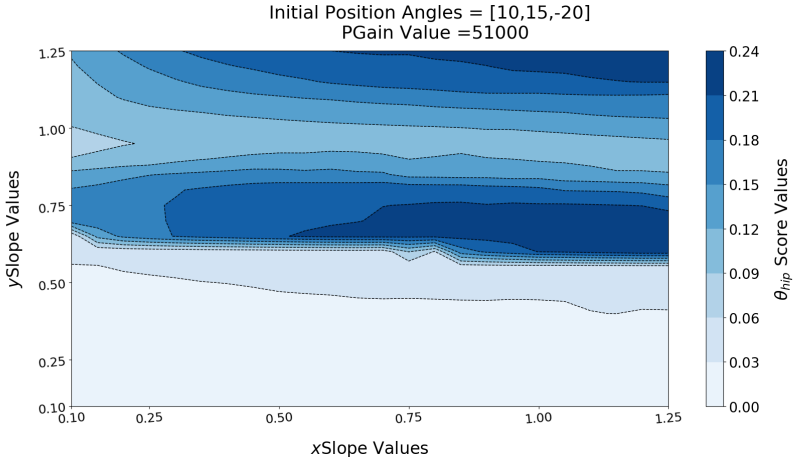

(d)

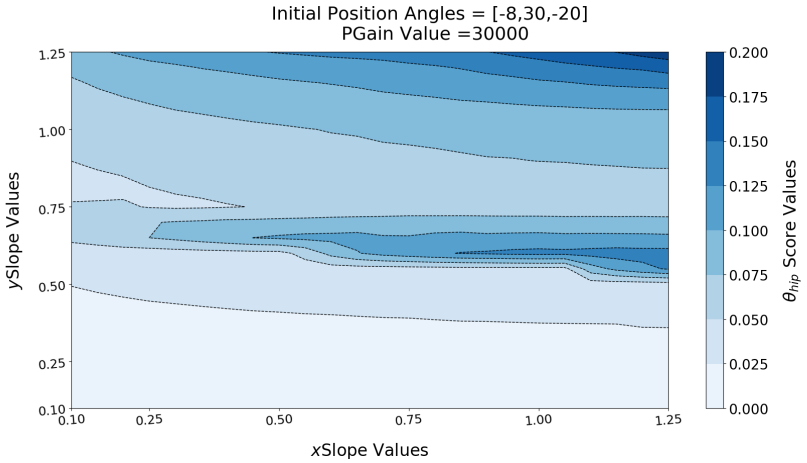

(e)

Figure C.1: Values of the θ_{hip} Score for different combinations of xSlope and ySlope values.

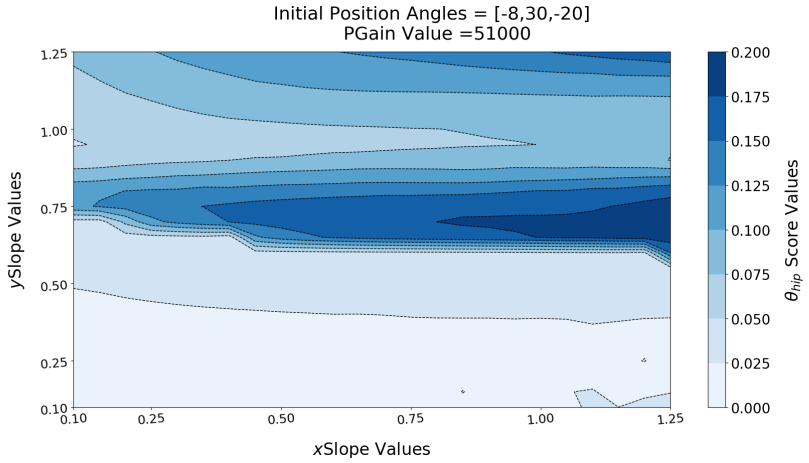

(f)

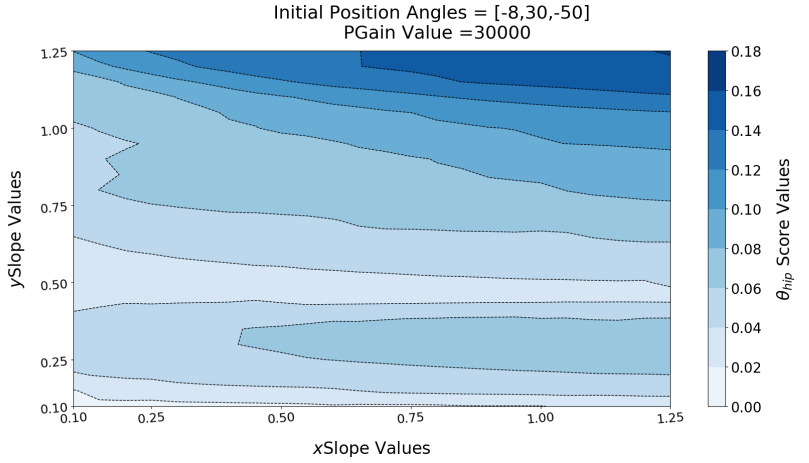

(g)

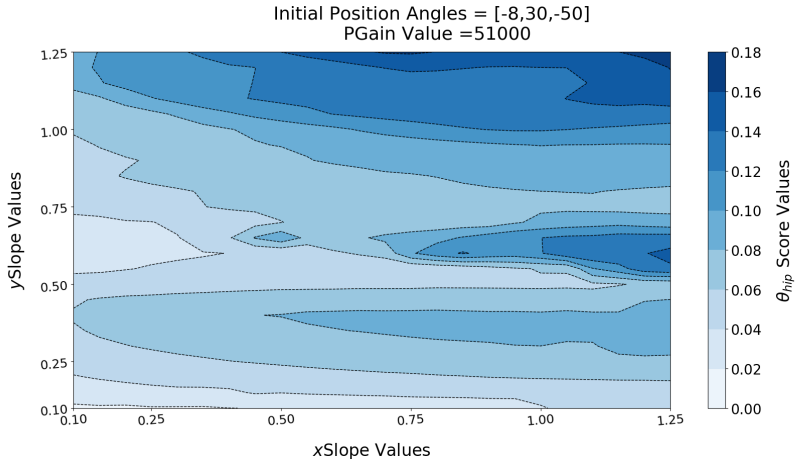

(h)

Figure C.1: Values of the θ_{hip} Score for different combinations of xSlope and ySlope values.

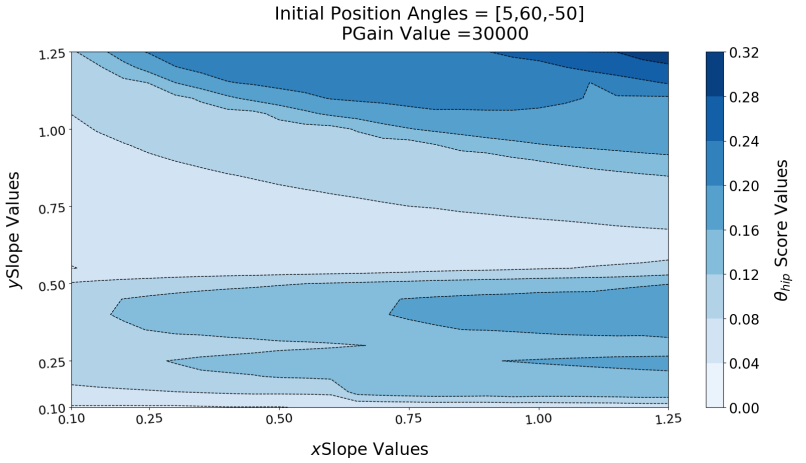

(i)

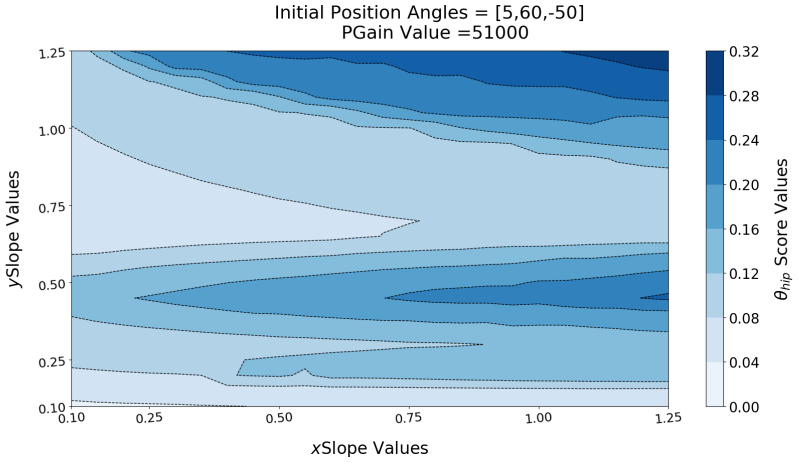

(j)

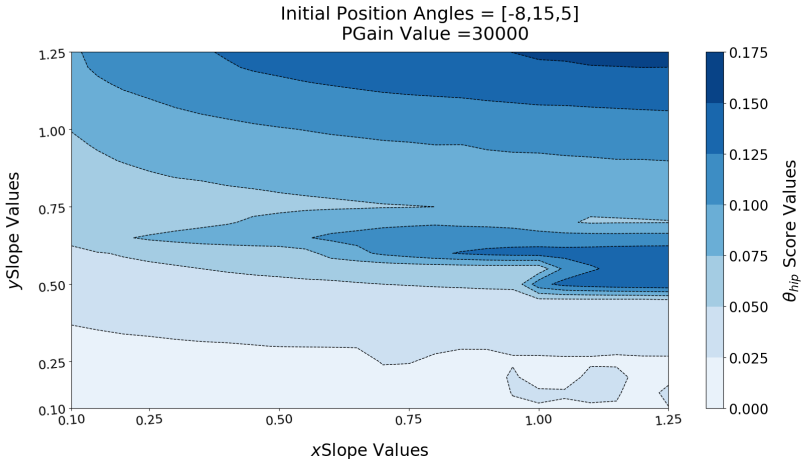

(k)

Figure C.1: Values of the θ_{hip} Score for different combinations of xSlope and ySlope values.

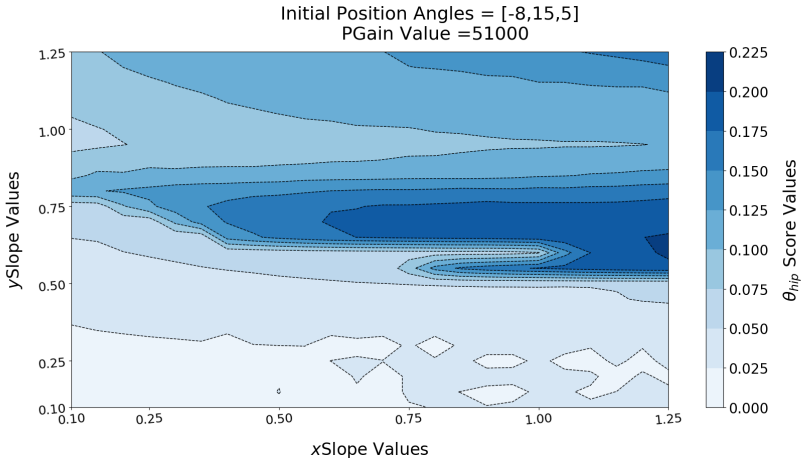

(l)

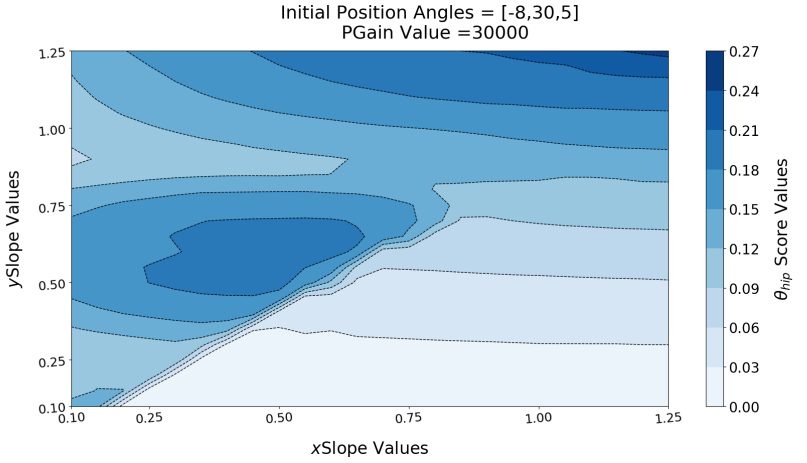

(m)

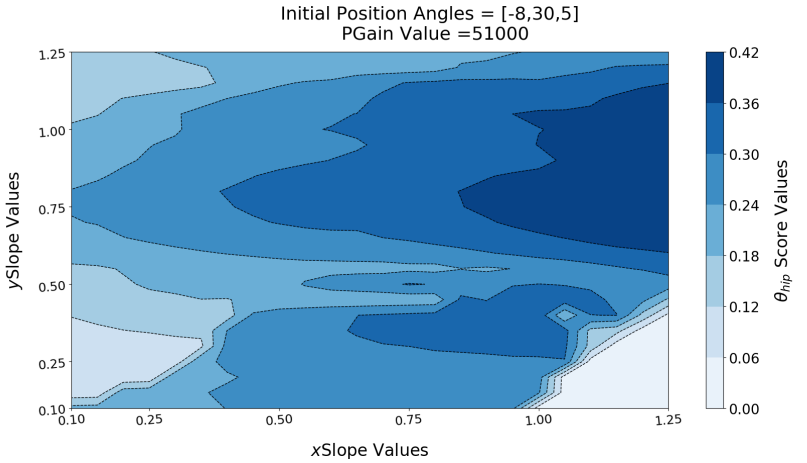

(n)

Figure C.1: Values of the θ_{hip} Score for different combinations of xSlope and ySlope values.

APPENDIX D

Average Joint Torque Integral Results

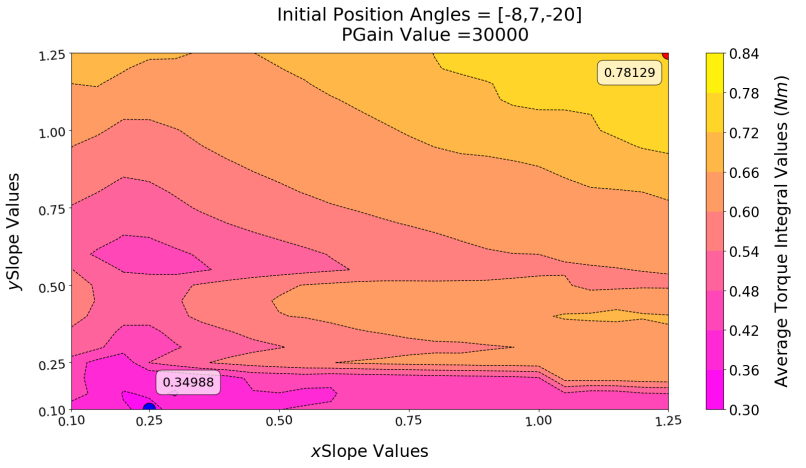

(a)

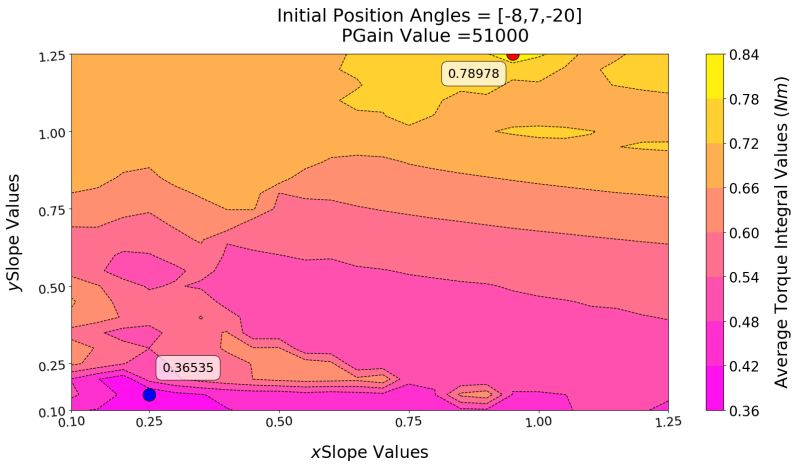

(b)

Figure D.1: Values of the average joint torque integral for different combinations of *x*Slope and *y*Slope values. The annotated values correspond to the highest (red) and lowest (blue) values.

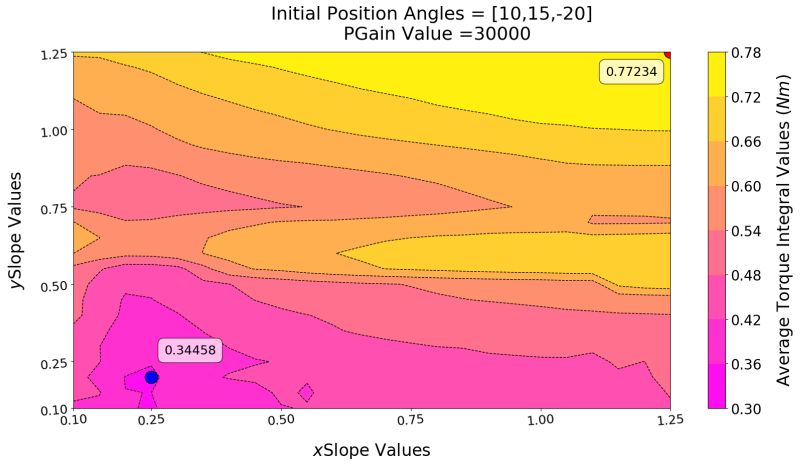

(c)

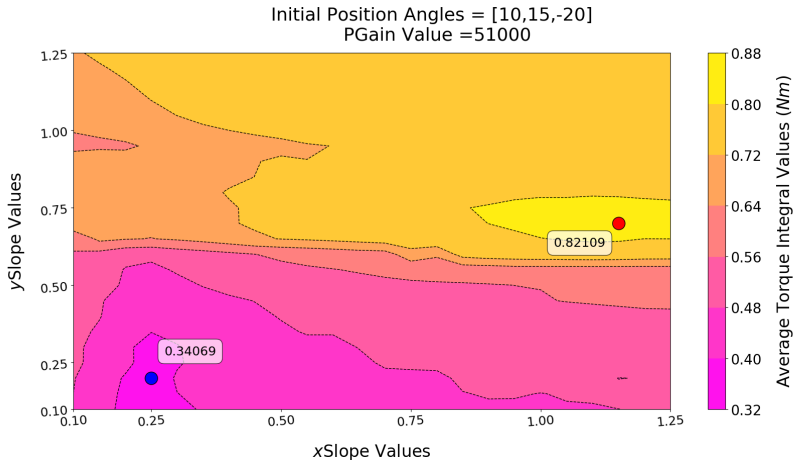

(d)

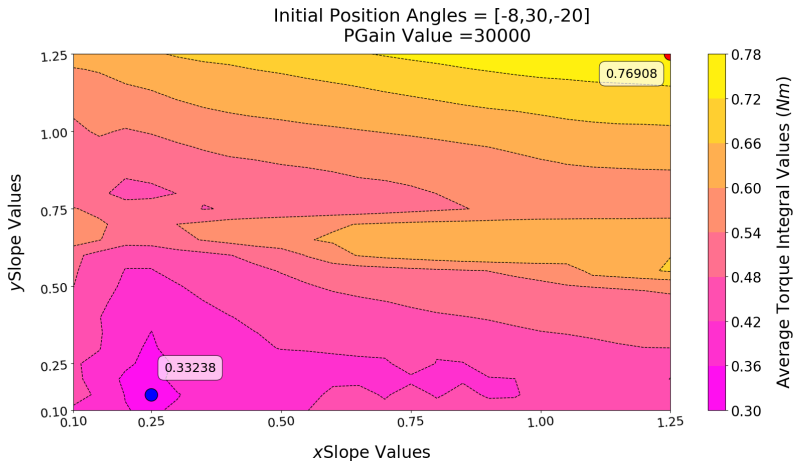

(e)

Figure D.1: Values of the average joint torque integral for different combinations of *x*Slope and *y*Slope values. The annotated values correspond to the highest (red) and lowest (blue) values.

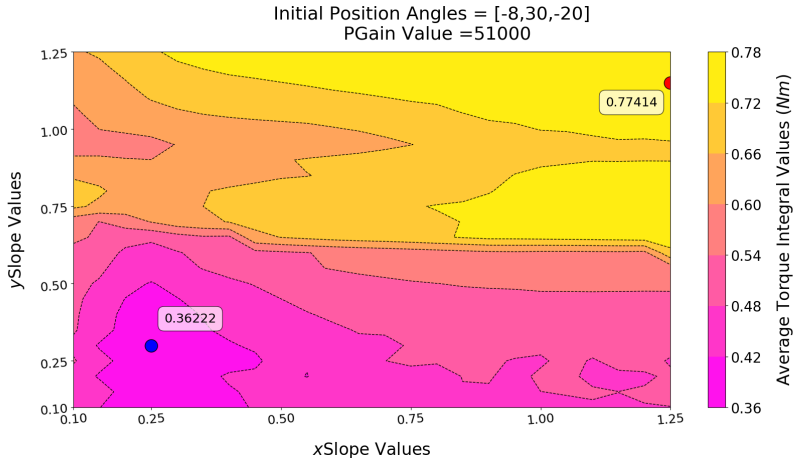

(f)

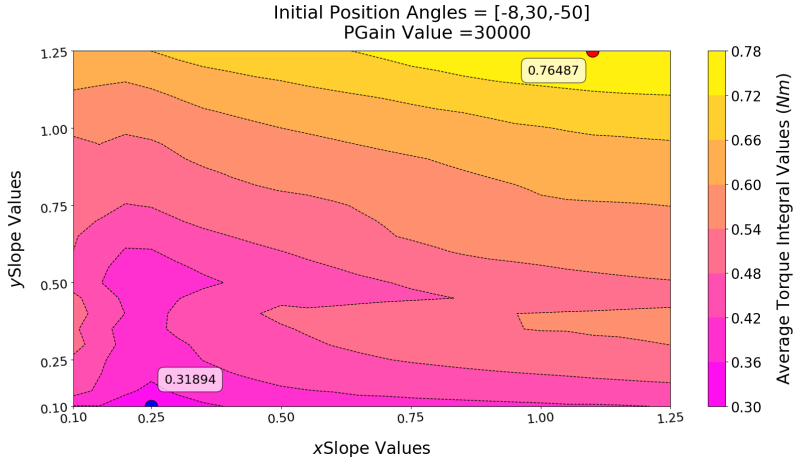

(g)

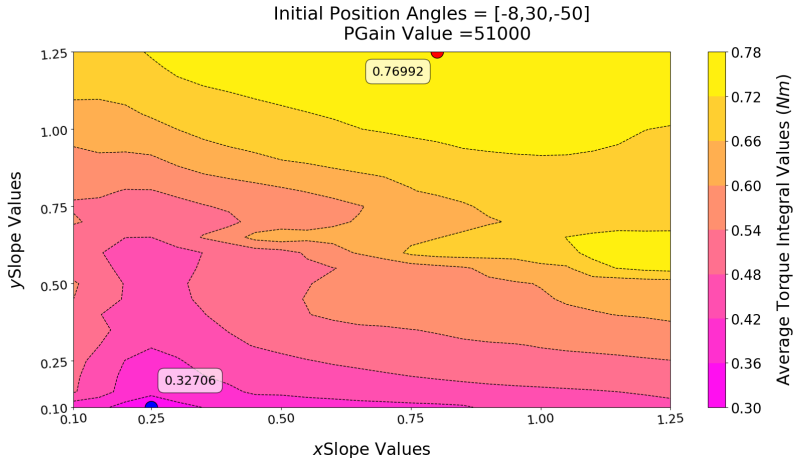

(h)

Figure D.1: Values of the average joint torque integral for different combinations of xSlope and ySlope values. The annotated values correspond to the highest (red) and lowest (blue) values.

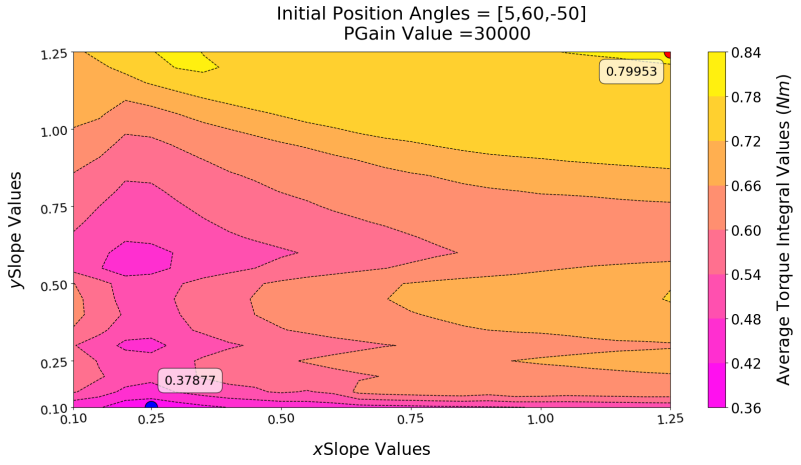

(i)

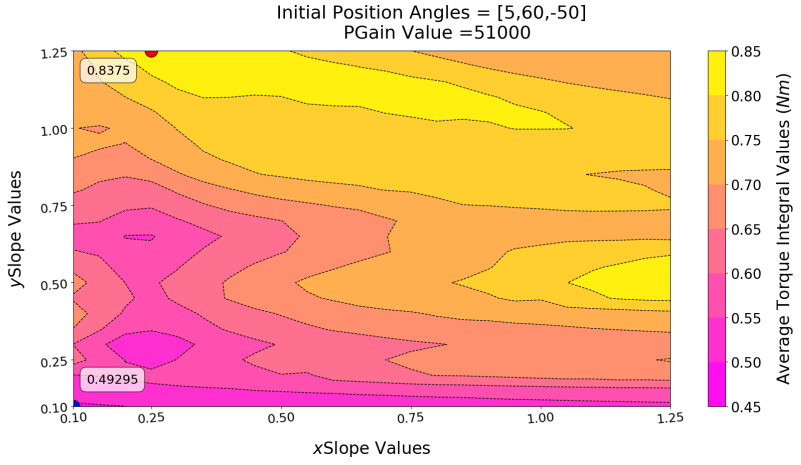

(j)

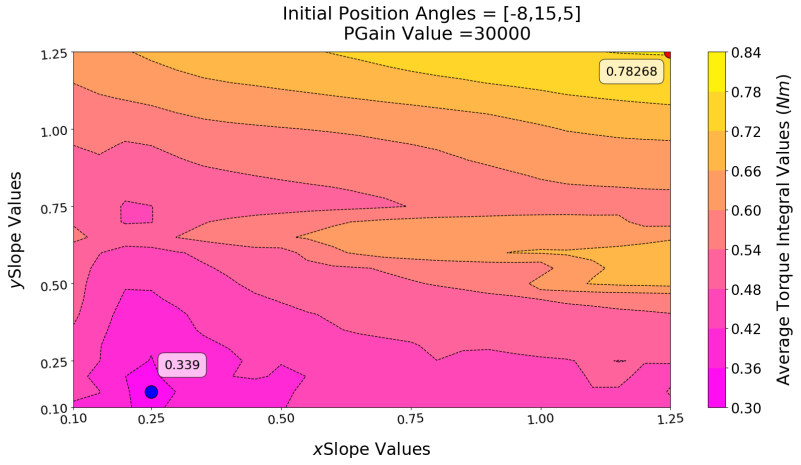

(k)

Figure D.1: Values of the average joint torque integral for different combinations of xSlope and ySlope values. The annotated values correspond to the highest (red) and lowest (blue) values.

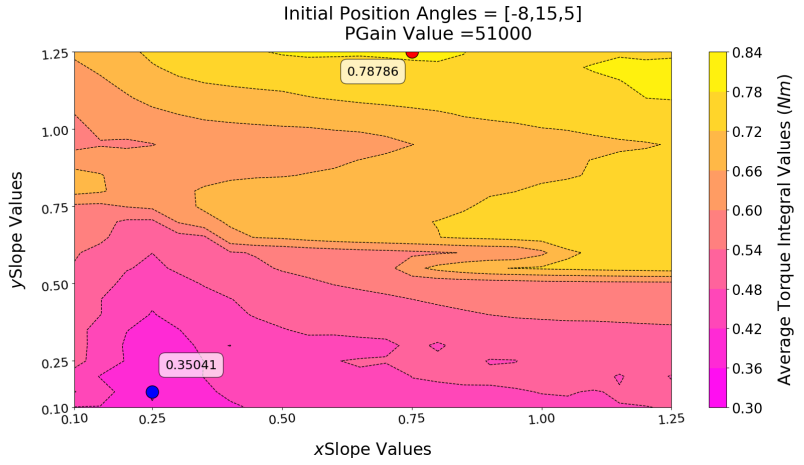

(l)

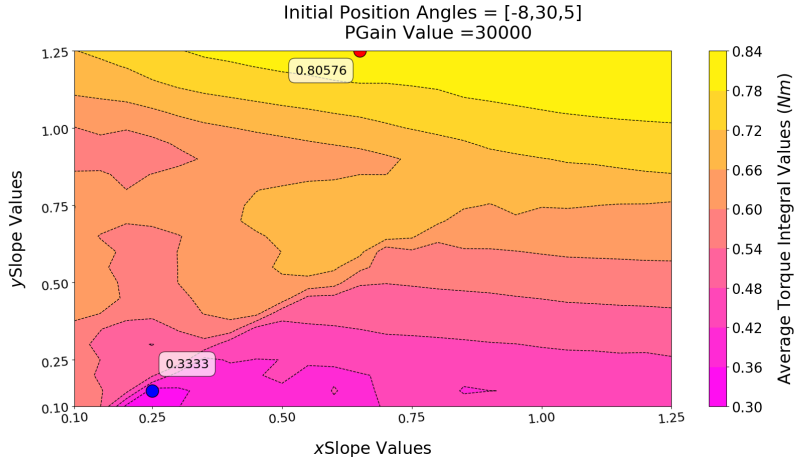

(m)

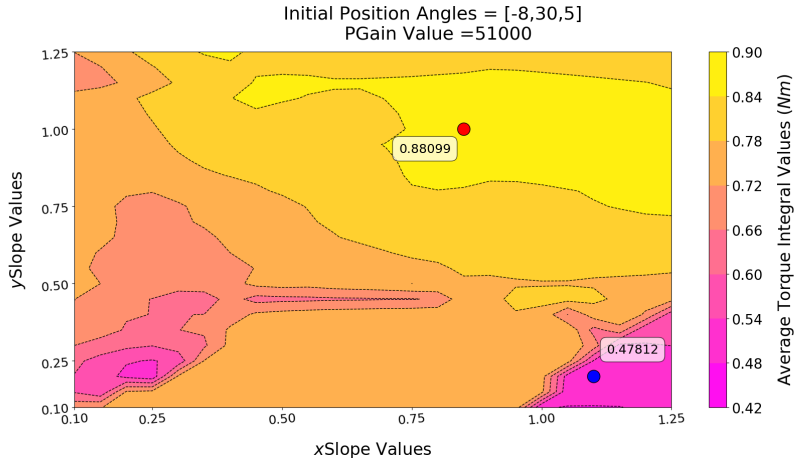

(n)

Figure D.1: Values of the average joint torque integral for different combinations of xSlope and ySlope values. The annotated values correspond to the highest (red) and lowest (blue) values.

APPENDIX E

Normalized Hip Vertical Velocity Results

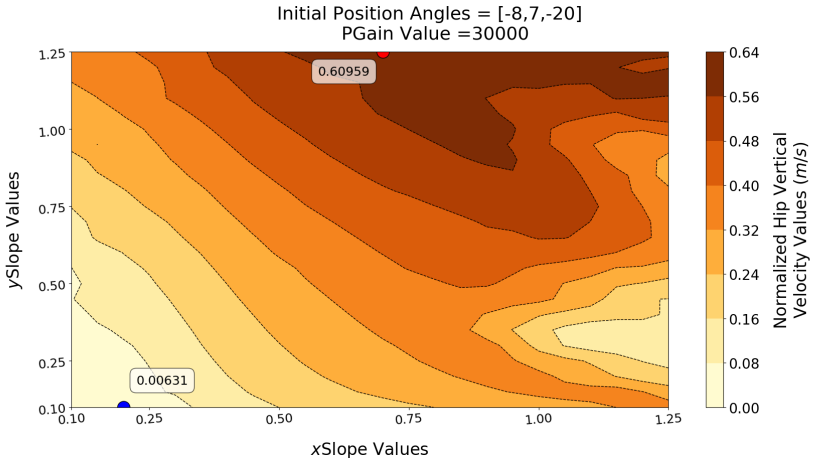

(a)

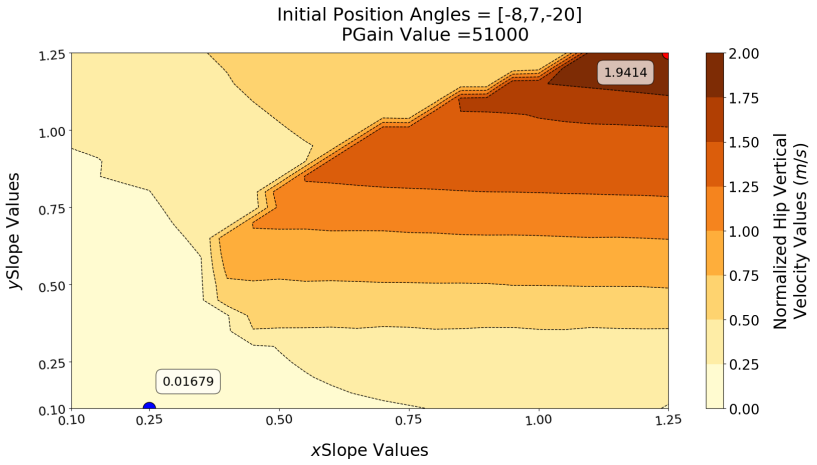

(b)

Figure E.1: Values of the normalized hip vertical velocity for different combinations of xSlope and ySlope values. The annotated values correspond to the highest (red) and lowest (blue) values for each set.

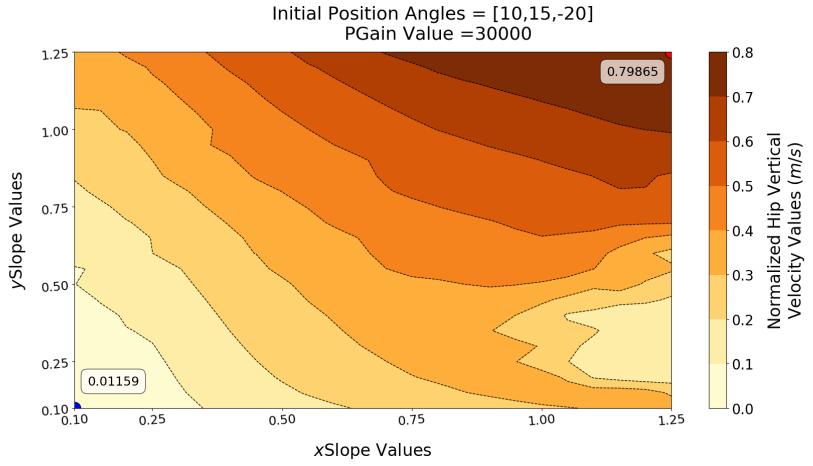

(c)

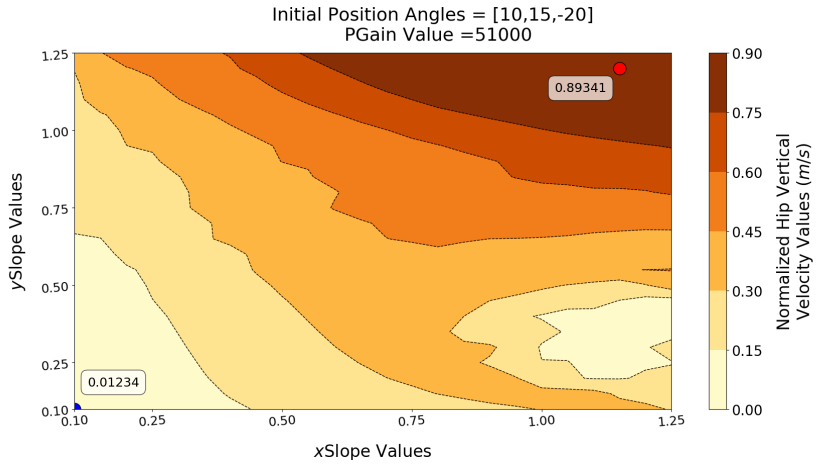

(d)

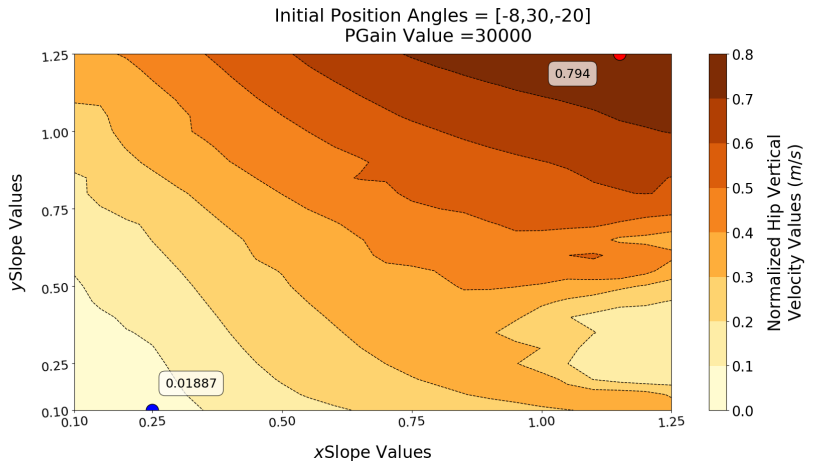

(e)

Figure E.1: Values of the normalized hip vertical velocity for different combinations of xSlope and ySlope values. The annotated values correspond to the highest (red) and lowest (blue) values for each set.

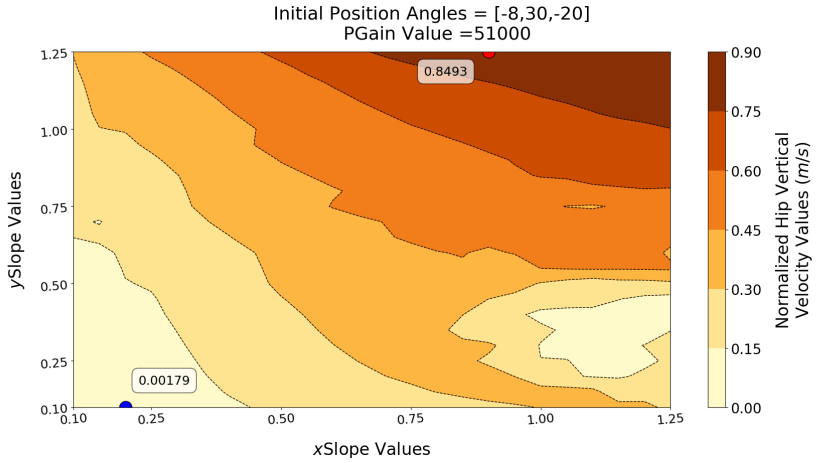

(f)

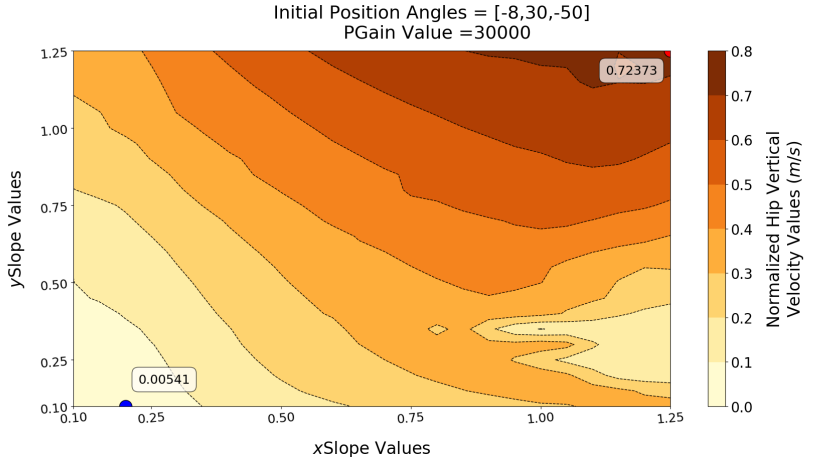

(g)

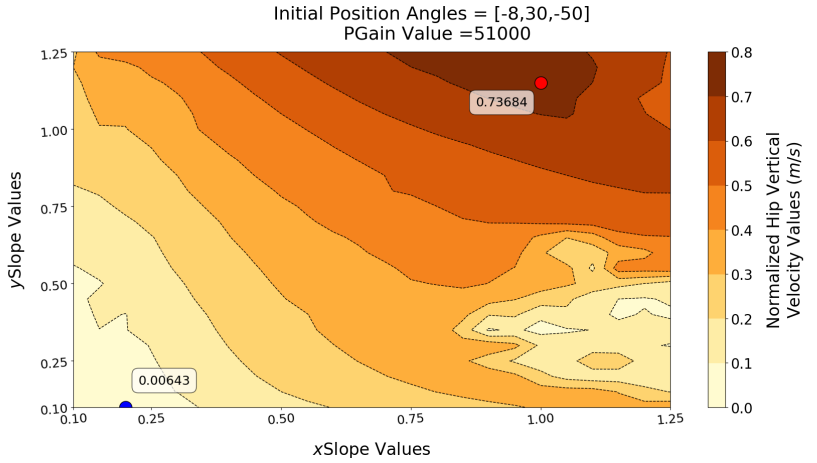

(h)

Figure E.1: Values of the normalized hip vertical velocity for different combinations of xSlope and ySlope values. The annotated values correspond to the highest (red) and lowest (blue) values for each set.

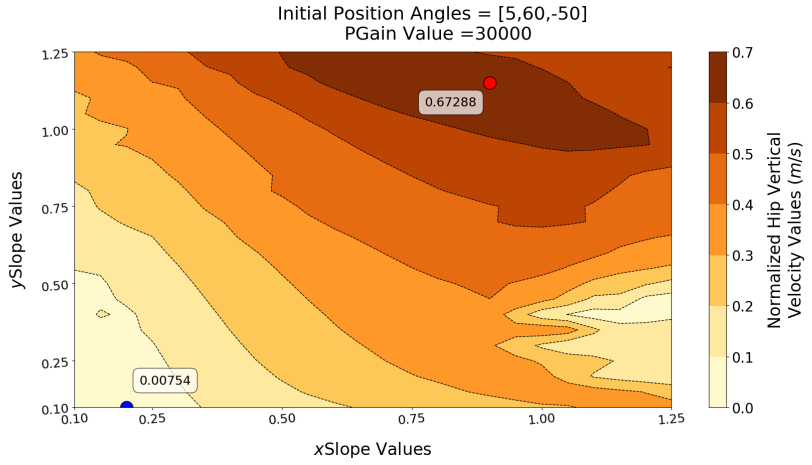

(i)

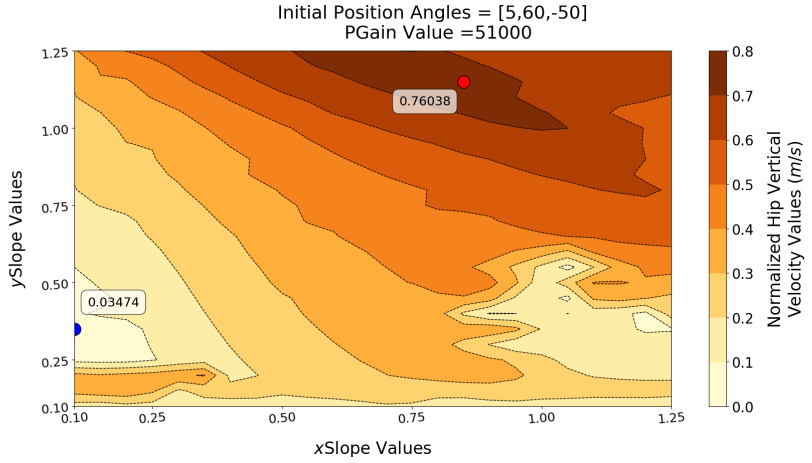

(j)

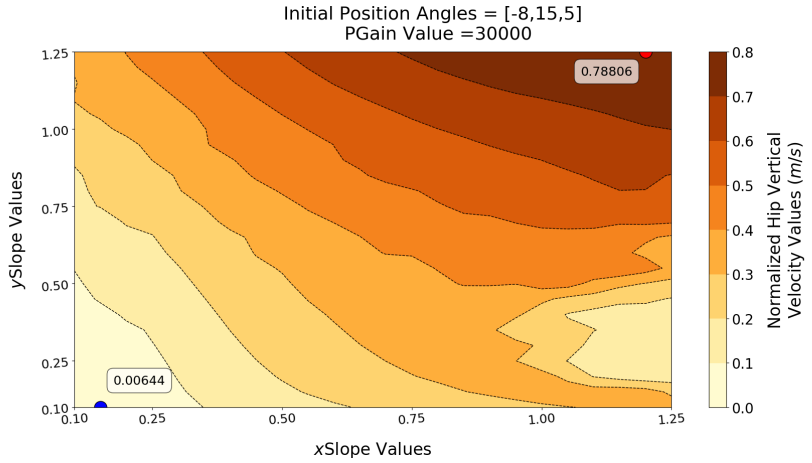

(k)

Figure E.1: Values of the normalized hip vertical velocity for different combinations of xSlope and ySlope values. The annotated values correspond to the highest (red) and lowest (blue) values for each set.

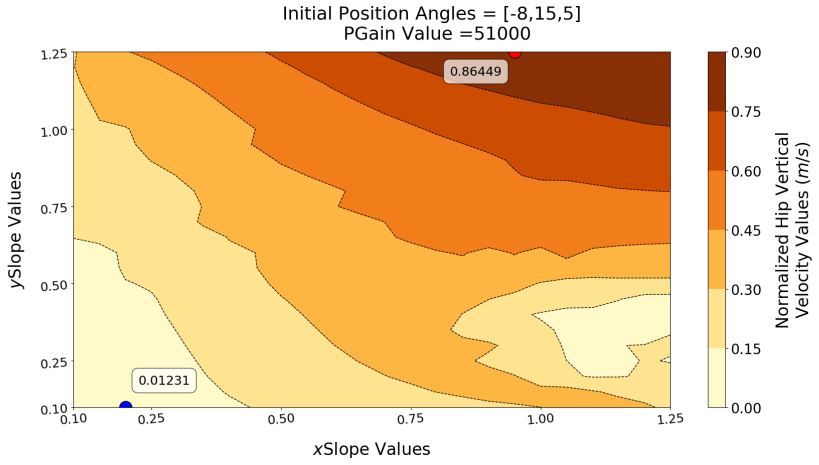

(l)

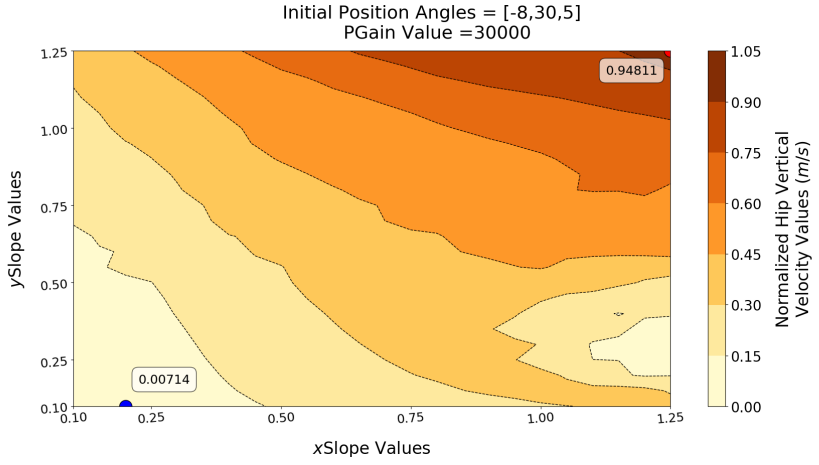

(m)

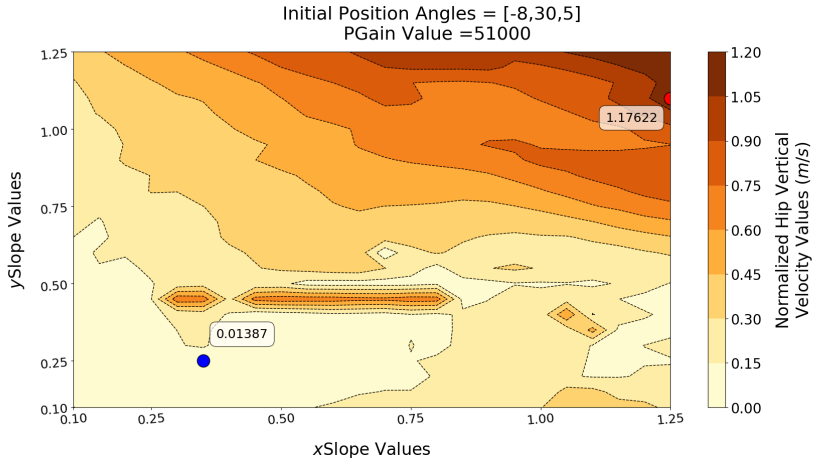

(n)

Figure E.1: Values of the normalized hip vertical velocity for different combinations of xSlope and ySlope values. The annotated values correspond to the highest (red) and lowest (blue) values for each set.

APPENDIX F

Performance Score Results

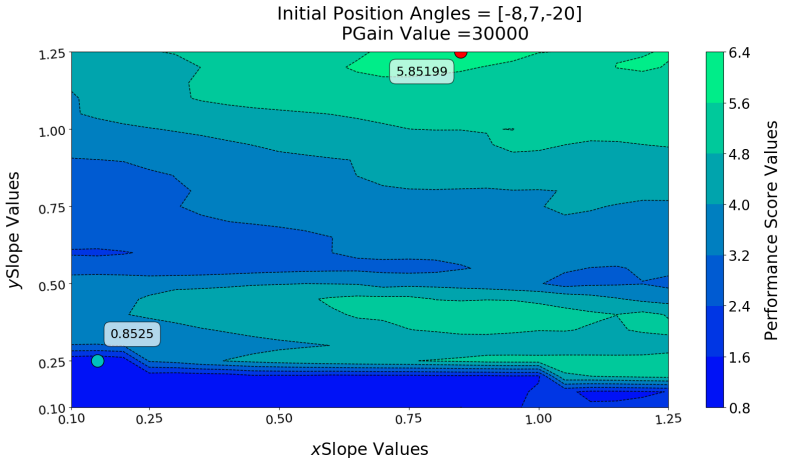

(a)

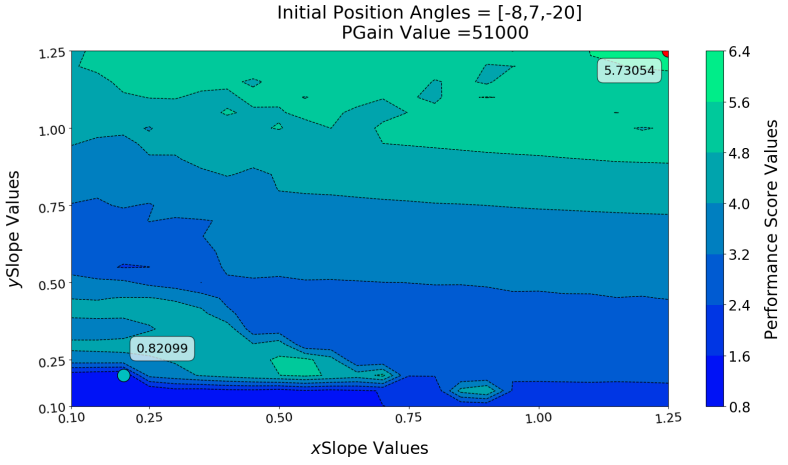

(b)

Figure F.1: Values of the performance score for different combinations of xSlope and ySlope values. The annotated values correspond to the highest (red) and lowest (cyan) values.

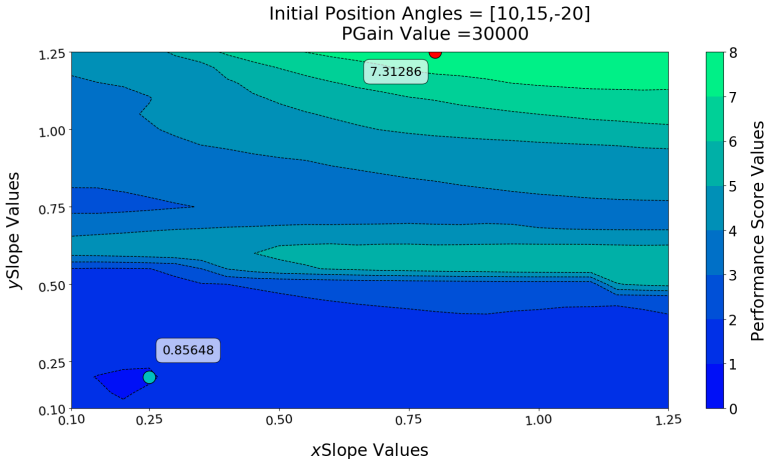

(c)

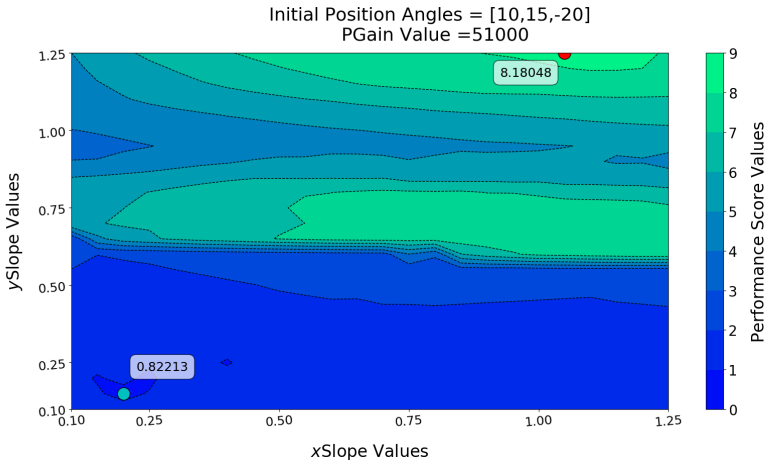

(d)

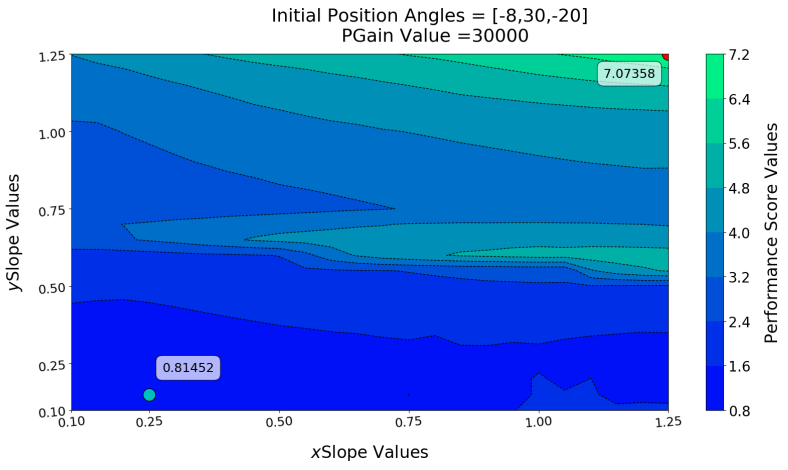

(e)

Figure F.1: Values of the performance score for different combinations of xSlope and ySlope values. The annotated values correspond to the highest (red) and lowest (cyan) values.

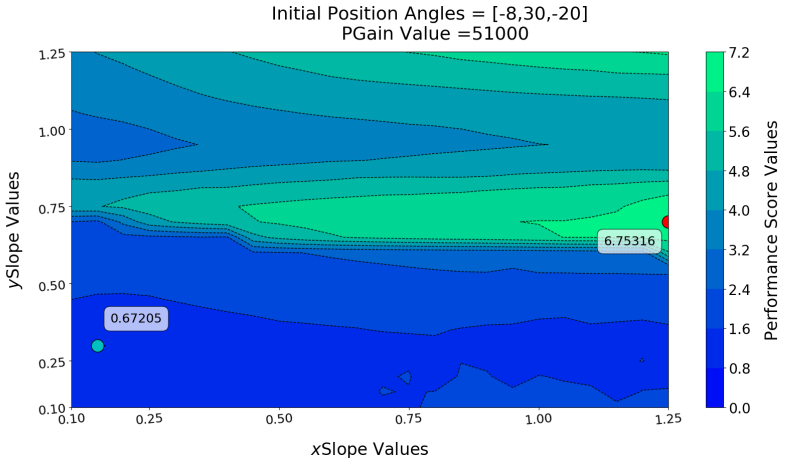

(f)

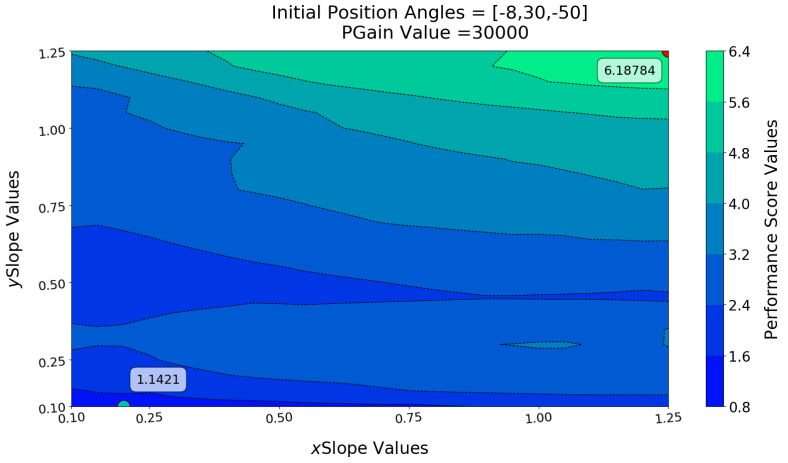

(g)

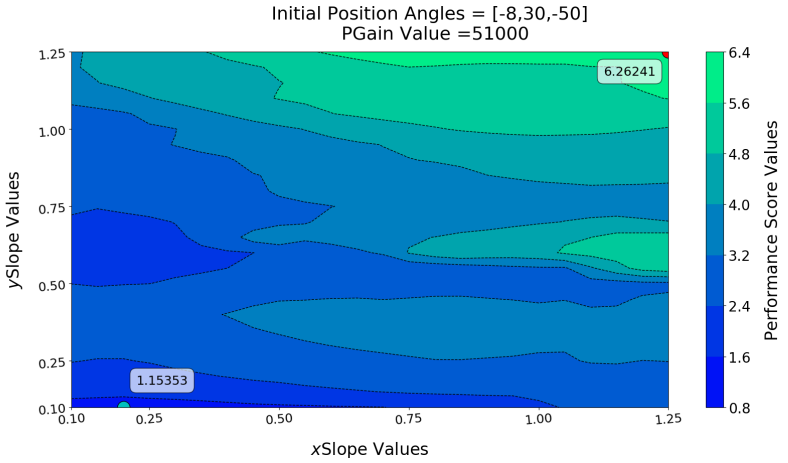

(h)

Figure F.1: Values of the performance score for different combinations of xSlope and ySlope values. The annotated values correspond to the highest (red) and lowest (cyan) values.

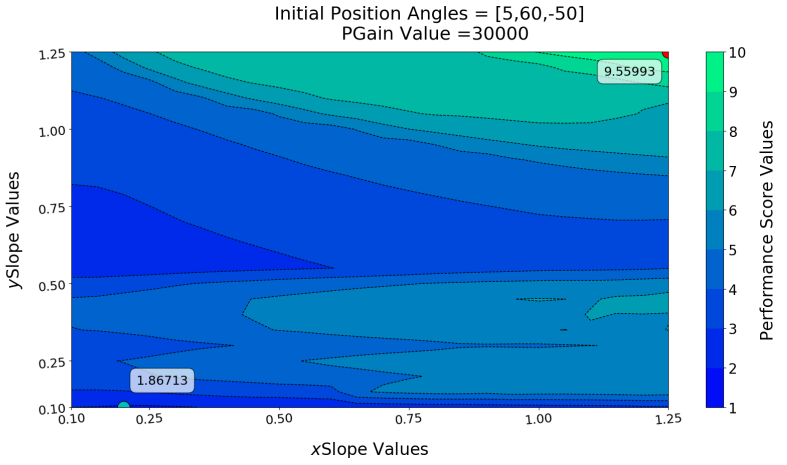

(i)

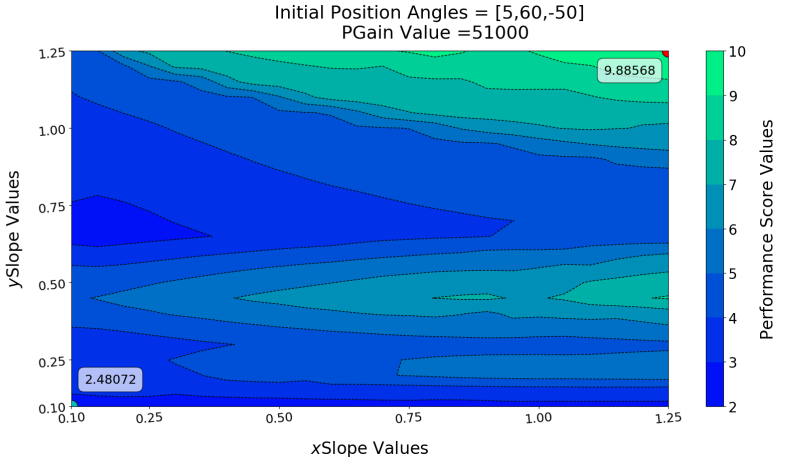

(j)

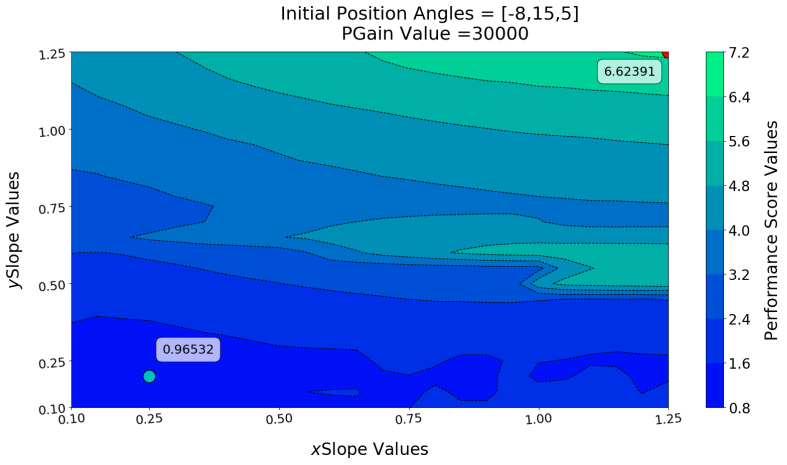

(k)

Figure F.1: Values of the performance score for different combinations of xSlope and ySlope values. The annotated values correspond to the highest (red) and lowest (cyan) values.

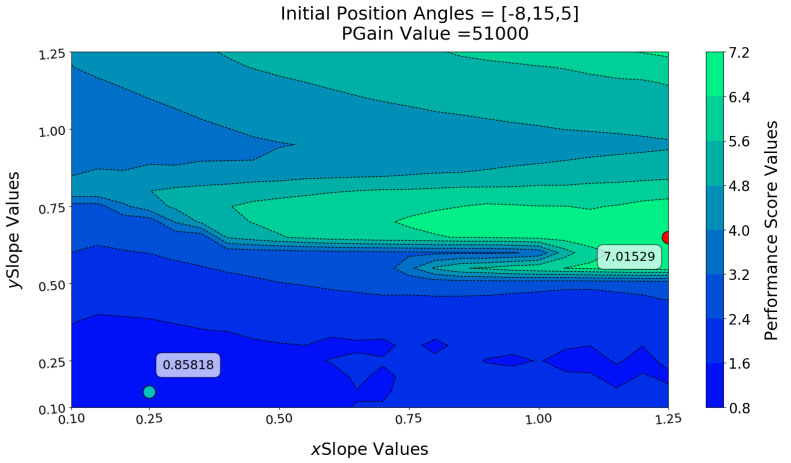

(l)

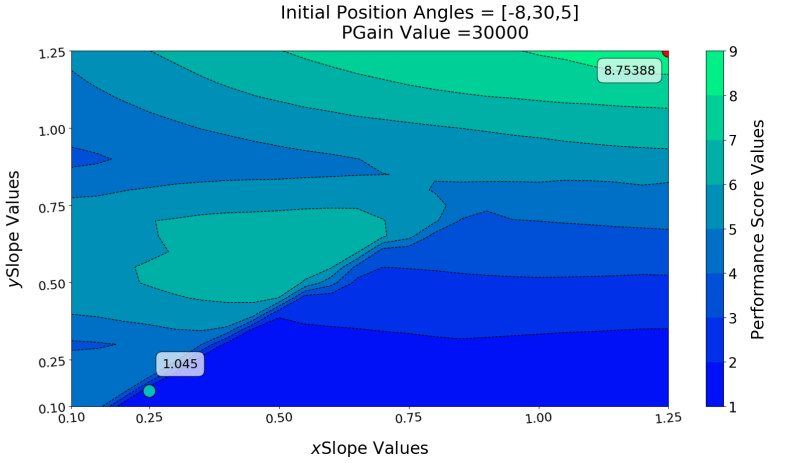

(m)

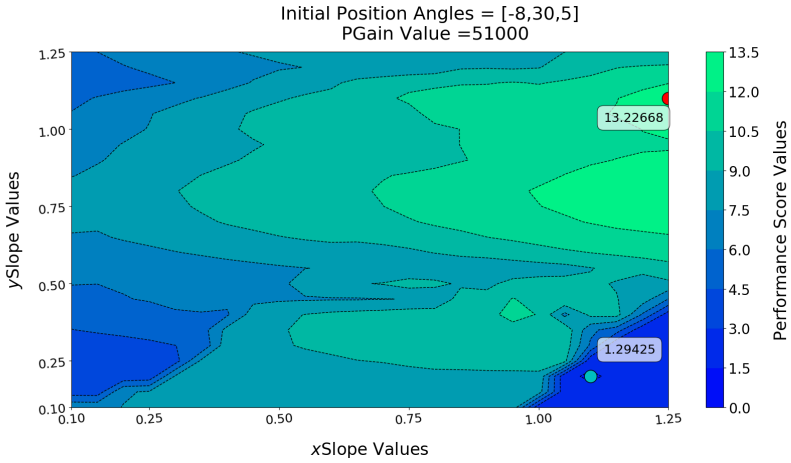

(n)

Figure F.1: Values of the performance score for different combinations of xSlope and ySlope values. The annotated values correspond to the highest (red) and lowest (cyan) values.